12-2006

INTERNAL COMBUSTION ENGINE COOLING STRATEGIES: THEORY AND TEST

John Chastain
Clemson University, jhchast@clemson.edu

INTERNAL COMBUSTION ENGINE COOLING STRATEGIES: THEORY AND TEST

A Thesis
Presented to
the Graduate School of
Clemson University

In Partial Fulfillment
of the Requirements for the Degree
Master of Science
Mechanical Engineering

---

by
John Howard Chastain, Jr.
December 2006

Accepted by:
Dr. John Wagner, Committee Chair
Dr. Richard Figliola
Dr. Darren Dawson

ABSTRACT

Advanced automotive thermal management systems integrate electro-mechanical components for improved fluid flow and thermodynamic control action. Progressively, the design of ground vehicle heating and cooling management systems require analytical and empirical models to establish a basis for real time control algorithms. One of the key elements in this computer controlled system is the smart thermostat valve which replaces the traditional wax-based unit. The thermostat regulates the coolant flow through the radiator and/or engine bypass to control the heat exchange between the radiator's coolant fluid and the ambient air. The electric water pump improves upon this concept by prescribing the coolant flow rate based on the engine's overall operation and the driver commands rather than solely on the crankshaft speed. The traditional radiator fan is belt driven and equipped with a clutch to limit parasitic loads during operating conditions that provide sufficient radiator heat rejection. A DC motor-driven radiator fan offers improved control over the air flow rate to better regulate radiator heat rejection while reducing power consumption. Ideally, the thermal management system will accept multiple engine sensor feedback including, but not limited to, the engine cylinder temperature, oil temperature, coolant temperature, engine block temperature, engine load, and throttle angle. To achieve this concept, these electrically driven system components must be mathematically described, computer controlled, and configured on an internal combustion engine.

A unique experimental platform has been developed featuring a 4.6L V8 engine, with extensive block-embedded thermocouples, attached to a water-brake dynamometer.

Three physical cooling system configurations were tested for prescribed engine temperature tracking and power consumption: an electrically driven fan in combination with a wax-based thermostat and a crank shaft driven cooling pump (Tests 1 & 2); a servo-motor driven radiator fan and smart thermostat valve in combination with the engine driven cooling pump (Tests 3 & 4); and an electrically driven radiator fan, smart thermostat valve, and servo-motor coolant pump (Tests 5 & 6). These cooling system configurations facilitated the testing of three different controller concepts based on factory emulation, classical control, and thermodynamic optimization. Each cooling system is evaluated with a test profile encompassing steady state and transient engine operation by including step changes in the engine speed, engine load, and air speed. Data acquisition and control activities were supported by a dSPACE DS1104 hardware board which managed the real-time interface between the Control Desk software and the physical system.

The experiments demonstrated that steady state coolant temperature regulation was improved with computer control of the radiator fan, thermostat valve, and coolant pump (Tests 5 & 6) which is noted by accurately tracking the set point temperature within ±0.5ºC. Most importantly this system (Test 5 & 6) was able to meet the cooling needs with 60W power consumption. A reduction of 478W parasitic energy use in situations where vehicle ram-air provided a sufficient heat rejection rate when compared to the factory emulation power use of 538W(Test 1). However, with this increased level of control, the system revealed temperature variations of ±3.0ºC in Test 3 versus ±0.1ºC in Test 1 during transient response to ram-air. Overall, computer control of the automotive cooling system enhances temperature tracking ability and reduces the parasitic loading.

ACKNOWLEDGEMENTS

It gives me great joy to thank my family who has supported me in all my endeavors with love and pride. My dad, John Chastain, Sr., is to be thanked, above all, for his support that has allowed me to focus full attention on this body of work. My mom, Cecilia Chastain, whose loving support in all areas of my life has been invaluable. I am forever indebted to my friends and colleagues who have provided the memories of a lifetime.

I would like to thank Dr. Wagner for his support on this project and the intellectual freedom he entrusted to me throughout. I give many thanks to my committee, Dr. Figliola and Dr. Dawson, for strengthening my work in engineering thermodynamics and control. I would like to acknowledge the continuous support of the mechanical engineering support shop, Jamie Cole for his assistance on the electric systems and Michael Justice for his extensive assistance in machining. Additional thanks are in order to the gentlemen at the Clemson University College of Engineering and Science Machining and Technical Support Shop for their expertise and knowledge in prototype development.

TABLE OF CONTENTS

Table of Contents (Continued)

LIST OF TABLES

LIST OF FIGURES

List of Figures (Continued)

List of Figures (Continued)

List of Figures (Continued)

List of Figures (Continued)

NOMENCLATURE

Symbol	Units	Description
a	-	coefficient
A	m^2	pump inlet area
A_r	m^2	cross-sectional area of radiator
A_v	m^2	cross-sectional area of valve
A_f	m^2	radiator flow area
A_t	%	fractional area of wax thermostat
b	-	coefficient
c	-	coefficient
c	kJ/kg·ºC	specific heat
c_a	kJ/kg·ºC	specific heat of air
c_c	kJ/kg·ºC	specific heat of coolant (water)
c_p	kJ/kg·ºC	isobaric specific heat
$c_{p,X}$	kJ/kg·ºC	minimum specific heat
c_v	kJ/kg·ºC	isochoric specific heat
$C_{p,m}$	kJ/kg·ºC	minimum thermal capacitance
d	-	coefficient
e	-	coefficient
e	ºC	temperature error
e	kJ/kg	specific energy of a control volume
$\dot{E}_d$	kJ/s	Exergy destruction rate

Nomenclature (Continued)

Symbol	Units	Description
f	Hz	frequency
f_c	Hz	chirp frequency
f_n	Hz	natural frequency
$\dot{f}_{loss,e}$	kJ/s	engine friction loss rate
$\dot{f}_{loss,j}$	kJ/s	junction friction loss rate
$\dot{f}_{loss,r}$	kJ/s	radiator friction loss rate
g	m/s^2	gravitational constant
h	kJ/kg	specific enthalpy
h_{fg}	kJ/kg	enthalpy of condensation
k	-	pipe number
K_i	-	integral gain
K_p	-	proportional gain
m_{cv}	kg	mass contained within a control volume
m_e	kg	mass of coolant contained within engine
m_j	kg	mass of coolant contained within junction
m_{pk}	kg	mass of coolant contained within the k^{th} pipe
m_r	kg	mass of coolant contained within radiator
$\dot{m}_a$	kg/s	mass flow rate of air at radiator
$\dot{m}_b$	kg/s	mass flow rate of coolant through bypass
$\dot{m}_c$	kg/s	mass flow rate of coolant

Nomenclature (Continued)

Symbol	Units	Description
$\dot{m}_{fg}$	kg/s	mass flow rate of condensate
$\dot{m}_{pk}$	kg/s	mass flow rate of coolant at the k^{th} pipe
$\dot{m}_r$	kg/s	mass flow rate of coolant at radiator
$\dot{m}_v$	kg/s	mass flow rate of coolant at valve
$\dot{m}_X$	kg/s	mass flow rate of minimum capacitant fluid
N	-	number of pipe segments
N_f	RPM	fan speed
$N_{\max}$	RPM	maximum pump speed
N_p	RPM	pump speed
p	kPa	pressure
$P_{1,a}$	kPa	radiator air side inlet pressure
$P_{2,a}$	kPa	radiator air side outlet pressure
P_v	kPa	pressure differential at valve
Q_c	LPM	volumetric flow rate of coolant
Q_r	LPM	volumetric flow rate of coolant at radiator
Q_v	LPM	volumetric flow rate of coolant at valve
$Q_{v,actual}$	LPM	actual volumetric flow rate of coolant at valve
$Q_{v,ideal}$	LPM	ideal volumetric flow rate of coolant at valve
$\dot{Q}_{cv}$	kJ/s	control volume heat transfer rate
$\dot{Q}_e$	kJ/s	engine combustion heat release rate

Nomenclature (Continued)

Symbol	Units	Description
$\dot{Q}_m$	kJ/s	maximum heat transfer rate
$\dot{Q}_{pk}$	kJ/s	heat transfer rate at the k^{th} pipe
$\dot{Q}_r$	kJ/s	radiator heat transfer rate
R	kJ/kg·K	ideal gas constant
s	kJ/kg	specific entropy
$\dot{S}_{gen,e}$	kJ/s	entropy generation rate at engine
$\dot{S}_{gen,j}$	kJ/s	entropy generation rate at junction
$\dot{S}_{gen,r}$	kJ/s	entropy generation rate at radiator
t_I	s	increased load time
t_{II}	s	ram-air on time
t_{III}	s	ram-air off time
t_{IV}	s	decreased load time
t_V	s	engine key-off time
t_p	s	peak time
t_r	s	rise time
t_s	s	settling time
T	ºC	temperature
$T_{a,e}$	ºC	air stream exit temperature
$T_{a,i}$	ºC	air steam inlet temperature
T_{cc}	ºC	combustion chamber temperature

Nomenclature (Continued)

Symbol	Units	Description
$T_{c,i}$	ºC	cold stream inlet temperature
T_e	ºC	engine temperature
$T_{e,e}$	ºC	engine exit temperature
$T_{e,i}$	ºC	engine inlet temperature
T_{fb}	ºC	feedback temperature
$T_{h,i}$	ºC	hot steam inlet temperature
T_{high}	ºC	wax-based valve upper temperature
$T_{j,1i}$	ºC	junction inlet temperature
$T_{j,2i}$	ºC	junction inlet temperature
$T_{j,e}$	ºC	junction exit temperature
T_{lb}	ºC	left engine bank temperature
$T_{lb\_\max}$	ºC	maximum left engine bank temperature
$T_{lb\_\min}$	ºC	minimum left engine bank temperature
T_{lb_ss}	ºC	steady state left engine bank temperature
T_{low}	ºC	wax-based valve lower temperature
T_o	ºC	ambient temperature
$T_{pk,e}$	ºC	k^{th} pipe exit temperature
$T_{pk,i}$	ºC	k^{th} pipe inlet temperature
$T_{r,e}$	ºC	radiator exit temperature
T_{r,e_ss}	ºC	steady state radiator outlet temperature

Nomenclature (Continued)

Symbol	Units	Description
$T_{r,i}$	ºC	radiator inlet temperature
T_{r,i_ss}	ºC	steady state radiator inlet temperature
T_{rb}	ºC	right engine bank temperature
T_{rb_ss}	ºC	steady state right engine bank temperature
T_{sp}	ºC	set point temperature
$T_{s,r}$	ºC	radiator surface temperature
P_f	W	fan power load
P_p	W	pump power load
P_{pl}	W	peak power load
P_{ssl}	W	steady state power load
u	kJ/kg	specific internal energy
U	kJ	internal energy
U_f	-	fan control signal
U_p	-	pump control signal
U_v	-	valve control signal
v	m^3/kg	specific volume
v_c	m^3/kg	specific volume of coolant
~~V~~	m^3	volume
V_e	m/s	exit velocity
V_f	V	fan voltage
V_{fc}	V	fan control voltage
V_i	m/s	inlet velocity

Nomenclature (Continued)

Symbol	Units	Description
V_n	m/s	velocity, normal to control volume boundary
V_p	V	pump voltage
V_{pc}	V	pump control voltage
V_r	m/s	air velocity at radiator
$\dot{W}_{cv}$	kJ/s	work rate at control volume
$\dot{w}_p$	kJ/s	work rate at pump
z	m	height above datum
$\Delta\dot{m}_a$	kg/s	change of ram-air mass flow rate
ΔN	kPa	change of engine speed
ΔP_b	kPa	differential pressure at bypass
ΔP_e	kPa	differential pressure at engine
ΔP_m	kPa	differential pressure at multi-pipe
ΔP_p	kPa	differential pressure at pump
ΔP_r	kPa	differential pressure at radiator
ΔP_v	kPa	differential pressure at valve
ΔT_e	ºC	engine temperature differential
$\Delta\tau$	N-m	change of engine torque
ε	-	heat exchanger effectiveness
η	-	efficiency
$\eta_{e/m}$	-	conversion efficiency (electrical to mechanical)

Nomenclature (Continued)

Symbol	Units	Description
$\eta_{m/h}$	-	conversion efficiency (mechanical to hydraulic)
θ_a	deg	actual angular valve position
θ_d	deg	desired angular valve position
θ_e	deg	angular valve position error
θ_{os}	deg	valve angular overshoot
$\theta_{v,\%}$	%	valve position
ρ	kg/m^3	density
ρ_a	kg/m^3	air density
ρ_w	kg/m^3	water density

CHAPTER 1

INTRODUCTION

Automotive thermal management systems vary in configuration and capacity but perform the primary function of cooling internal combustion engines. These systems generally feature a radiator, radiator fan, coolant pump, and thermostat valve which dissipate the engine's waste heat through the coolant fluid. The valve is a proportioning device which ensures that the engine coolant temperature remains within a specified range. Also, system designs require the engine ethylene-glycol fluid to remain below its boiling point for the engine's entire operating range including its maximum heat load. Advancements (i.e., automotive based electronic control) have created the opportunity to continuously tailor the heat dissipation by implementing and controlling electrically actuated cooling system components allowing better temperature modulation and energy management.

Automotive cooling system configurations will be evaluated with both mechanical and electrical actuation (e.g., servo-motor driven valve, pump, and fan). These components will be computer controlled using thermostatic control techniques where the set point, control point, and actuator are extensively connected by the coolant (Miles, 1965). To define and control the actuators, proportional plus integral controllers have been implemented and tuned (O'Dwyer, 2003). In an effort to compare all control strategies and benefits, an experimental system is developed with the actuators controlling the temperature of a 4.6L V8 two valve engine. This system is reconfigurable

to support alternative cooling system architectures which feature integrated sensors for feedback of the system's temperatures, pressures, flow rates, and power consumption.

A common basis for the evaluation of cooling system architectures has been established with concise testing procedures. Engine cooling systems are exposed to variability in both the engine load and the radiator air flow conditions. The testing procedure will simulate the engine's power output variability with a dynamometer. Environmental conditions at the radiator, such as ram-air, will be simulated by way of adjustable air blower. Each configuration will be evaluated based on temperature response to the disturbances and analyzed through steady state characteristics. The experimental apparatus provides the ability to evaluate the engine cooling system power consumption load and effective operation.

Research Objective and Goals

The main objective to this research project has been to design an advanced automotive cooling system. A series of five goals were identified which include: component selection, component design, empirical and analytical modeling, system integration, and on-engine experimental testing. The cooling requirements of a 4.6L V8 two valve engine provided the basis for the selection of an electric fan and a pedestal pump. An electrically controlled butterfly valve was specified and designed based on specifications for a thermostat valve. This valve was machined and built since an off-the-shelf solution did not exist. Empirical models for the fluid action of the system were developed to benchmark the valve and pump. Also, the radiator's heat dissipation capacity was determined experimentally with various fan operating conditions. Analytical modeling based on thermodynamics has been utilized to develop a model of the cooling system's transient thermal action. Finally, the sensors and actuators were

integrated in the engine testing environment designed to evaluate cooling system configurations and real-time control algorithms.

Thesis Organization

Chapter 2 presents a literature review which examines the recent advancement of automotive cooling systems and the foundation for further development. Chapter 3 demonstrates the design process utilized for the smart thermostat control valve including a description of the controller design and scale bench testing method. Chapter 4 reports the experimental characteristics for thermal system components such as the valve, pump, coolant circuit flows, and radiator heat dissipation capacity. Chapter 5 establishes the analytical modeling intended for simulation based studies and also applicable in cooling system experimental evaluations. Chapter 6 presents the cooling system configurations and control architectures applied to a 4.6L V8 internal combustion engine. Also included in this chapter is the test profile, available sensors and the engine control console details. Most importantly this chapter outlines the key observations and challenges revealed in the testing. Conclusions and recommendations will be presented in Chapter 7. Appendix A describes a valve design detail drawings. Appendix B presents the Matlab code used to identify the transfer function of the valve's response. The valve design tool based on the prototype smart valve is included in Appendix C. Appendix D describes the analytical development of the radiator friction losses on the air side and coolant side. Appendix E presents the subroutines that are used within the thermal system modeling with experimental data from a thermal system simulation of the scale thermal bench. Appendix F presents the engine test time histories and the data acquisition settings.

CHAPTER 2

LITERATURE SURVEY

Automotive Cooling Systems

To introduce the work in the field of automotive cooling systems, a list of references is presented which offers insight to the past and current work. Chalgren and Barron (2003) considered an advanced thermal management system capable of fuel efficiency benefits of up to 5%. The electric water pump introduced a 1.9 kW reduction in parasitic losses. Chanfreau *et al.* (2003) introduced the need of an electrical water valve for the thermal management intelligent system as an alternative to the passive wax thermostat operating as a water bypass valve. Wagner *et al.* (2003) presented a smart thermostat and coolant pump to control engine thermal management. The presented valve was a linearly actuated three way valve to control the bypass and radiator coolant flow. Eberth *et al.* (2004) introduced a smart thermal management system that reduced warm-up time, temperature tracking errors and power consumption of the electrically actuated cooling components.

Luptowski *et al.* (2005) presented an enhanced vehicle and engine cooling system simulation through the coupling of advanced engine and cooling system computer-based simulation tool. This active cooling simulation was applied to a Detroit Diesel series 60 engine where power consumption and engine warm-up time reduction was studied. Rigorous models have been used in development of the simulation system. A classical PID controller, with combinations of feedback and feed-forward control, was used as well as special transport delays. Chalgren and Allen (2005) presented a light duty diesel

on vehicle application for complete electrification of the cooling system. A Ford Excursion was tested and showed the ability of the advanced cooling system to reduce under hood packaging, reduce power consumption, and provide better temperature modulation. Page *et al.* (2005) applied the advanced thermal management concept to an army vehicle that attained lower power consumption. Redfield *et al.* (2006) presented a thermal management application on a Class 8 tractor equipped with an auxiliary power unit (fuel cell) to power an advanced thermal management system which introduced significant fuel savings for a cross-country trip. This short list describes the trend of implementing electrical actuators in automotive cooling systems for increased system controllability.

Further improvements have been suggested which are truly innovative in that the cooling system configuration is modified. Vagenas *et al.* (2004) propose a novel cooling jet system to maintain temperatures in the thermally critical exhaust valve bridge or cylinder head. The addition of the cooling jets to the base system allows lower coolant flow rates through the water jacket. Ap and Tarquis (2005) compare different types of engine cooling systems that can be characterized as innovative. One of the most interesting in the group of systems presented is the nucleate boiling engine cooling which allows the coolant in the engine to boil requiring an expansion tank to absorb the additional volume. This system is reported to have higher engine head and oil sump temperatures while attaining the benefit of reduced coolant flow.

Thermodynamic Modeling and Performance Evaluation

Research has concluded that implementing controlled actuators will reduce cooling system parasitic loads and reduce emissions. Simulation based system design and control development activities have been used to address the increased complexity

and increased design time typically required by these advanced systems. Wagner *et al.* (2002) presented a simulation based on a multiple node resistor-capacitor representation of the cooling system which described the cooling system thermal behavior. Some other application benefiting from cooling system modeling is its use as control basis for the action of the thermal management components (Setlur *et al.*, 2005).

Thermal management system performance analysis can be based on energy consumption and enhanced with a second law of thermodynamic based analysis. Li and Figliola (2004) present an exergy-based analysis for optimizing the design of an automotive cooling system. This analysis is particularly useful for initial system design and can apply to transient system performance evaluation. Figliola and Tipton (2000) use this exergy based methodology to address the design of aircraft thermal systems. This analytical technique lays the foundation for the definition of an objection function which can be minimized to achieve efficient system design.

System and Component Design

Driskell (1983) presented the performance equations for control valves to aid their specification and design. Driskell's contribution on control valves accounts for the selection and application of control valves where equations are used to develop a descriptive dimensionless valve (Hutchison, 1976). Stoecker (1971) presented many modeling techniques for use in the design of thermal systems. In addition, many thermal system modeling applications and design analyses are presented with mathematical modeling techniques. Shinskey (1978) applies controls in thermal systems while utilizing the second law of thermodynamics to realize improved performance.

CHAPTER 3

SMART THERMOSTAT VALVE DESIGN

Advanced thermal management systems require active components which can be controlled using feedback variables. In this thesis, a smart thermostat valve has been developed to control fluid routing at the radiator. For current vehicles, a wax-based thermostat provided the flow control. The thermostat opening characteristics are designed based on a defined cooling system set point temperature. Furthermore, the system action is greatly influenced by the valve's location. This may be attributed to the wax-based unit's concurrent locations for fluid flow actuation and temperature feedback. For proper modulation of coolant temperature, this unit must observe the highest coolant temperature which occurs by installing the valve close to the engine block. In the proposed smart valve, the system integration constraints are eased with the separation of the actuator control point and its temperature feedback mechanism. Temperature feedback for the actuator was accomplished electronically with temperature sensors such as thermocouples (or thermistors). These sensors can be installed in thermally demanding areas such as the cylinder head and in locations outside the controlled media, such as the engine lubrication oil. This chapter discusses the design of the valve and its accompanying controller.

Valve Design Method

The smart thermostat valve prototype design features a DC gear motor and rotational potentiometer to control valve position as shown in Figure 3.1. The valve body is machined from aluminum and equipped with a permanent magnet DC gearmotor

(Dayton 1L475) coupled to the valve shaft. Opposite the motor is a voltage dividing potentiometer for valve position feedback (Penny and Giles SRS). The butterfly to housing seal interface uses an oblique conical surface geometry. The valve utilizes a series of o-rings (not shown) that maintain water tight integrity. The butterfly is mounted to the valve shaft such that the seals on the shaft experience low pressures downstream when in the closed position.

Table 3.1 Prototype valve component list with part numbers referenced in Appendix A

Valve Component	Part No.
Valve Body	B269S05805 - prototype
Seal Bushing	B269S05808 - prototype
Butterfly Plate	B269S05806 - prototype
Valve Pin	B269S05807 - prototype
Sensor Bracket	B269S05809 - prototype
Motor Bracket	B269S05810 - prototype
DC Gear Motor	Dayton 1L475
O-ring	Standard AS568A-008 & -011
Rotary Sensor	Penny & Giles SRS280/120/D/IP50/A

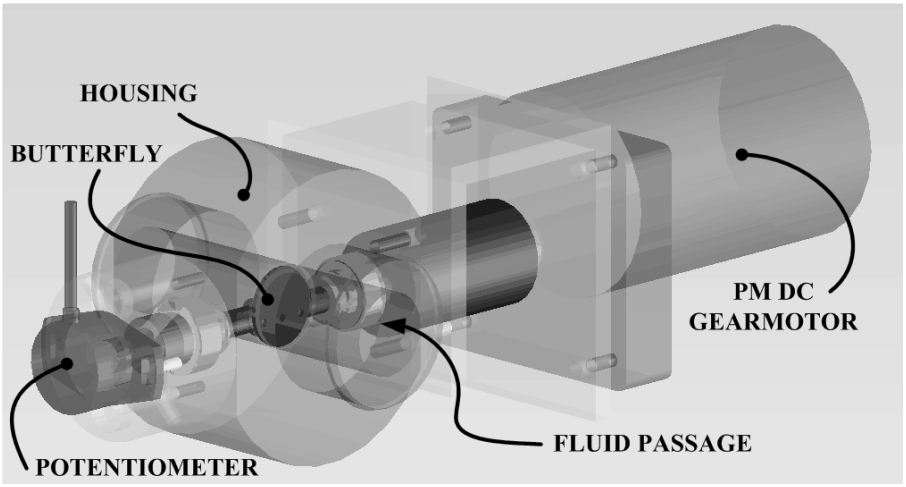

Figure 3.1 Prototype smart valve assembly with integrated servo-motor and rotational potentiometer

In selecting the valve's diameter, the performance parameters of pressure, flow, speed of response and controllability are considered. Designing the valve required knowledge of the cooling system which the valve will be controlling coolant flow. The main concern is matching the valve size with the cooling system application to ensure proper controllability with respect to the radiator or bypass flow characteristics. If the valve is too large, then insufficient restriction will be offered at a given flow rate and the flow controllability will be diminished. These oversized valves result in small operation ranges (near the fully closed position) which is not desired. In contrast, a small valve will develop a large pressure head, even at fully open condition, negatively impacting the coolant flow control. Proper valve sizing and design is essential to valve function. Accordingly, the prototype valve orifice size is designed to meet the controllability of flow for this specific cooling system application.

The valve's hydraulic performance has been studied using a fluid analysis approach. In the design stage, calculations of the valve's flow area for different butterfly positions provide performance feedback. An important design factor includes the effective flow area which requires geometric inspection of the flow passages within the valve. Through the use of solid modeling software (Solid Works), the geometry of the flow area was investigated providing information for a theoretical mapping of the valve where the flow rate, pressure, and valve position are interrelated. This feedback in the design process establishes the basis for the characterization of the valve's orifice diameter. Figure 3.2 illustrates geometric inspection that produced an analytical valve map, where the relationship between the valve position and the flow area was defined. The valve's cross sectional area, determined by the geometric inspection at various valve

positions, allows the construction of Figure 3.3. The unique valve action, where it rotates about an axis that is not centered on the valve flow passage or on the butterfly plate, causes the slightly nonlinear valve position to area relationship.

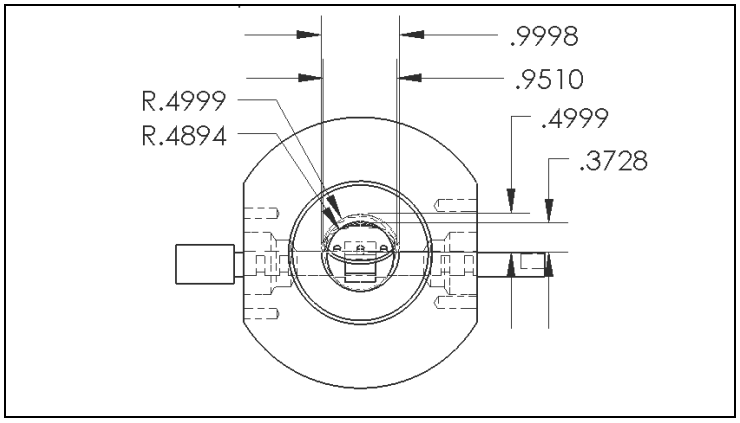

Figure 3.2 Top view of smart thermostat valve with flow passage geometry (note: valve shown at 66%)

The definition of the valve's cross sectional area of flow for various valve positions defines the theoretical valve map. Ideally, the valve's flow rate, Q_v, may be determined using the valve cross sectional area, A_v, and pressure head, P_v, as

$$Q_{v,ideal} = A_v \sqrt{\left(2 \cdot \Delta P_v / \rho_w\right)} \tag{3.1}$$

However, the actual flow rate is less than the ideal this reduction is determined by a correction factor, C, which is a function of the Reynold's number and fluid momentum.

$$Q_{v,actual} = C Q_{v,ideal} \tag{3.2}$$

In Figure 3.4, the analytically-based pressure, valve position, and flow relationship is displayed for the prototype valve using the nonlinear relation between the valve opening and the cross-sectional area of flow (refer to Figure 3.3). An empirically defined valve map is presented in Figure 4.3 utilizing empirical data from prototype tests.

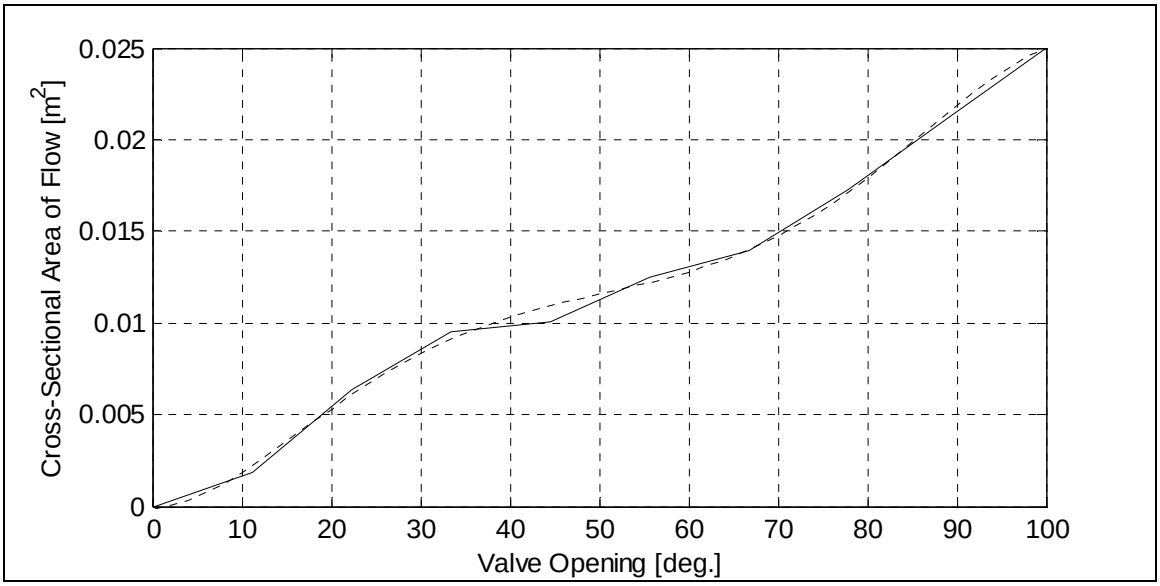

Figure 3.3 Geometric analysis of smart thermostat valve orifice

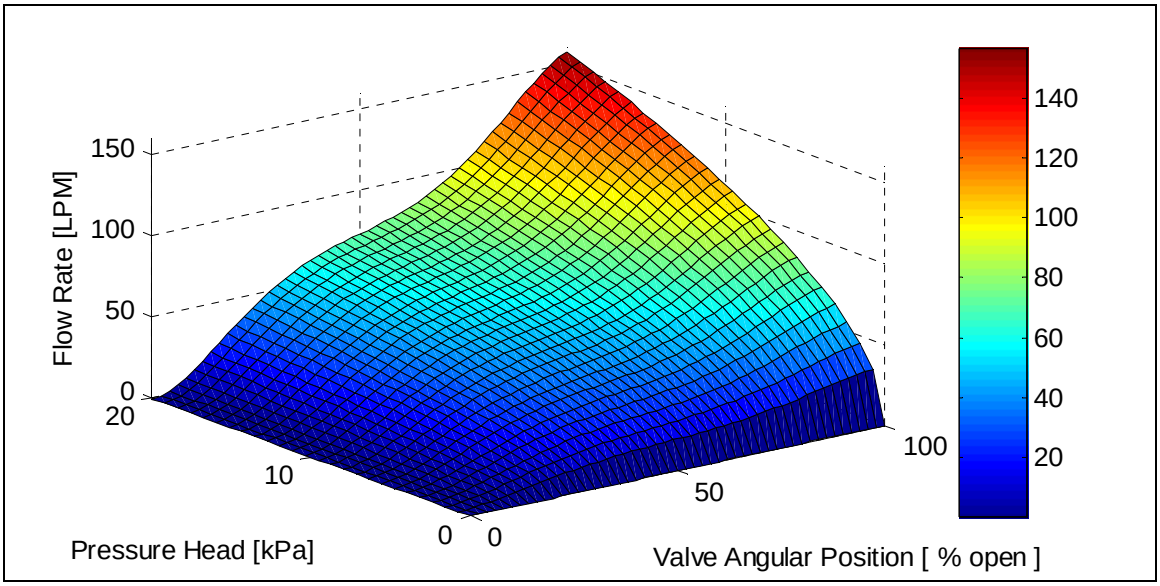

Figure 3.4 Analytical smart thermostat valve map
featuring pressure, ideal flow, and valve position

Controller Development

After realization of the smart thermostat valve, the unit was benchmarked by testing its mechanical response and fluid operation. A hardware-in-the-loop configuration was created with a proportional control algorithm and a software saturation block to avoid motor damage. Also featured was a block sequence that acted as a relay where the valve drive motor will not function unless there is a position feedback signal. The controller gains were selected to obtain acceptable step and frequency response characteristics. The test procedures and results for the mechanical response characteristics are now discussed.

Bench Testing Method

To test the valve's capabilities, the response to step, ramp, and sinusoidal waveforms were considered. The step response test was accomplished using various sized valve opening increments. The transfer function estimate utilized a chirp signal with defined frequency limits and target times. As shown in Figure 3.5A, the valve command tracking for a 22.5º step holds the steady state error to within $\theta_e = \pm 0.5º$. The actual valve position shows approximately $\theta_{os} = 0.25º$ overshoot with a peak time at $t_p = 0.5s$. For both tests, the valve settles with negligible oscillation. In Figure 3.5B, the valve rise time to a 45º step is approximately $t_r = 0.8s$. The rise time increases with increasing step size due to the constant saturation value (angular velocity). The steady state error remains within $\theta_e = \pm 0.5º$ for both step tests.

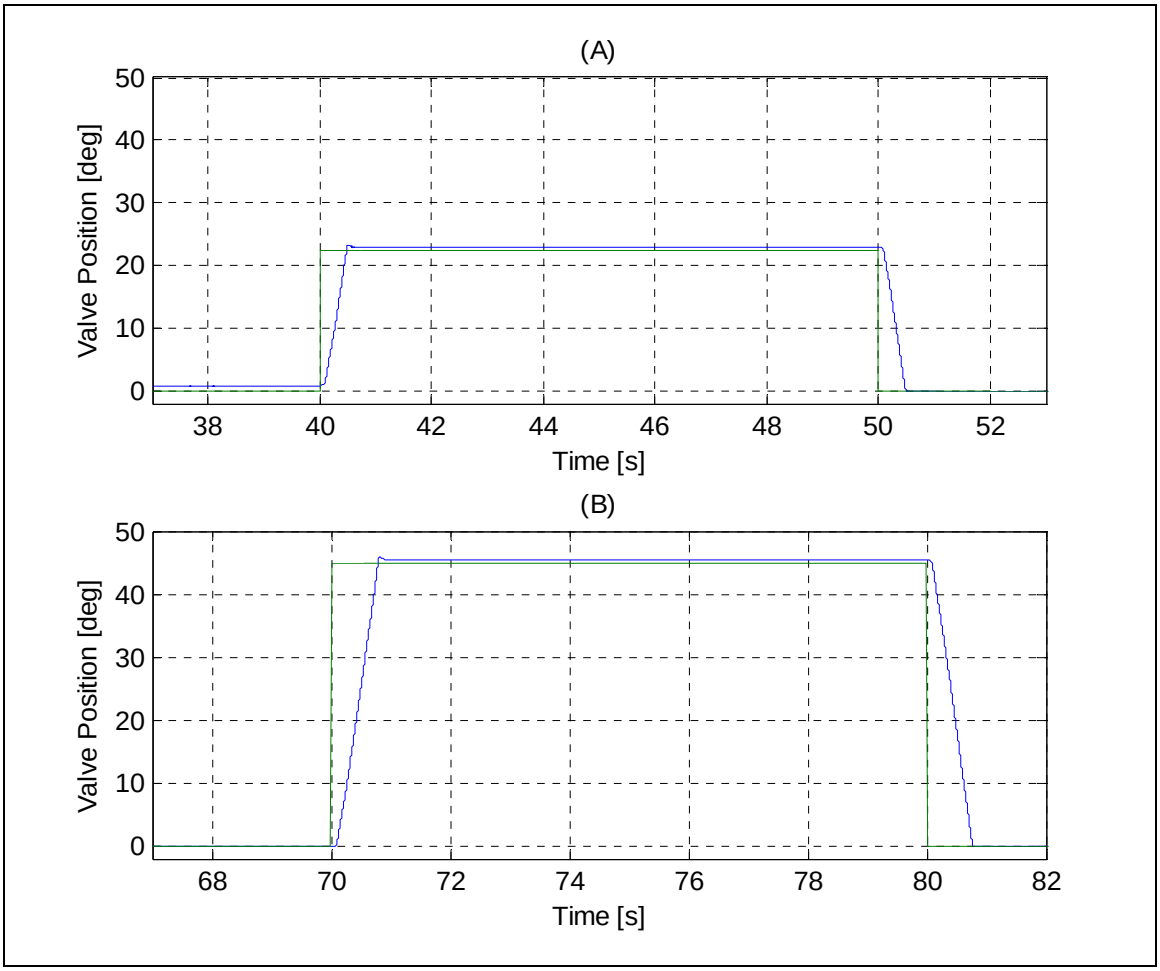

Figure 3.5 Smart thermostat valve plate's rotational response for (A) 22.5º, and (B) 45º step input

The valve step response reveals acceptable dynamic performance. Inspection of the two step response plots show the system has a natural frequency of approximately f_n = 4 Hz. Observed in all response plots is the constant slope during the rise time which is due to the saturation block limiting valve control voltages between ±6 VDC. The saturation component may hold the angular velocity to a constant which restricts the overshoot and reduces power consumption while the controller gain maintains sufficient gain at small error signals to seek desired position. The valve was also evaluated using a 1.2º/s ramp response. Note that in Figure 3.6, the steady state error is θ_e = 0.8º.

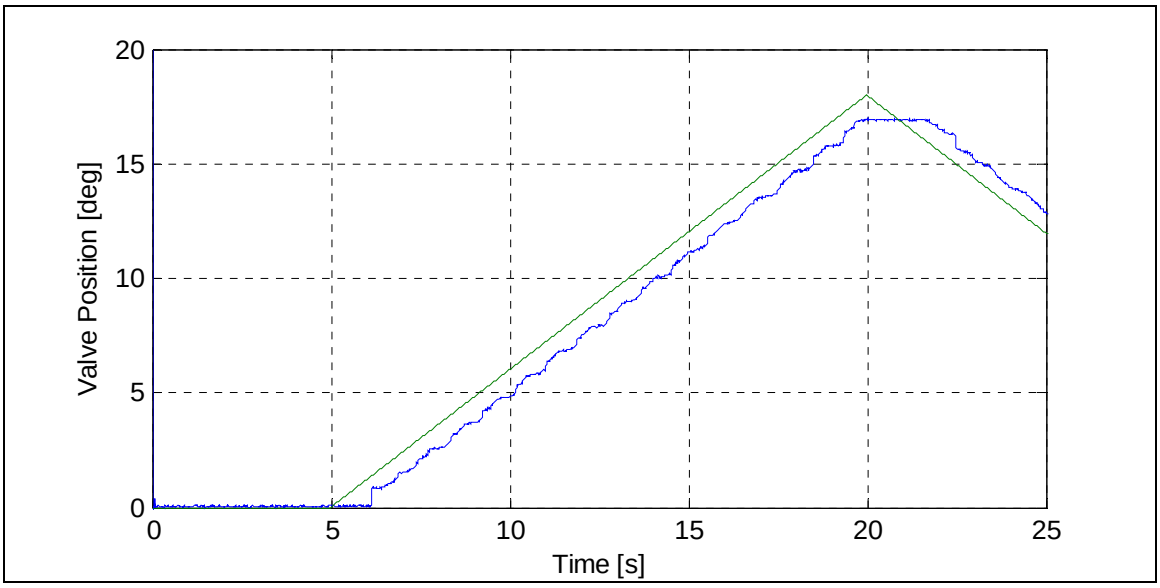

Figure 3.6 Smart thermostat valve response to a ramp input

Finally, the thermostat valve is subjected to a chirp signal ranging from $0.1 \leq f_c \leq$ 2 Hz. The desired, θ_d, and the actual, θ_a, valve positions are compared using the Matlab function 'tfe or tfestimate' that estimates the transfer function. The magnitude and phase plots, presented in Figure 3.7, give the frequency response of the valve based on experimental data. The valve shows good response between $0.1 \leq f \leq 2.0$ Hz with

negligible magnitude reduction or amplification. The valve drive mechanism fails to respond at frequencies greater than $f \geq 2$ Hz. This trait is common in many electro-mechanical systems where the command signal frequency exceeds the system's natural frequency.

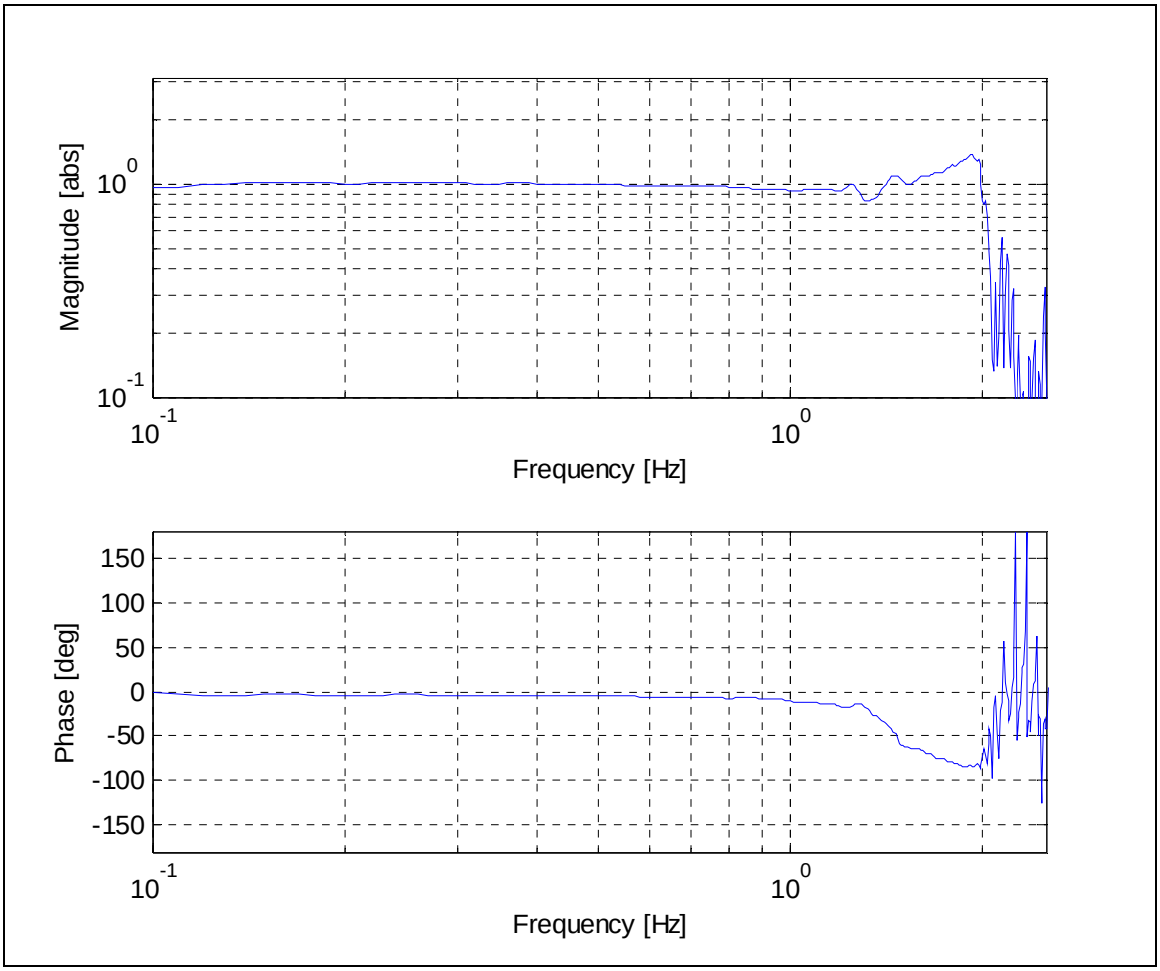

Figure 3.7 Smart thermostat valve's transfer function estimate (θ_a / θ_d) for an input signal amplitude of ±15º

CHAPTER 4

EXPERIMENT-BASED MODELS

Thermal system design and control vary in automotive applications depending on the engine's thermal load and under-hood packaging. These variations in require the development of generic test routines for individual system components that can be applied to any development activity. In this study, a typical thermal management system has been designed which includes three electronically actuated cooling components; radiator fan, thermostat valve, and coolant pump. This experimental system will be used to develop an empirical model of fluid dynamic behavior that accounts for the complex geometries that typically lead to analytical modeling difficulties resulting in modeling error. This empirical modeling method begins with the prototype smart thermostat valve which is benchmarked by measuring the flow and pressure head while varying valve positions. Next, a multi-pipe system, where the bypass valve loop (with benchmarked valve) and radiator are connected in parallel, will require models that describe the bulk flow rates related to the pressure losses at varying valve positions. Finally, the pump model is developed by varying the pump speed while measuring the pressure head and flow rate.

The system fluid flow behavior can be applied to the system thermal response analysis resulting in increased accuracy. Note that the thermal system design and under hood packaging constraints will not readily allow for reliable and accurate measurement of flow observation in the radiator and bypass coolant passages. The thermal model

developed for the radiator uses a novel approach (i.e., utilizes steam as the hot fluid in the radiator which decreases the number of measured variables and overall control required for testing in comparison to working with coolant) which minimizes the experimental uncertainty (Chastain and Wagner, 2006). This approach, using steam as the hot fluid, allows the heat transfer rate to be quantified with minimal experimental uncertainty when compared to the coolant based testing which requires measurement and control of coolant temperatures and flow rates.

Pump Characteristics

The development of the pump's empirical model uses the smart valve to control the pressure head in the system at various pump operating speeds. The experimental setup has a flow meter, controllable valve, and a variable speed centrifugal pump as shown in Figure 4.1. The pump is operated at various shaft speeds while varying the valve from a fully open to a fully closed position. The experimental data that depicts the lower flow characteristics of the pump is presented in Figure 4.2. The pump is rated for flows up to 220 LPM for a negligible pressure head and maximum pump speed (3,450 RPM). Modeling the pump is secondary to the pump selection where manufacturers typically furnish test data. In the pump selection process, the choice of the pump type (i.e., axial or centrifugal) should be based on the system requirements. Allen and Lasecki (2001) discuss an axial pump to implement controlled coolant flow. In this study, a centrifugal pump has been selected.

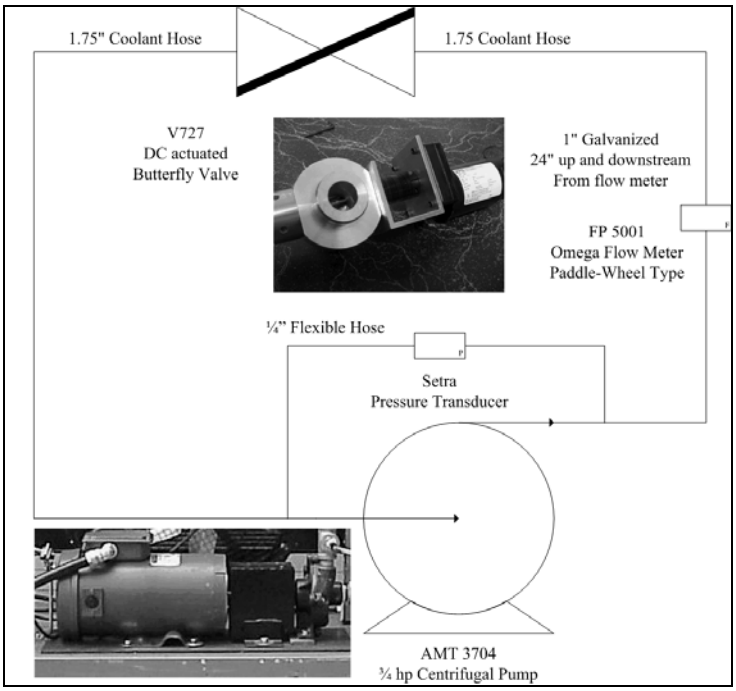

Figure 4.1 Process diagram of the electric coolant pump

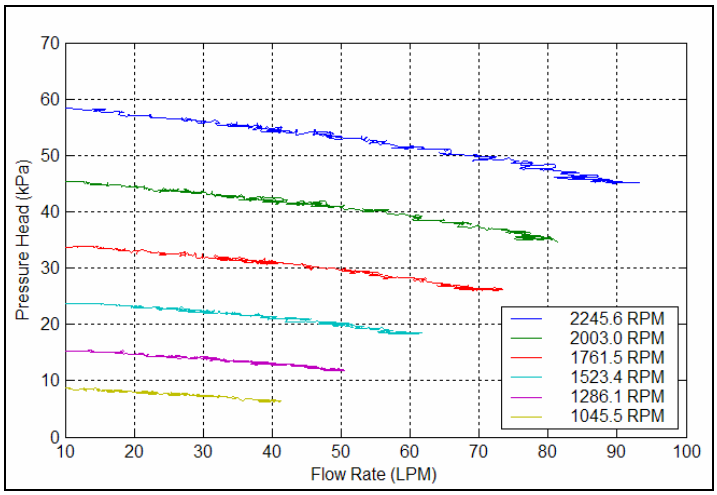

Figure 4.2 Pump characteristics featuring the pressure head versus the flow rate

Valve Characteristics

The development of the valve's empirical model will account for the interaction between the flow rate, pressure head, and valve position by varying the valve's angular position. A three variable mathematical description (e.g., flow rate, differential pressure, and valve positions) yields a surface map for the valve's operating characteristics. Note that the placement of a flow meter in the bypass loop would not be successful due to space limitations causing undeveloped flow measurement where flow sensors generally require fully developed flow for reasonably accurate flow measurement. By placing the flow meter upstream of the valve and blocking off the radiator, the flow in the valve loop can be measured.

A valve map of the empirical data with fitted surface (provided by TableCurve3D) will be introduced to describe the valve's with three input variables; valve position (percent open), pressure head (kPa), and flow rate (LPM) as shown in Figure 4.3. The empirical valve map reveals zero flow rates for zero pressure head and/or a fully closed valve position. The maximum flow in the valve loop occurs at the fully open position and the maximum pressure head. The empirical data of the prototype valve provides a means to fit a surface map in three dimensions. This surface fit equation becomes

$$Q_v = a\theta_{v,\%}{}^{b}\Delta P_v^{c} \tag{4.1}$$

where a= 7.21, b= 0.25 and c=0.54, effectively describe the flow rate attained at a given pressure head, ΔP_v, and valve position, $\theta_{v,\%}$. This equation allows the flow through the bypass to be determined during simulations.

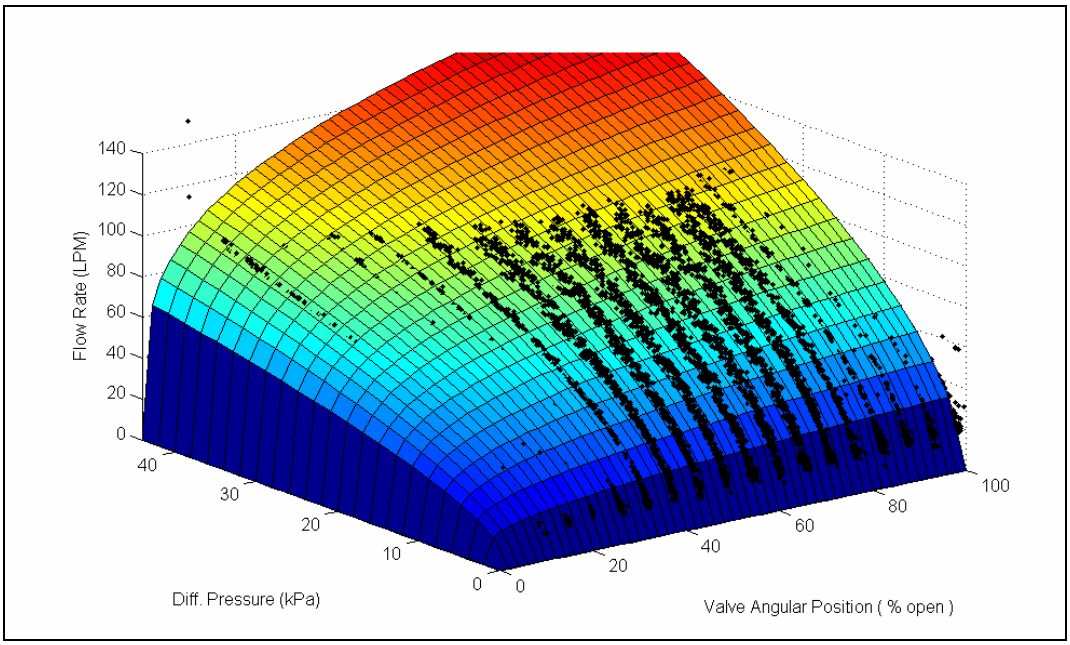

Figure 4.3 Valve map using experimental differential pressure, flow rate, and angular valve position data

Multi-Pipe System

A multi-pipe system empirical model is necessary to quantify the mixing at the junction of the bypass and radiator loops. As shown in Figure 4.4, the multi-pipe system's bypass and radiator loops are parallel and does not show the flow meter, placed upstream, used to determine the bulk coolant flow rate. The differential pressure transducer provides measurement of the pressure head across the multi-pipe system. By way of fluid mechanics applied to the multi-pipe system, where two passages are in parallel, the pressure head in either passage is equal to the pressure drop across the multi-pipe (White, 2003). Thus, the flow rate in either passage can be determined using a pressure measurement and empirical data.

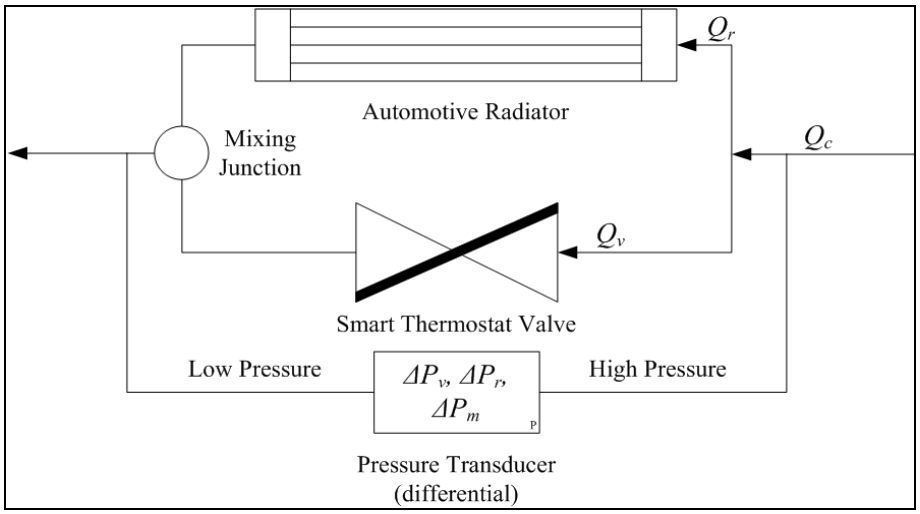

Figure 4.4 Multi-pipe system process diagram

For this system analysis, the pressure drop for the multi-pipe system is equal to the pressure drop in either loop. Further, the multi-pipe pressure drop is determined through a function of the coolant flow rate and the valve position as given by the expression

$$\Delta P_m = \Delta P_v = \Delta P_r, \quad \Delta P_m = f\left(Q_c, \theta_{v,\%}\right) \tag{4.2}$$

The pressure drop and valve position can now be used to determine the radiator and valve loop flow rates as

$$Q_r = f\left(\Delta P_m, \theta_{v,\%} = 0\right), \quad Q_v = f\left(\Delta P_m, \theta_{v,\%}\right) \tag{4.3}$$

The multi-pipe system requires measurement of the pressure head as a function of the flow rate and the valve position. Two test procedures are used to determine the empirical map of the multi-pipe system:

(1) Varied valve position with constant pump speed ($0 \le \theta_v \le 90^o$; $N_p = fixed$).

(2) Varied pump speed with constant valve positions ($0 \le N_p \le N_{max}$; $\theta_v = fixed$).

The testing produced the empirical maps of the multi-pipe system as shown in Figure 4.5. Plotting the data in three dimensions with surface fitting allows the flow rate,

valve position, and pressure head to be displayed where the pressure head is also related to the pump speed. Due to the nature of the modeling effort to be used in both simulations and control architectures, the pump model parameters can be altered to a more convenient form such as pump control voltage or pump speed. The flow rate may be replaced with the pump speed to allow direct control of the pump which is primary in developing the coolant flow and pressure head expressed as

$$\Delta P_m = a\left(\frac{1}{1+\left(\theta_{v,\%}/b\right)^{-c}}\right)\left(\frac{1}{1+\left(N_p/d\right)^{-e}}\right) \tag{4.4}$$

where a=39.3, b= 150.4, c= -1.2, d= 1747.5, and e= 2.1. This empirical expression can be used to obtain the three dimensional surface illustrated in Figure 4.5.

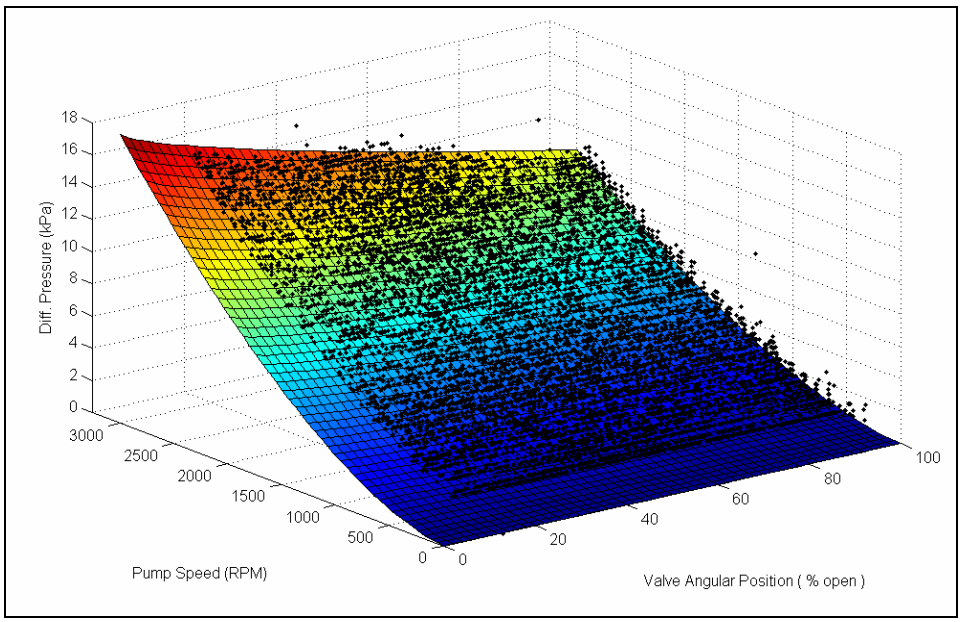

Figure 4.5 Fluid analysis map for the radiator/valve multi-pipe system with differential pressure, pump speed and valve position

Radiator Characteristics

Although many methods exist to experimentally benchmark radiators, the primary purpose of this test is to minimize calculation uncertainty while fully characterizing the radiator's thermal capacity at various fan operating conditions. These methods require the ability to control the fluid flow rate with a pump which can lead to high experimental errors. Also, this test arrangement requires temperature measurement at the fluid's inlet and outlet locations. Fortunately, some of the difficulties in this test arrangement are alleviated through the use of steam as the hot fluid and noting that the phase change of the steam can indicate the heat transfer rate at the radiator, since the radiator heat transfer rate capacity is primarily influenced by the air flow stream. This test protocol reduces the number of variables measured in the experiment and consequently reduces the inherent uncertainty.

Using effectiveness (e.g., the capability of a heat exchanger to dissipate heat) as a measure of radiator performance, a fan control strategy can be developed to dissipate the radiator's thermal energy. The radiator's ability to dissipate energy is largely dependent on the fan's rotational speed (control voltage). Quantifying this relation is integral in defining a control strategy to maintain an accurate engine set point temperature. Managing the fan's parasitic load will be possible using a description of the heat transfer rate for various combinations of fan and pump speeds. The radiator effectiveness factors necessitate an analysis of the thermal energy exchanged in the radiator that is to be implemented in the cooling system. The two points of interest are: (i) the effect of air cross-flow on the actual transfer of energy, and (ii) the maximum transfer of energy. It will be necessary to analyze the air stream cross flow while observing steady-state conditions of the radiator's hot fluid. Specifically, the trends in the relationship between

the fan-speed (air mass flow rate) and the effectiveness of the automotive radiator will be quantified experimentally.

Experimentally, benchmarking the radiator's effectiveness necessitates the measurement of many variables. The test method requires the recording of the air/cold stream inlet temperature and mass flow rate. The hot stream utilizes steam at atmospheric pressure. The measurement of the condensation rate provides the hot stream energy transfer rate (i.e., the amount of saturated steam condensed to saturated liquid represents the amount of energy transfer).

Radiator Experimental Apparatus

The experimental setup (refer to Figure 4.6) collected condensed steam to measure the energy transfer. The setup requires a low pressure steam supply which feeds saturated steam at atmospheric pressure into the radiator. The outlet condition from the radiator is a mixture of liquid and vapor at 100ºC. The amount of liquid exiting the radiator is representative of the heat exchange since the vapor leaving has not changed phase. This outlet liquid flow rate is measured by way of a scale and timer as shown in Figure 4.6. Taking this quantity with the knowledge of the enthalpy of condensation at 100ºC, the experimental energy transfer rate is determined. This experimental energy transfer rate can be compared to coolant by considering the differences in the convection coefficients. Also consider that the air stream has a smaller heat capacity, which can justify the air side having the dominant contribution in the energy transfer process.

Radiator Analysis

The radiator is subjected to forced steam which is reduced to condensate during heat transfer which varies over the fan operating range. The mass flow rate of condensate, $\dot{m}_{fg}$, is measured as the quantity of steam that has changed phase through the process described in Figure 4.6. This flow rate and the enthalpy of condensation, h_{fg}, fully defines the experiment heat transfer rate, $\dot{Q}_r$, as

$$\dot{Q}_r = \dot{m}_{fg} h_{fg} \tag{4.5}$$

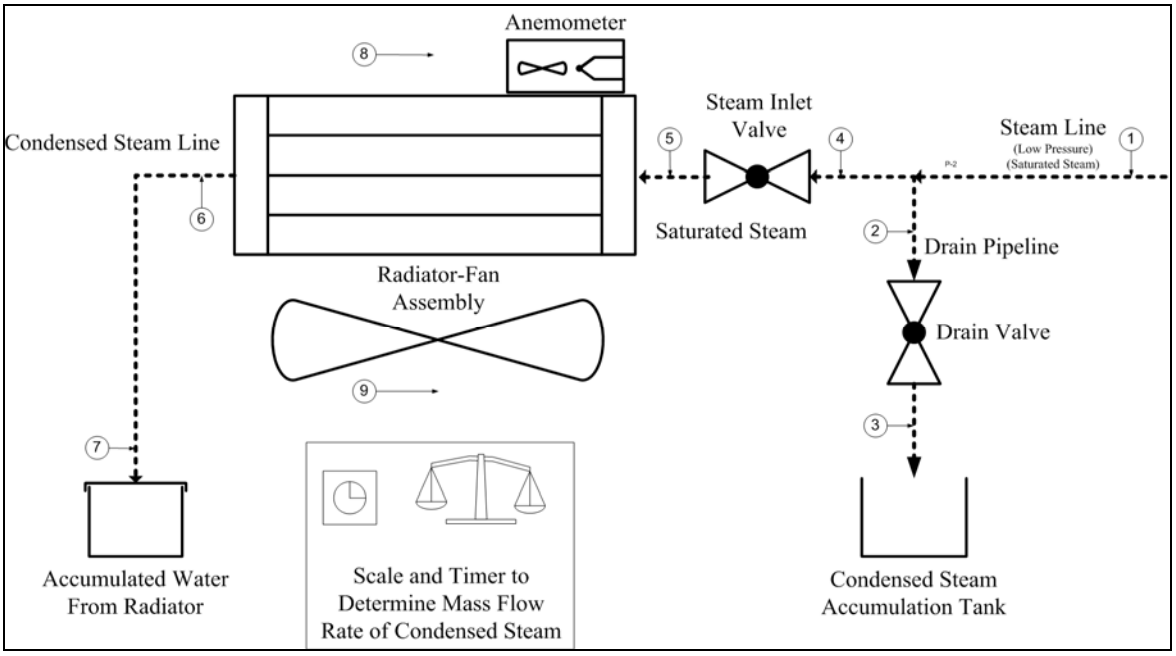

Figure 4.6 Experimental process diagram

In Figure 4.8, the heat transfer rate from the steam to the air stream is displayed for an automotive radiator for a 4.6L V8 and 12V fan (18" diameter) ranging over $850 \leq N_f \leq 1{,}500$ RPM. The information can be used in the development of fan control algorithms which exceed in sophistication over the on/off fan controller operations. It

should be noted that the air stream temperature as well as air stream flow rate influence the maximum heat transfer rate and the actual heat transfer rate.

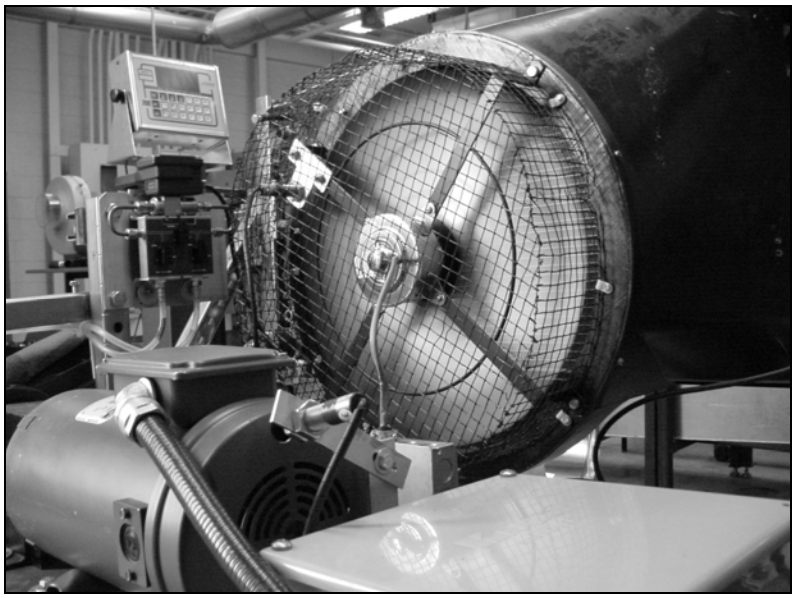

Figure 4.7 Experimental apparatus system photograph

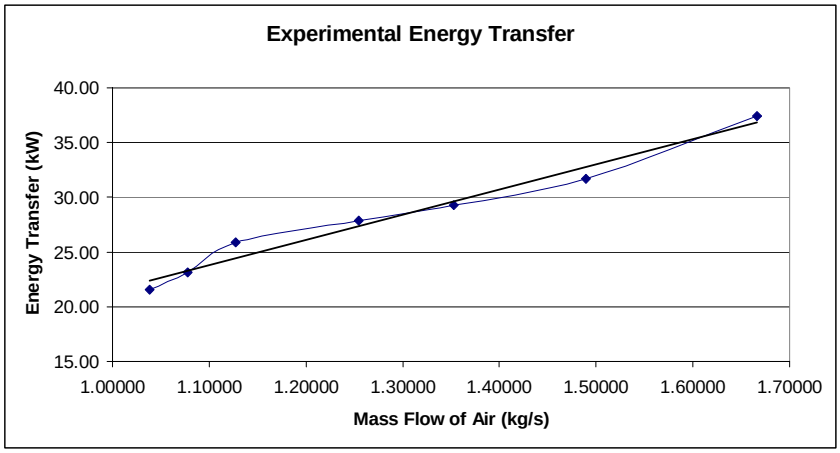

Figure 4.8 Radiator analysis of heat transfer rate

Radiator Air Flow Distribution

The cross flow air stream parameters determine the maximum energy transfer since it typically represents the minimum capacious fluid. The mass flow rate of air across the radiator measured via an anemometer may be placed upstream of the radiator. Analysis of radiator data yields the velocity profiles shown in Figure 4.9 for the fan operating at maximum speed. Using these measurements, the velocity distribution of air across the face is surface plotted with interpolation. The analysis of the flow profile uses area weighted average of the measurements to yield a descriptive air velocity for the radiator.

The small non-uniformity of the flow pattern requires proper placement of the anemometer with an area weighted average velocity of 1.54 (m/s) which is achieved by the fan operating at full speed. The placement will create an average cross flow velocity, V_r, which can serve as assumed uniform velocity when calculating the air flow rate as

$$\dot{m}_a = \rho_a A_r V_r \tag{4.6}$$

According to Incropera and Dewitt (2002), the maximum heat transfer rate, $\dot{Q}_m$, becomes

$$\dot{Q}_m = \dot{m}_X \cdot c_{p,X}\left(T_{h,i} - T_{c,i}\right) = C_{p,m}\left(T_{h,i} - T_{c,i}\right) \tag{4.7}$$

where $T_{h,i}$ and $T_{c,i}$ represent the hot stream and cold stream inlet temperatures, respectively. When analyzing heat exchangers, the important fact is the effectiveness differs from efficiency in mechanical systems. However, in actual vehicles there will be a greater opportunity for non-uniformities in the flow distribution due to front-end module designs that contain a number of auxiliary heat exchangers. The main goal in this section is to experimentally quantify the radiator's effectiveness.

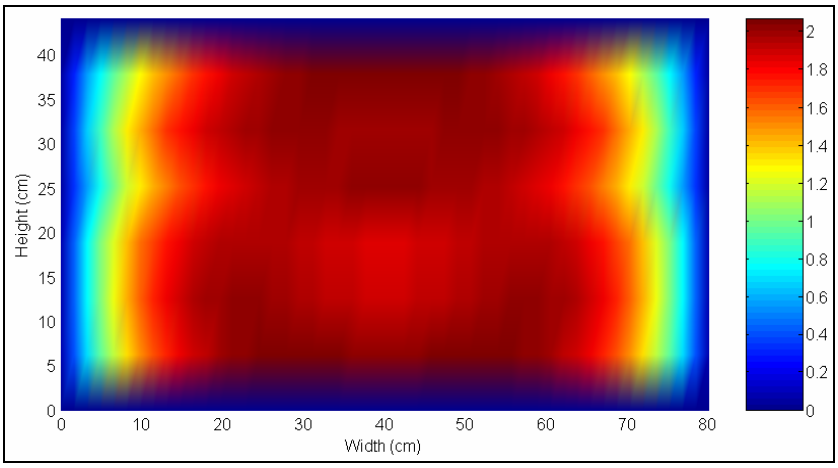

Figure 4.9 Radiator velocity distribution contour plot

Automotive Radiator Effectiveness

The steam condensation rate determines the actual energy transfer, while the air stream flow rate and temperature determine the maximum energy transfer rate. The ratio of these two energy transfers combine to calculate the overall effectiveness of the automotive heat exchanger, ε, as

$$\varepsilon = \dot{Q}_r / \dot{Q}_m = \frac{\dot{m} h_{fg}}{C_{p,m}\left(T_{h,i} - T_{c,i}\right)} \tag{4.8}$$

The relation defined must be corrected as the true hot fluid in automotive application will be a mixture of water and ethylene glycol. In spite of this, this heat exchange rate can provide a viable preliminary estimate since it is a stronger function of the cross flow air conditions in such compact heat exchangers. Realizing the relationship between effectiveness and cool stream conditions will allow the definition of a control strategy and energy conservation algorithm for the DC controlled fan.

In an effort to provide an easy reference for the important data, Table 4.1 summarizes the empirical models that have been developed.

Table 4.1 Empirical model equations

System Component	Empirical Model Equation	Coefficients				
		a	b	c	d	e
Valve	$Q_v = a\theta_{v,\%}{}^b \Delta P_v^c$	7.21	0.25	0.54		
Multi-pipe	$\Delta P_m = a\left(\frac{1}{1+\left(\theta_{v,\%}/b\right)^{-c}}\right)\left(\frac{1}{1+\left(N_p/d\right)^{-e}}\right)$	39.3	150.4	-1.2	1747.5	2.1
Fan Flow	$\dot{m}_a = aV_{fc}$	0.126				
Radiator Experimental Heat Transfer Rate	$\dot{Q}_r = aV_{fc}$	2.75				
Radiator Maximum Heat Transfer Rate	$\dot{Q}_m = aV_{fc}$	9.56				
Fan Power	$P_f = aV_{fc}^2 + bV_{fc}$	0.4682	-0.7306			
Fan Speed	$N_f = aV_{fc}^2 + bV_{fc}$	-1.9036	126.22			
Pump Power	$P_p = aV_{pc}^2 + bV_{pc}$	4.96	-2.19			
Pump Speed	$N_p = aV_{pc}$	287.24				

CHAPTER 5

ANALYTICAL MODELS

A transient thermal response model, applying thermodynamic principles, evaluates the coolant properties and states within the engine cooling system simulation in this chapter. For a complete automotive cooling system thermal evaluation, individual cooling components must be analyzed using an energy balance capable of representing transient operating conditions. The resulting dynamic model will be used to evaluate cooling system performance within a simulated environment. Additionally, this transient model introduces thermodynamic principles to measure energy consumption and temperature regulation performance for various cooling system configurations and control architectures. Overall, tradeoffs often arise in system design and operation that need to be considered using an additional second law analysis (e.g., entropy balance). This procedure permits the deficiencies that exist in these waste heat rejection systems to be quantified.

The analytical modeling of a system's thermal response requires an acceptable level of mathematical detail to represent the physical traits. The goal of this modeling effort is to estimate the thermal characteristics within 5% of the actual system while maintaining the capability of real-time execution. These constraints require simplified empirical models to describe the actuators' capabilities and dynamic behaviors within the automotive cooling system. Overall, this model will assist automotive engineers in their initial system design, controller development, and system performance assessment tasks.

Incompressible Substance Model

The transient analysis of automotive cooling systems can be simplified using an incompressible substance assumption. This incompressible substance is automotive cooling fluid, traditionally an ethylene-glycol and water mixture, and its properties are assumed to be that of water (as shown in Table 5.1).

Table 5.1 Properties of saturated water (Moran and Shapiro, 2000)

Temperature, K	Specific Heat, c_p, kJ/kg-K	Density, ρ, kg/m^3
275	4.211	999.9
300	4.179	996.5
325	4.182	987.1
350	4.195	973.5
375	4.22	956.8
400	4.256	937.4

The assumption that the coolant is incompressible also allows the definition of the constant specific volume and specific heat. Furthermore, the internal energy of the control volume can be defined as a function of the temperature (Moran and Shapiro, 2000)

$$c_v(T) = \frac{\partial u}{\partial T} \tag{5.1}$$

This assumption has some implications on the calculation of the enthalpy that varies with both the temperature and pressure as

$$h(T, p) = u(T) + pv \tag{5.2}$$

The derivative of equation (5.2) at pressure constant, the specific heats are equal

$$c = c_p = c_v \tag{5.3}$$

The system model utilizes this simplification to facilitate the evaluation of water states during transient simulations by selecting appropriate property values from Table 5.1. Some of the interesting thermodynamic states include the internal energy, enthalpy, and entropy that can be written as

$$u_2 - u_1 = \int_{T_1}^{T_2} c(T)dT = c(T_2 - T_1) \tag{5.4}$$

$$h_2 - h_1 = \int_{T_1}^{T_2} c(T)dT + v(p_2 - p_1) = (u_2 - u_1) + v(p_2 - p_1) \tag{5.5}$$

$$s_2 - s_1 = \int_{T_1}^{T_2} \frac{c(T)}{T}dT = c\ln\frac{T_2}{T_1} \tag{5.6}$$

The thermodynamic properties calculated with only temperature enable the development of energy balance equations to be evaluated by differential equation solvers. These equations must account for external energy transfer, (i.e., heat and work), and energy flux transport, (i.e., energy accompanying mass transfer) across control volume boundaries to characterize the transient thermal response in a simulated environment. Also, the energy contained within a control volume during transient system operation must be evaluated. Moran and Shapiro (2000) report that the energy balance equation for a control volume is

$$\underset{(1)}{\frac{\partial E_{cv}}{\partial t}} = \underset{(2)}{\dot{Q}_{cv}} - \underset{(3)}{\dot{W}_{cv}} + \underset{(4)}{\dot{m}_i\left(h_i + \frac{V_i^2}{2} + gz_i\right)} - \underset{(5)}{\dot{m}_e\left(h_e + \frac{V_e^2}{2} + gz_e\right)} \tag{5.7}$$

Accounting for the time rate in change of energy contained within a control volume, (1), is provided by external energy transfers with the environment in the form of positive heat addition, (2), and negative work extracted, (3). It is also necessary to account for the fluid states and the flow rates into, (4), and exiting (5) the control volume boundary.

To begin the model development process, the conservation of mass and mass rate must be justified. For each control volume, the conservation of mass can be stated as

$$\frac{\partial}{\partial t}\int_{\forall} \rho d\forall = \sum_i \left(\int_A \rho V_n dA\right)_i - \sum_e \left(\int_A \rho V_n dA\right)_e \tag{5.8}$$

where ρV_n is the mass flux per unit area (Moran and Shapiro, 2000). This statement of conservation of mass, where mass is not allowed to accumulate within a control volume or leak from a control volume, may be presented as

$$\sum_i \left(\int_A \rho V_n dA\right)_i = \sum_e \left(\int_A \rho V_n dA\right)_e \tag{5.9}$$

Next, if the flow is steady, one dimensional, uniform with position, and normal to the control volume surface, then the mass flow across a control volume becomes

$$\dot{m} = \int_A \rho V_n dA \tag{5.10}$$

This may be further justified when the control volume boundaries in the system are rigid. In addition, the rigid control volume boundaries provide negligible leakage, expansion, or contraction which permits the integral

$$m_{cv} = \int_{\forall} \rho d\forall \tag{5.11}$$

to yield a constant amount of mass.

The energy contained within a control volume is developed in its time rate form as

$$\frac{\partial E_{cv}}{\partial t} = \frac{\partial}{\partial t}\int_{\forall} \rho\left(u + \frac{V^2}{2} + gz\right) d\forall \tag{5.12}$$

where u is the internal energy, V is the velocity, g is the gravitational constant, ρ is the fluid density, and z is the height of the control volume (Moran and Shapiro, 2000).

Because, the velocity of the cooling system with respect to the car body will be zero, the kinetic energy of each control volume is neglected. The potential energy has negligible influence in the thermal system and hydraulic models, since there are small height differences concerning components within the cooling system relative to the car body. Also, utilizing a fixed control volume mass, equation (5.12) may be expressed as

$$\frac{\partial E_{cv}}{\partial t} = m_{cv}\frac{\partial u}{\partial T}\frac{\partial T}{\partial t} = m_{cv}c\frac{\partial T}{\partial t} \tag{5.13}$$

In this expression, the mass, m_{cv}, is defined in equation (5.11) which is calculated from the amount of coolant stored in a given control volume and the constant specific heat, c, as defined in equation (5.4) with the time rate of temperature change. A change in temperature develops as heat transfer occurs with the surroundings and energy transfers across the control volume boundary. Equation (5.13) represents the dynamic description of the control volume energy and introduces the thermal lag behavior.

The system elements that reveal a large thermal lag, due to coolant volume and metals, are the radiator and the engine block. Other coolant system elements such as piping for fluid routing reveal small temperature lags. In previous studies, these elements have been lumped into appropriate neighboring nodes to reduce the system equations for model based control applications (Wagner *et al.*, 2003, Setlur *et al.*, 2003). The proposed model includes these pipe elements, and related equations, to provide a sufficient description of the system transient behavior.

Thermal Model

The various control volumes within the thermal model of a typical automotive coolant system are illustrated in Figure 5.1. Some important elements to consider are the engine and radiator which account for the high temperature heat addition to the system

and the low temperature heat rejection from the system, respectively. At steady state, the pipe elements account for the small temperature drop due to the secondary heat transfer from the pipes to the environment via convection and radiation. The junction element reveals the effect of the thermostat on the temperature response. In previous modeling efforts, the junction control volume has been considered as a mass flow rate weighted average of the dissimilar coolant stream temperatures (Setlur *et al.*, 2005). To reveal the dynamic response of an automotive cooling system, these elements have been analyzed with a thermodynamic energy balance.

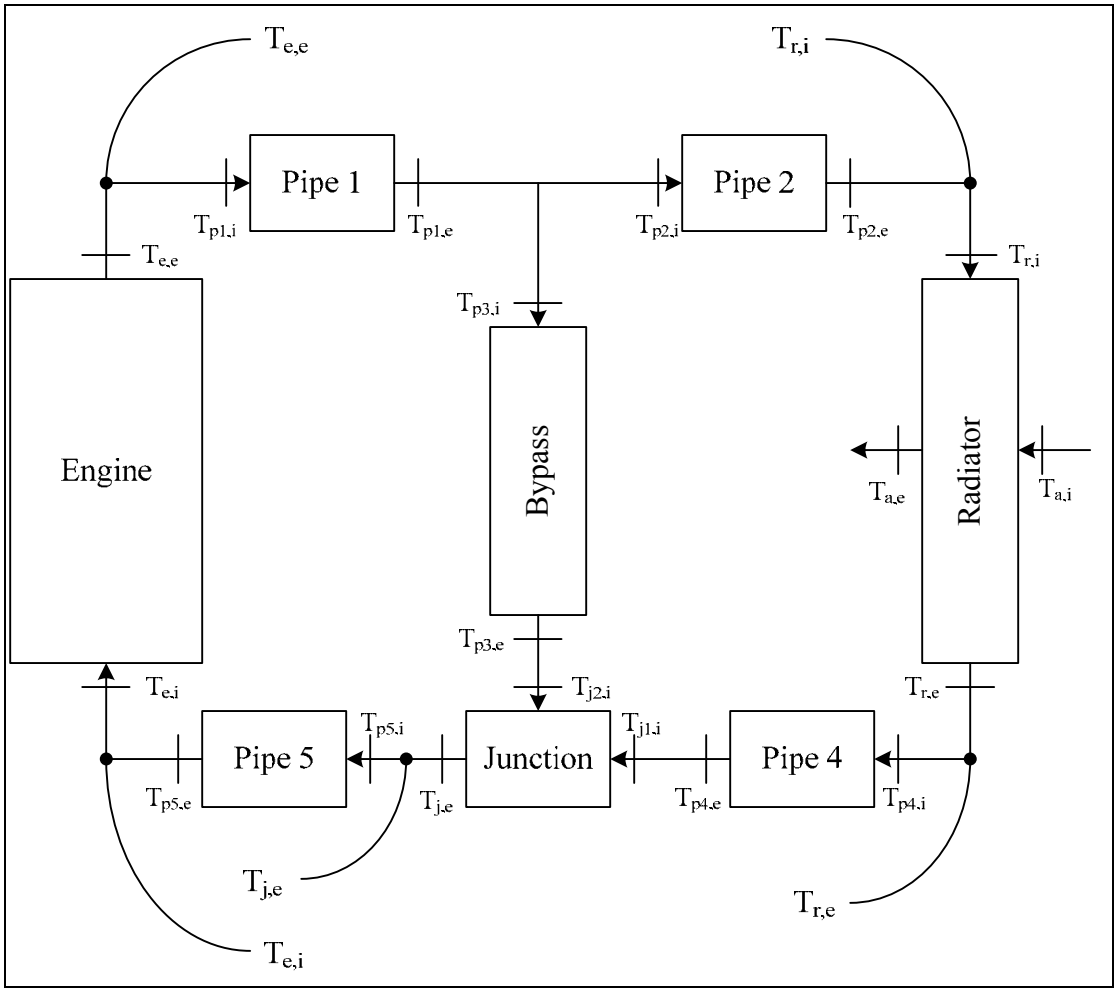

Figure 5.1 Dynamic model control volumes – thermal

Hydraulic Model

Hydraulic (pressure drop) evaluations are employed to account for the flow work and the losses due to fluid friction. Previous studies have modeled the distributed pressure drops in a lumped throttling device (Li and Figliola, 2004). Alternatively, the proposed model accounts for the distributed flow work in a rigorous assessment of the system design and operation. This approach will facilitate an exergy account on a component-by-component basis which provides insight into overall system performance. As illustrated in Figure 5.2, these distributed pressure drops are due to the coolant flow at the engine, ΔP_e, in the bypass, ΔP_b, and at the radiator, ΔP_r. For simplicity, individual pipe element pressure drops were comparably less significant and, consequently, were neglected. The pump supplies the pressure head to overcome these friction losses by ΔP_p.

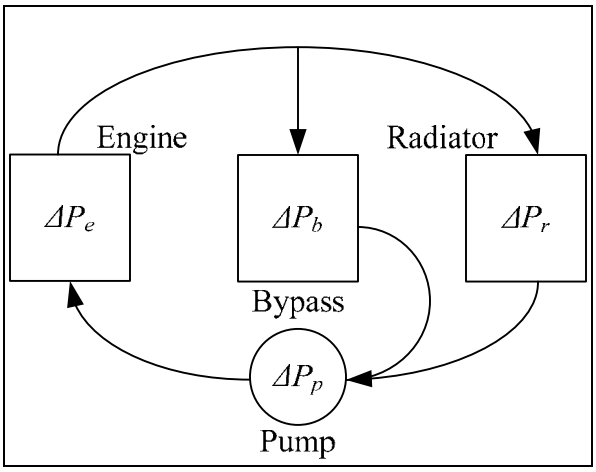

Figure 5.2 Pressure model with distributed fluid dynamic blocks

System Control Volumes

Each system control volume in Figure 5.1 is modeled according to the incompressible substance assumption. Next, the control volumes are combined for an accurate and descriptive system representation. The energy balances and assumptions are applied to each system control volume (i.e., engine, bypass, and radiator). Furthermore, individual pipe segments are included in the thermal response to account for the time lag represented in the energy flux accompanying mass flow between system elements.

Radiator Energy Balance

The radiator energy balance relies on an experimental description of the radiator effectiveness which, through experimentation, was shown to be constant (refer to Chapter 4). The hot and cold streams interaction with the radiator control volume is shown in Figure 5.3. For heat transfer between the coolant and air streams, the convective heat transfer coefficients are a function of the coolant and air flow rates. Additionally, a tradeoff exists between the air and coolant side flow rates and heat transfer coefficients. This tradeoff is exposed in the exergy accounting (i.e., entropy generation minimization). The radiator energy balance equation can be expressed as

$$m_r c_c \left(\frac{\partial T_{r,e}}{\partial t} \right) = -\dot{m}_r c_c \left(T_{r,i} - T_{r,e} \right) - \varepsilon \dot{m}_a c_a \left(T_{r,i} - T_{a,i} \right) \tag{5.14}$$

and on the air side, the energy transfer must be conserved so that

$$\dot{m}_r c_c (T_{r,i} - T_{r,e}) = \dot{m}_a c_a (T_{a,e} - T_{a,i}) \tag{5.15}$$

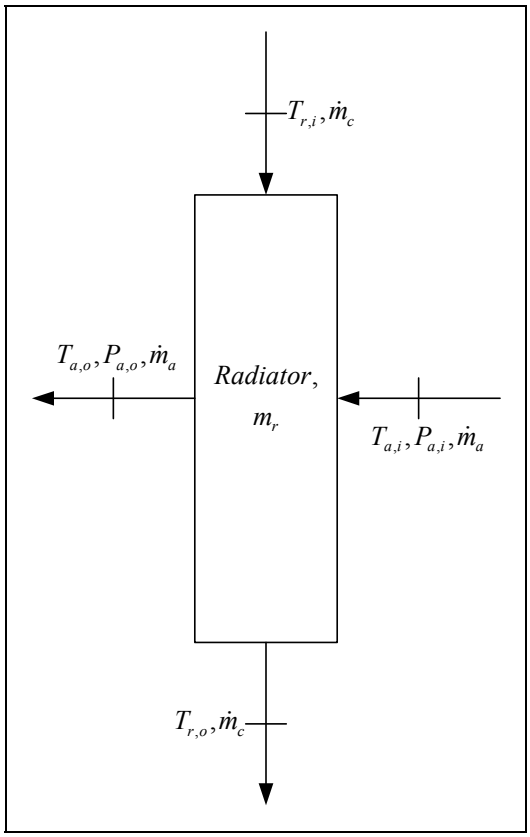

Figure 5.3 Radiator control volume

Junction Energy Balance

The cooling junction is an important component in the thermal system which mixes two fluid streams based on the interactions of the valve flow control and the radiator heat dissipation. At steady state, the junction outlet temperature can be modeled as a mass flow rate weighted average of the two inlet stream temperatures (Setlur *et al.*, 2005). However, the proposed model considers the time lag response associated with the coolant contained within the junction, m_j, which is illustrated in Figure 5.4. The junction element may be thermally described as

$$m_j c_c \left(\frac{\partial T_{j,e}}{\partial t} \right) = -\dot{m}_c c_c T_{j,e} + \dot{m}_r c_c T_{j1,i} + \dot{m}_b c_c T_{j2,i} \tag{5.16}$$

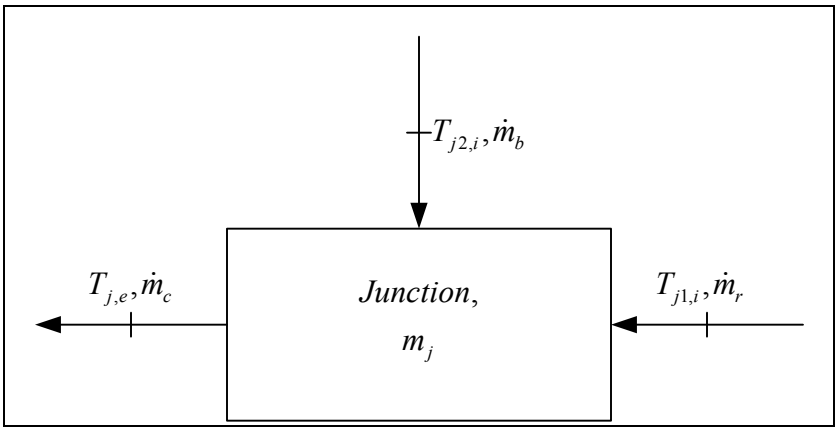

Figure 5.4 Junction control volume

Engine Energy Balance

The next control volume quantifies the waste heat transfer rate associated with the internal combustion engine's output power. Sophisticated models for the combustion process heat release require the measurement of the fuel consumption rates and instantaneous cylinder pressures (Freidrich, 2006, Zeng, 2004, Chmela, 1999). In the automobile the heat released by the combustion process produces crankshaft work and requires heat rejection to the environment. Under optimal engine operating conditions, the engine operates at an efficiency of approximately 30%, an equal portion (30%) of the heat released leaves with coolant where the remaining, 40%, exits in the exhaust stream. However, operating the engine at partial load, more thermal energy is rejected to the coolant than mechanical energy at the crankshaft (Kays, 1989). This proposed model should employ a simplified, empirically determined thermal load estimate based on the engine's operation, load and power. In Figure 5.5, the energy flux into and out of the engine water jacket is shown and thermodynamic energy balance can be expressed as

$$m_e c_c \left(\frac{\partial T_{e,e}}{\partial t} \right) = -\dot{m}_c c_c T_{e,e} + \dot{m}_c c_c T_{e,i} + \dot{Q}_e \tag{5.17}$$

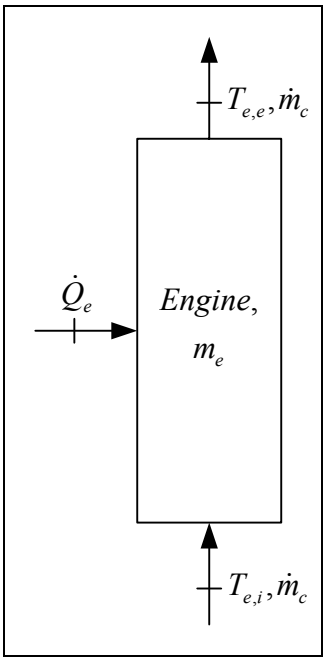

Figure 5.5 Engine control volume

Pipe Energy Balance

The energy balance on the pipe segments will account for uncontrolled heat loss through the pipe walls resulting in small temperature gradients. During transient conditions, the addition of pipe control volumes and associated energy balance create a more accurate system response by accounting for the thermal time lags. A pipe segment energy balance assumes that some of the heat transfer occurs due to effects such as free convection and radiation which are constant and a function of the exposed pipe area to ambient air (refer to Figure 5.6). The differential equation for the pipe segment temperature becomes

$$m_{pk} c_c \left(\frac{\partial T_{pk,e}}{\partial t} \right) = \dot{m}_{pk} c_c \left(T_{pk,e} - T_{pk,i} \right) - \dot{Q}_{pk} \qquad \left(k = 1 \ldots N \right) \tag{5.18}$$

where N represents the number of pipes within the system. The number of pipe sections to be simulated is at the discretion of the modeling needs.

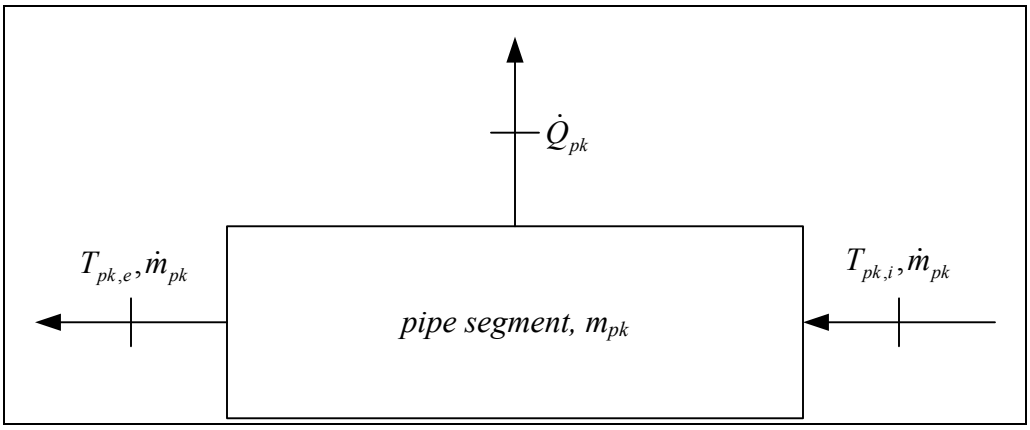

Figure 5.6 Pipe segment control volume

Exergy Audit – Entropy Generation

The system performance can be evaluated with increasing scrutiny utilizing information determined in the thermal response model. Specifically, the level of optimum performance realized by a given system design and control architectures can be analyzed. Automotive cooling systems can be designed to meet cooling requirements while minimizing entropy generation. During the vehicle's operation, a variety of conditions are imposed by the engine and the environment that demand flexible systems which offer cooling controllability while maintaining efficient system operation. The equations developed in this Chapter account for the entropy generation which offers a measure of optimum system performance. Shinskey (1978) utilized these principles to define guidelines for controller designs which enhance system function. This analysis is advantageous since it accounts for the effective use of energy by revealing performance trade-offs that a first law analysis cannot evaluate.

Past researchers have concluded that processes which utilize energy wastefully impart large losses and should be avoided (e.g., Shinskey, 1978). Automotive thermal management systems utilize fluid mixing which cause system losses. However, the heat

energy could be utilized for another process since it contains some available energy (Goldstick, 1943). For instance, the automobile cabin temperature control can utilize this waste heat by circulating engine coolant to a heat exchanger capable of warming the cabin air through the heater core. Unfortunately, extracting more useful work from this waste heat is not feasible due to its low intensity and must be dissipated in an effective manner. However, there are challenges to increase the efficiency and feasibility of thermo-electric generation devices which could convert this heat energy into electrical energy. Any heat engine operating between the coolant and ambient temperature reservoirs can reach a thermal efficiency of only 20%, as represented by the Carnot efficiency (Moran and Shapiro, 2000). The goal of the following analysis is to realize the most efficient method to dissipate the coolant's thermal energy to the environment using the least amount of energy. The use of exergy destruction minimization, also stated as entropy generation minimization, can be used to achieve more efficient system performance by controlling the actuators at the radiator fan, thermostat valve, and coolant pump.

This exergy accounting provides the backbone for achieving improved second law system performance (Li and Figliola, 2004, Figliola and Tipton, 2000, Bejan, 1996, Bejan, 1982). This second law performance evaluation is greatly influenced by the control strategies employed in maintaining system function and efficiency (Shinskey, 1978). By implementing control strategies that perform real-time measures of the entropy generation rates, much more effective system operation can be realized which can further improve automotive cooling systems.

Bypass Exergy Account

The bypass loop in the automotive cooling system is used to maintain the coolant temperature inside the engine block. When the coolant temperature increases, the thermostat valve routes fluid to the radiator where it is cooled thereby influencing the mixing of fluids to maintain engine temperature. However, the improved modulation of the bulk coolant flow rate (i.e., thermostat valve and pump control) will reduce the amount of energy wasted by mixing the radiator and engine temperature fluids. Therefore, exergy destruction equations must be developed so that both the flow related losses and the fluid mixing are considered. The flow work component in the entropy account is, as suggested by White (2003), expressed as

$$\dot{f}_{loss,j} = \dot{m}_b v_c \Delta P_m \tag{5.19}$$

where the pressure drop, ΔP_m is due to fluid friction, and the mass flow rate and specific volume are $\dot{m}_b$, v_c , respectively. Furthermore, the collective entropy generation relation for the junction element, as suggested by Bejan (1996), becomes

$$\dot{S}_{gen,j} = \dot{m}_b c_c \ln \frac{T_{j,e}}{T_{j2,i}} + \dot{m}_r c_c \ln \frac{T_{j,e}}{T_{j1,i}} - \frac{\dot{f}_{loss,j}}{T_{j,e}} \tag{5.20}$$

The reader may refer to Figure 5.4 for an illustration of the location of the states in equation (5.20). The first term in the equation is the entropy generated due to the coolant flow from the bypass and, similarly, the second term is due to flow coming from the radiator and the third term is lost work due to friction in flow passages. These terms account for the entropy generation from the mixing process. By utilizing equation (5.20), a function can be developed to minimize the entropy generation at the junction by utilizing these equations and imposing flow control to reduce the pressure drop and

mixing. Experimental based models in Chapter 4 provide the information necessary to determine the distributed pressure loss terms in the cooling system including.

Radiator Exergy Account

The use of the entropy generation minimization concept at the radiator allows development of a minimization function that is constrained by the energy dissipation required to maintain engine temperature. An exergy audit for the radiator provides the information necessary to determine the tradeoff between the air coolant flow rates. As suggested in literature (Bejan, 1996), accounting for the friction losses and generation of entropy on both the air and coolant streams results in the relationship

$$\dot{f}_{loss,r} = \dot{m}_a R \ln\left(\frac{P_{a,e}}{P_{a,i}}\right) + \dot{m}_r v_c \Delta P_{r,c} \tag{5.21}$$

$$\dot{S}_{gen,r} = \dot{m}_a c_a \ln\left(\frac{T_{a,e}}{T_{a,i}}\right) + \dot{m}_r c_c \ln\left(\frac{T_{r,e}}{T_{r,i}}\right) - \frac{\dot{f}_{loss,r}}{T_{a,i}} \tag{5.22}$$

Equation (5.21) breaks the friction loss term into two components where the first term is the friction loss on the air side, based on an ideal gas model for the ambient air (Moran and Shapiro, 2000). Additionally, the second term in equation (5.21) is the coolant side pressure drop caused by the fluid friction in the radiator tubes which can be calculated by way of empirical or theoretical models. The first term in equation (5.22) accounts for the entropy generation due to the temperature gradient on the air side of the radiator. The second term accounts for the coolant side losses. Friction loss is accounted in the third term of equation (5.22). At the radiator, there exists an optimum operating point between the two fluids flow rates. Bejan (1996) suggests that balancing the heat capacitance of the two streams will reduce the entropy generated.

Engine Entropy Account

In the engine cooling system, entropy generation minimization is only effected by the temperature at which the waste heat is rejected. Increasing this temperature will inevitably reduce the entropy generation from a thermal perspective. However, material constraints, coolant boiling curve, and engine combustion environment limit the amount by which this temperature can be increased. Generally, the coolant flow through the engine can be reduced to lower the effect of fluid friction within the water jacket thereby reducing losses at the engine. For improved exergetic efficiency, the extracted energy from the engine will be maximized while reducing the parasitic operating cost of the cooling system. The frictional pressure loss term associated with the engine water jacket can be influenced by the coolant flow rate as

$$\dot{f}_{loss,e} = \dot{m}_c v_c \Delta P_e \tag{5.23}$$

The total entropy generated at the engine is the sum of the heat transfer, as suggested by Moran and Shapiro (2000), and the friction loss term so that

$$\dot{S}_{gen,e} = \left(1 - \frac{T_{e,i}}{T_{cc}}\right)\frac{\dot{Q}_e}{T_{e,i}} - \frac{\dot{f}_{loss,e}}{T_{e,i}} \tag{5.24}$$

The first term in equation (5.24) is based on an expression for the amount of exergy destroyed with the transfer of heat from the combustion environment to the coolant. The reader should refer to Figure 5.5 for an illustration of the temperature locations. The second term of this equation is the friction loss due to fluid flowing in the engine water jacket.

Pump Exergy Account

At the pump, some power is lost due to conversion inefficiencies between the electrical and fluid domains. For all pumps, there exists an optimum point that minimizes the amount of wasted energy which is influenced by impeller design. To comply with a rigorous exergy account, the pumping loss is included as the amount of pumping power lost due to electrical, mechanical, and hydraulic factors. The pump inefficiency based entropy generation term, as suggested by Li and Figliola (2004), is written as

$$\dot{S}_{gen,p} = \frac{(1-\eta)\dot{w}_p}{T_e} \tag{5.25}$$

This term is developed by accounting for the work rate being put into the pump, $\dot{w}_p$, and the efficiency of the drive mechanism, η. The efficiency term accounts for electrical to mechanical inefficiencies, η_{e-m}, (e.g., heat generated, bearing friction), and mechanical to fluid inefficiencies, η_{m-h}, (e.g., fluid friction and impeller-body clearances) and can be expressed as

$$\eta = \eta_{e-m} \cdot \eta_{m-h} \tag{5.26}$$

These efficiencies are illustrated in Figure 5.7.

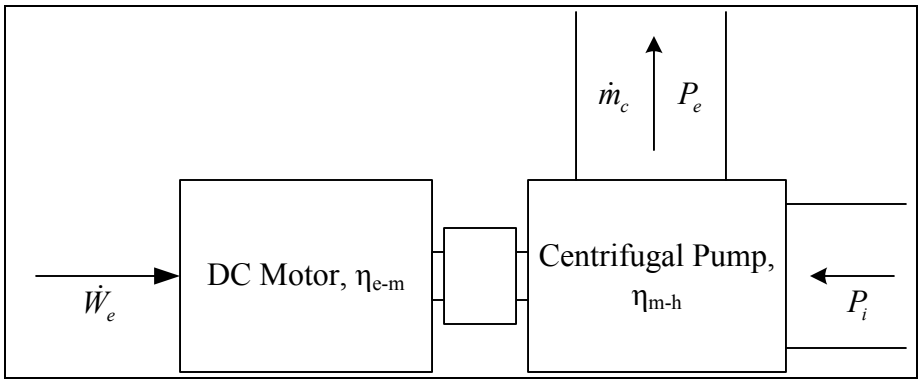

Figure 5.7 Flow of energy at pump

CHAPTER 6

EXPERIMENTAL – 4.6 LITER ENGINE TESTING

Automotive cooling system configurations can integrate different system components and control strategies to provide improvements to engine temperature modulation. This chapter presents the engine test configurations, control strategies, test parameters, and performance evaluation for various cooling system scenarios. In the first section, the cooling system configuration details are discussed. Next, the control strategy applied to these actuators will be explored as well as the available control feedback variables. In the third section, the test routine for each configuration will be presented. The on-engine implementation and available sensor discussion are presented in the fourth and fifth sections, respectively. Next, two separate tables (Table 6.3 & 6.4) are provided with details related to the system evaluation: (i) initial temperature tracking, (ii) disturbance rejection, (iii) power consumption, and (iv) actuator response evaluations.

Experimental time histories are included in Appendix F where Test 4 is presented in Figures 6.15 through 6.18. Some key elements selected from all tests are presented in the final section which discusses the observations revealed through the engine testing. These observations provide important cooling system function considerations and challenges for future cooling system configurations and controller designs. This chapter will conclude with a description of the most effective cooling system configuration and most harmonious controller architecture.

Cooling System Configurations

From an initial perspective, the cooling system utilizes a water jacket in the engine metal casting surrounding the combustion chamber to maintain its environment by controlling the coolant temperature. Coolant flow is provided by a water pump driving coolant through the water jacket and the radiator. The thermal energy is released to the coolant and then transferred through the convection and radiation heat transfer at the radiator to the ambient air and engine bay environment. Unfortunately, traditional cooling systems lack active control of the coolant flow and radiator air flow with belt driven components such as the fan and pump. This results in a system that will not accurately control the coolant temperature in the water jacket. To reduce the passive nature and inaccurate temperature control, electric actuators are implemented such as an electrically controlled thermostat, fan and pump.

The goal of the engine testing is to determine the benefits of active cooling systems. The configurations implement different active cooling system elements. The first configuration integrates an electric fan where the belt driven pump and wax thermostat provide the coolant flow modulation. The first control strategy implemented is based on typical crank driven fan function where the control voltage is based on the engine speed. Further testing of this configuration utilizes a proportional plus integral fan controller. The next configuration implements an electric thermostat valve in addition to the fan using two PI controllers on both the fan and valve. An additional control strategy based on efficient radiator function determines the fan control based on the cooling system fluid flow conditions. The testing continues with the implementation of an external DC motor driven pump. This pump control is determined based on the valve PI controller. The pump speed increases from its base speed once the valve is fully

saturated at its open position. The first test in this configuration utilizes the PI control structure on the fan. Next, the balanced fan control strategy is tested with the pump control as well. In total, there are three basic cooling system configurations, each adding an additional level of engine temperature and cooling system functional control. These configurations are controlled based on a typical system operation, linear control theory, and optimal thermodynamic behavior. Table 6.1 illustrates the configuration and controller combinations explored in this research.

Table 6.1 Control strategy and configuration test matrix

Test	Configuration	Component	Actuation	Controller
1	Factory Fan Operation	Fan	DC motor	Crankshaft
		Valve	Wax-based Element	Proportional
		Pump	Engine Speed	Crankshaft
2	Controlled Fan Operation	Fan	DC motor	PI (K_p=1.013, K_i=0.049)
		Valve	Wax-based Element	Proportional
		Pump	Engine Speed	Crankshaft
3	Controlled Valve w/ Controlled Fan Operation	Fan	DC motor	PI (K_p=1.013, K_i=0.049)
		Valve	DC motor	PI (K_p=0.135, K_i=0.005)
		Pump	Engine Speed	Crankshaft
4	Controlled Valve w/ Balanced Fan Operation	Fan	DC motor	Balanced
		Valve	DC motor	PI (K_p=0.135, K_i=0.005)
		Pump	Engine Speed	Crankshaft
5	Controlled Pump & Valve w/ Controlled Fan Operation	Fan	DC motor	PI (K_p=1.013, K_i=0.049)
		Valve	DC motor	PI (K_p=0.135, K_i=0.005)
		Pump	DC motor	Cascade (K_p=2.5)
6	Controlled Pump & Valve w/ Balanced Fan Operation	Fan	DC motor	Balanced
		Valve	DC motor	PI (K_p=0.135, K_i=0.005)
		Pump	DC motor	Cascade (K_p=2.5)

DC Actuated Fan

In traditional systems, the fan is driven by the crankshaft, a viscous clutch and, is sometimes, actuated with a bimetallic strip. However, the fan speed is primarily based on crankshaft speed which yields heat rejection at the radiator that is not directly controlled on an intelligent basis. As illustrated in Figure 6.1, a belt-driven pump and wax-based thermostat emulates the factory configuration and will be used to provide experimental data for baseline performance of the factory configured cooling system (Test 1). The fan will simply be operated in a manner that is directly related to the engine crank shaft speed; typical to factory radiator fan operation. With the fan operating through a DC motor drive, other more sophisticated control strategies are evaluated to control the heat transfer rate at the radiator through the use of a controller based on linear control theory, such as a PI controller (Test 2).

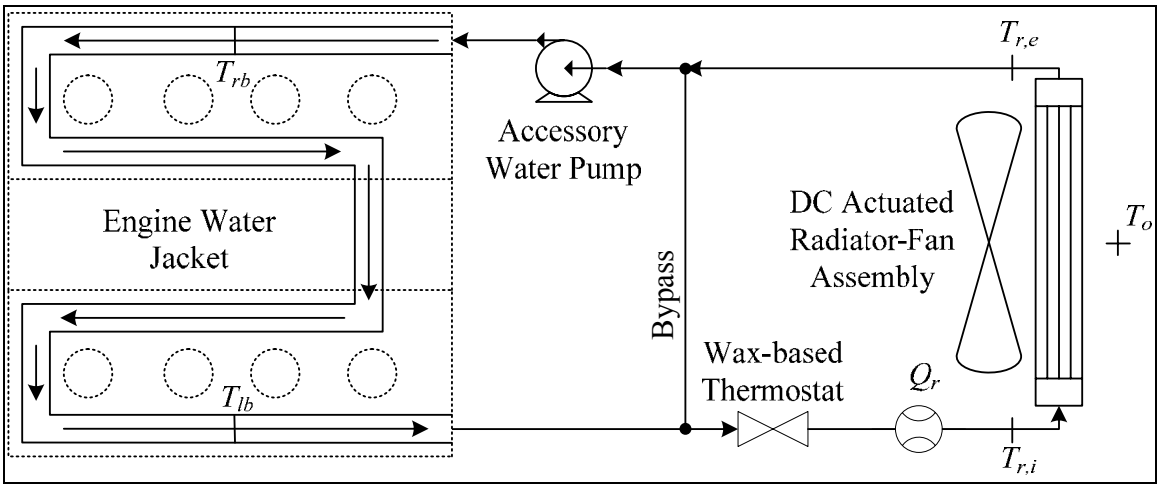

Figure 6.1 Engine testing configuration 1– baseline layout and fan control

DC Actuated Fan and Smart Valve

Thermostats control the engine temperature by routing coolant flow through various system passages (e.g. bypass or radiator loop). For instance, flow is routed through the radiator during cooling scenarios and through the bypass during warm-up. In traditional systems, the wax element actuates the thermostat valve when the coolant temperature reaches a certain magnitude typically 90ºC. Inherent in thermostats and traditional cooling systems is proportional control action which results in the system temperature variance for different operating conditions. Improved actuation of the thermostat is investigated with this configuration by implementing a PI controller on the thermostat valve (Test 3). This configuration utilizes a blank engine thermostat housing which allows the use of an on-engine bypass loop that provides a coolant flow route during all operating conditions.

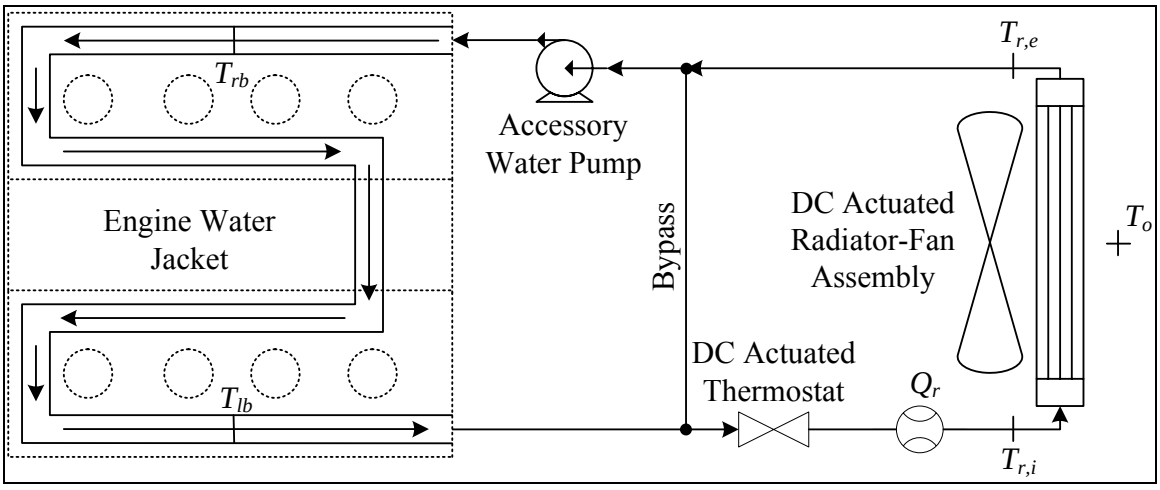

Figure 6.2 Engine testing configuration 2–
smart thermostat and variable speed fan

DC Actuated Fan, Smart Valve, and Pump

The third configuration integrates a controlled coolant pump which allows the coolant flow rate to be adjusted. Since the engine speed is only partially indicative of the heat load, this addition will allow the coolant flow rate to more accurately meet the system's cooling needs. This type of system, where the coolant flow rate is controlled, provides the ability to quantify the benefits of decoupling the pump from the engine speed. This system architecture, illustrated in Figure 6.3, represents the complete computer controlled architecture of the cooling system and will be evaluated with different control strategies based on classical control theory and thermodynamic optimization.

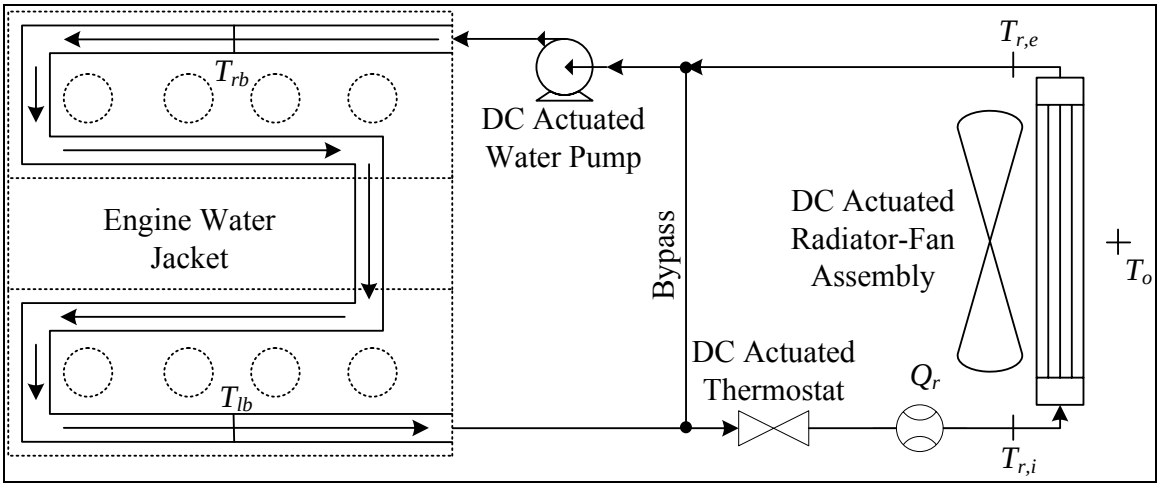

Figure 6.3 Engine testing configuration 3– fan, smart valve, and variable speed pump

Control System Architectures

Engine cooling system architectures, integrated with electrically actuated devices, have the ability to improve cooling control for increased system performance. This trend is driven by technological improvements in actuators and sensors with real time computer control in automotive environments. This work explored the improvements that such an electronically integrated system can provide to the engine cooling system. The control systems were classical control algorithms which are consistently defined throughout testing. This trait focused attention on the configuration aspect of the engine cooling system and its actuators. Also, thermodynamic principles are considered for energy conservation and exergy destruction minimization which provide greater thermal energy dissipation with minimum actuator power consumption.

Fan Control Structure

Implementing a servo-motor, controlled viscous drive (Bhat *et al.*, 2006), or hydraulic motor drive (Frick *et al.*, 2006) for controlled fan speed requires a control algorithm to improve operation over the traditional fan drive system. The fan control effort can be defined by classical control concepts. The controller, proportional and integral gain, was tuned with knowledge of the slow response of the thermal system and PI tuning rules (O'Dwyer, 2003). The error signal is developed as

$$e = T_e - T_{sp} \tag{6.1}$$

with the PI controller defined as

$$U = K_p e + \int K_i e dt \tag{6.2}$$

Another example of fan control is based on entropy generation minimization principles applied to the radiator function. The entropy analysis was conducted by Bejan (1996) and concluded that heat exchanger should be operated in a balanced manner. For

example, this entropy generation minimization principle is utilized for fan control where the fan speed based on coolant flow rate so that the capacities of the two fluids are balanced so that

$$\dot{m}_c c_c = \dot{m}_a c_a \tag{6.3}$$

The fan operation will be described as flow balance control and represents the concepts from a second law thermodynamic analysis as applied to the cooling system's radiator operation. To successfully implement this control method, a reliable measure of the radiator's coolant flow is required. This feedback can be from either a coolant flow measurement via flow metering or empirical modeling. The later requires that the controller monitors the pump speed and valve position.

Smart Valve Control Structure

In the traditional cooling system where the radiator flow rate is controlled by the wax-based thermostat. The valve opening area, A_t, is dependent solely on the coolant temperature as prescribed by Equation 6.4. This passive, wax element is problematic in its implementation for strict temperature control since the valve cannot account for operating condition variances. This can be revealed in the fact that the valve will not accurately prescribe flow rate during all conditions to maintain 90ºC. Also, air flow rates at the radiator are subject to large fluctuations due to changes in vehicle speed. This ram-air effect can be noticed in the reduced need for fan induced air flow as the ram-air sufficiently provides heat rejection. Valve control should be defined by prescribing a temperature set point with a temperature feedback location within the system boundary and a PI control structure to specify valve position (Equation 6.2).

$$A_t = \frac{T_e - T_{low}}{T_{high} - T_{low}} \tag{6.4}$$

Pump Control Structure

With the traditional system consisting of an engine driven coolant pump, the water pump is left to simply function based on the engine speed in an uncontrolled manner. However, the cooling system coolant flow needs are not always proportional to the engine speed and may produce unnecessary parasitic loads during warm-up and low load conditions. This research explored pump speed control by completely decoupling the pump from the engine speed. The pump control voltage is determined by the valve's PI controller which serves as the control input to the pump motor driver. This approach is supported from the perspective of controlling the radiator's heat rejection rate. Furthermore, by coupling the action of these two devices the control authority will be justified by increasing the pump speed after the valve reaches its fully open position

$$U_p = K_p U_v \tag{6.5}$$

Engine Test Profile

To provide a basis of comparison for each of the configurations and their control methods, a common test profile has been created. In developing this test profile, two main types of system disturbances are considered which will challenge the cooling system's ability to maintain the set point temperature. The first disturbance is the engine load increase. Changes in terrain, vehicle speed and driving styles will be represented by a single load increase, t_I and decrease, t_{IV}. Also important in this evaluation is the effect of "ram-air" on the cooling system from t_{II} through t_{III}. This is an additional source of air flow at the radiator that is uncontrolled.

Steady state system operating conditions are also evaluated using this engine test profile. During idle conditions, there is no ram-air present and represents a parked vehicle. The coolant system must accommodate both highway driving from t_{II}, at

t=1,000s, to t_{III}, at t=1,700s, and strenuous low speed, high torque vehicle operation t_{III} through t_{IV}, at t=2,100s. To consider both of these scenarios, the system is allowed to reach steady state during loading with ram-air t_{II} to t_{III} and without ram-air t_{III} to t_{IV}. After sufficient time for steady state operation to be reached, a full on ram-air condition is initiated which represents the air side disturbance t_{II}. The system is allowed to reach steady state after the ram-air is turned off at t_{III}. Soon after, the loading condition is removed and the vehicle returns to parked condition at t_{IV} with an engine key off at t_V, at t=2,450s. This test schedule is represented by Figure 6.4.

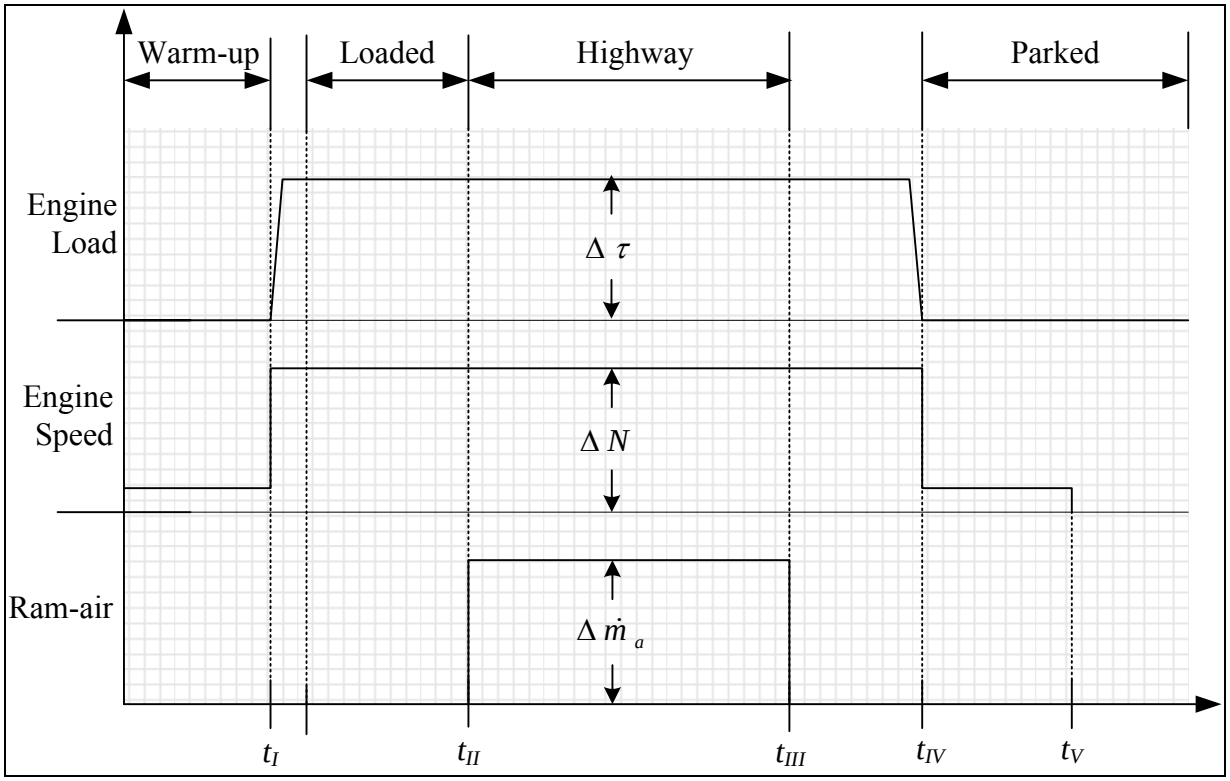

Figure 6.4 Engine test profile

On-Engine Implementation

Implementing the various configurations required connecting the thermal management system to the existing engine coolant jacket. Each configuration was implemented in a manner to maintain similarity which can be seen in the comparison of Tests 1 and 2 to Tests 3 and 4. A large variance occurs in the implementation of the off-engine pump which required the design of an off-engine bypass. The on-engine test configurations will be described in the following paragraphs and illustrated in Figures 6.5 through 6.7.

The first configuration simply implements a DC controlled fan-drive into the cooling system. A wax-based thermostat is maintained in the on-engine thermostat housing. The configuration is illustrated in Figure 6.5. The second configuration implements an electronic thermostat placed at the radiator outlet. This location is chosen since it has the lowest system temperature. The smart valve will provide the ability to evaluate thermostat control with a PI controller. Also, the two fan control algorithms, PI and Balanced, are tested utilizing the cooling system configuration illustrated in Figure 6.6. The third configuration utilized an external coolant pump drive consisting of a one hp DC motor coupled to a pedestal centrifugal pump. The external pump also requires an off-engine bypass loop which is illustrated in Figure 6.7. The effect of this off-engine bypass is an increased coolant volume at the engine. This configuration represents the fully computer controlled cooling system and provides some interesting insight into the challenges and improvement available with computer controlled actuators.

Figure 6.5 On-engine implementation: Configuration 1

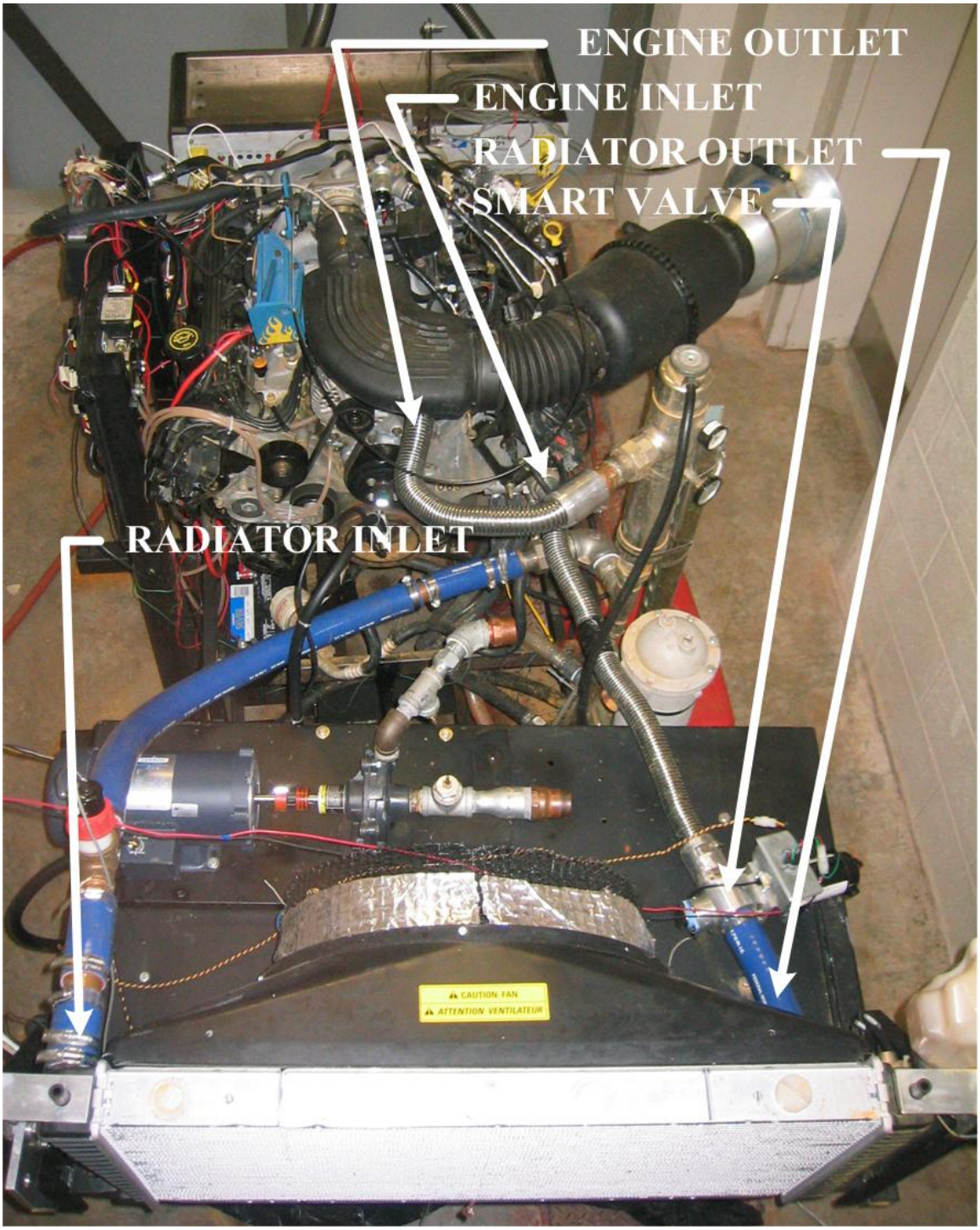

Figure 6.6 On-engine implementation: Configuration 2

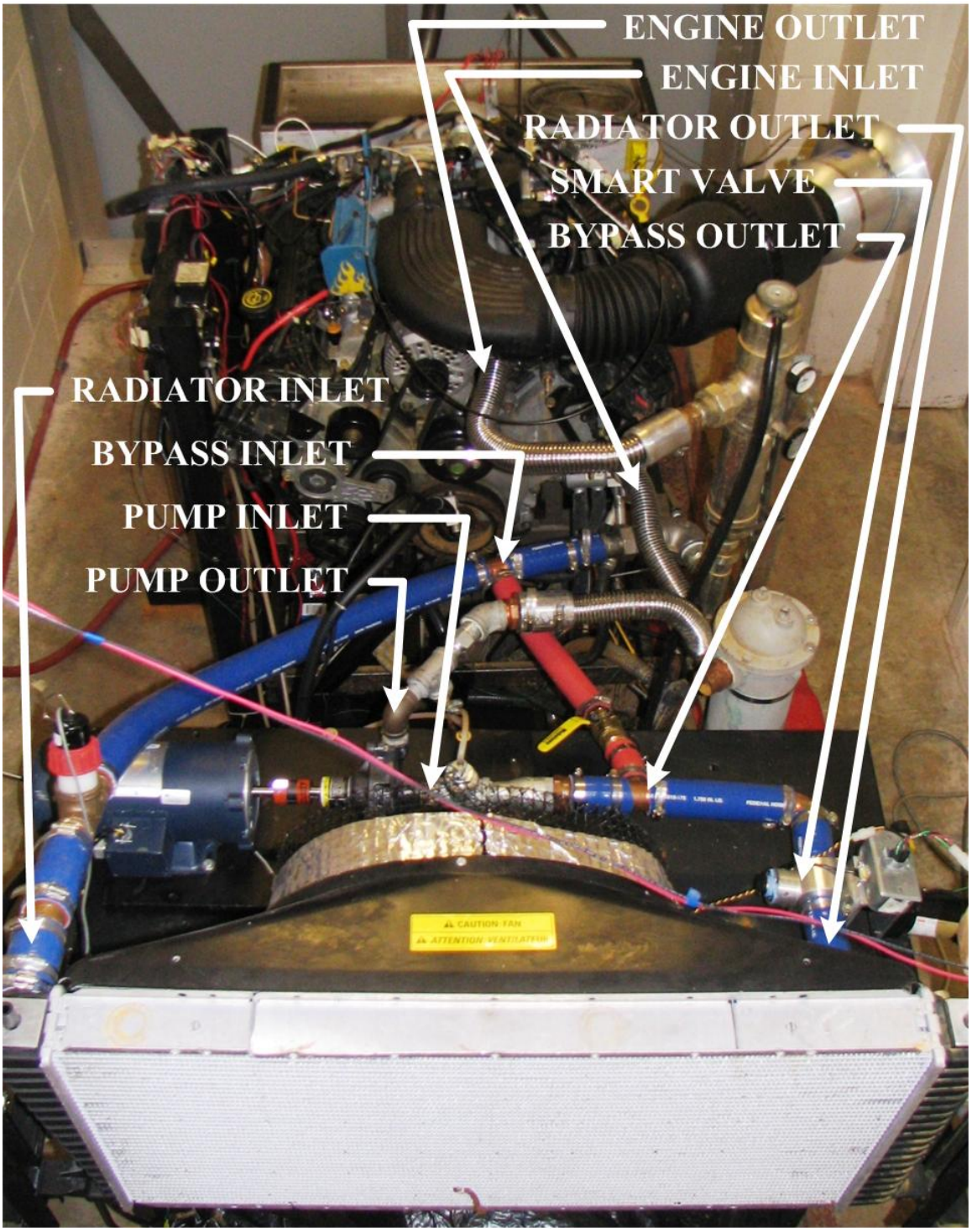

Figure 6.7 On-engine implementation: Configuration 3

Available Sensors

To evaluate the cooling system configurations for temperature tracking, power consumption, and thermodynamic action, a data acquisition system is implemented with various sensors to provide fluid flow, pressure sensing, temperature measurements. In the engine block and cooling system, various thermocouples are available for measurement as shown in Figure 6.8. The engine thermocouples are organized by the head, top, middle, and bottom of each cylinder. There are a total of 32 embedded thermocouples across the engine water jacket where temperatures are chosen from the left and right hand side engine banks. These two temperatures provide feedback of the engine temperature homogeneity where a large temperature difference indicates large temperature gradients on the engine. Increasing the number of measured engine temperatures will provide increased insight into the temperature gradients in the engine water jacket. This engine provides the ability to fully measure the temperature of the coolant across the engine at any given time. Unfortunately, the data acquisition system limited the number of temperatures measured. Increasing the number of temperatures measured will increase the ability to observe the impact of various flow controls when implementing an external water pump.

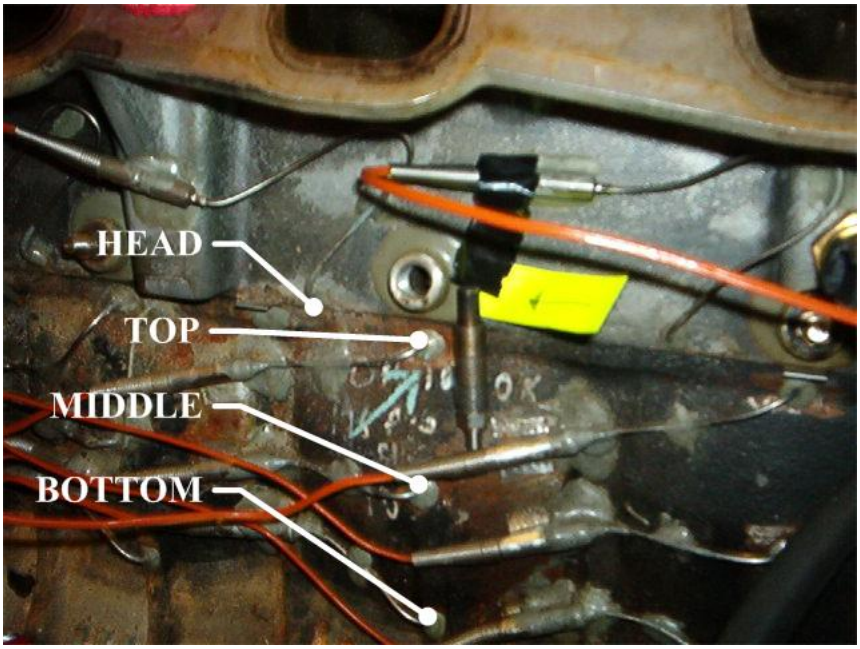

Figure 6.8 Embedded engine thermocouples - locations

The engine has pressure taps located at the pump inlet and outlet to provide real-time measure of the pressure head (refer to Figure 6.9). This pressure head at the engine provides an indication of the pump's parasitic load on the engine. However, to truly measure the pump power consumption, torque and speed measurements are necessary. The comparable DC motor driven pump performance will act as an indicator of pump load. For the external pump, the pressure is measured in a similar manner where pressure taps are placed on the coolant passages near the pump inlet and outlet locations (refer to Figure 6.10).

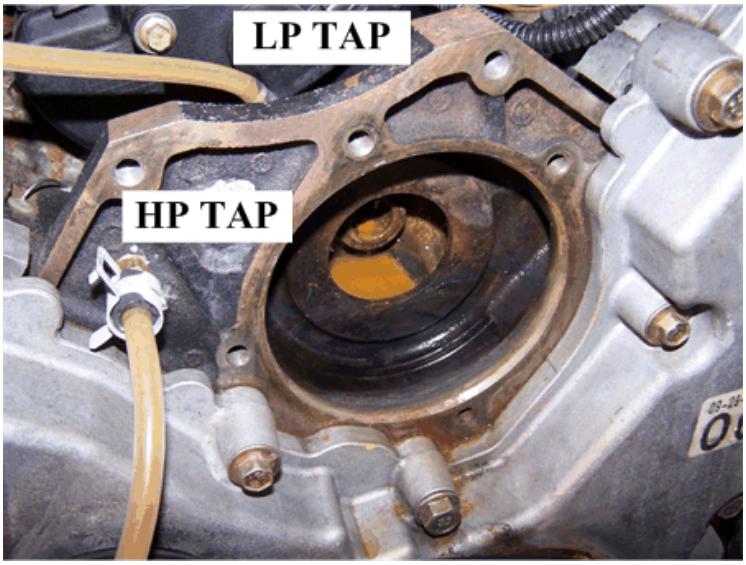

Figure 6.9 Engine pump pressure taps

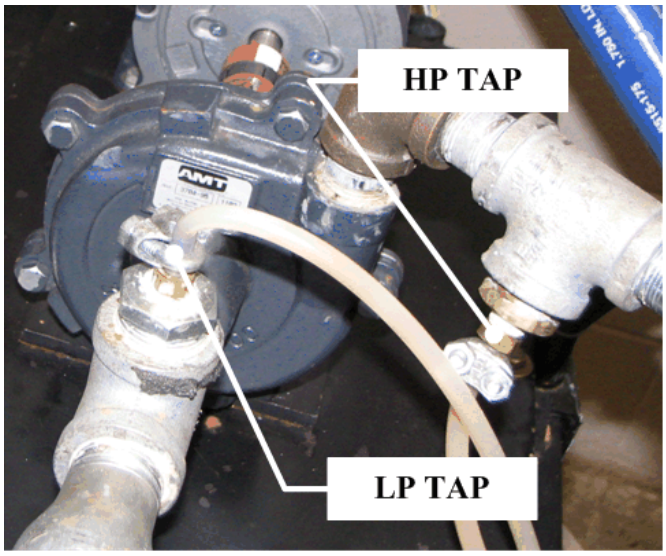

Figure 6.10 Off-engine pump – pressure taps

In the radiator passage, a paddle wheel flow meter is installed to measure the coolant flow rate (refer to Figure 6.11). In the balanced control system, radiator flow rate is a feedback variable. However, an estimate of the radiator flow rate is provided by the

pump speed and smart valve position feedback. This approach has been developed due to the flow meter's inability to measure flow rates below 10 LPM in an accurate manner.

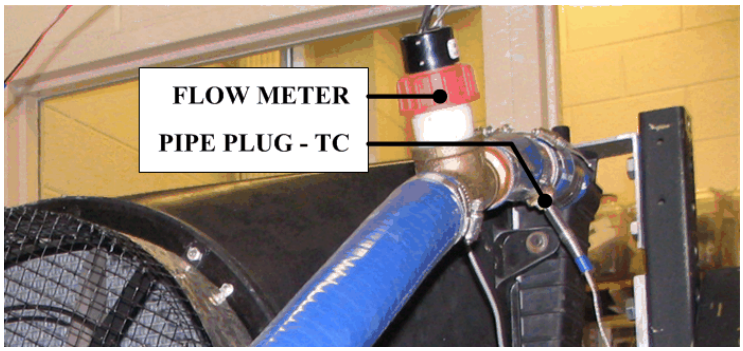

Figure 6.11 Flow meter and pipe plug thermocouple

The pump speed is may be measured directly or processed from the pump control signal. The speed sensor produces a voltage pulse when the reflective tape mounted on the pump pulley passes by the sensor (refer to Figure 6.12). This voltage pulse provides the input to a frequency counting software algorithm which measures the time between pulses to determine speed of both the water pump and the driving crankshaft.

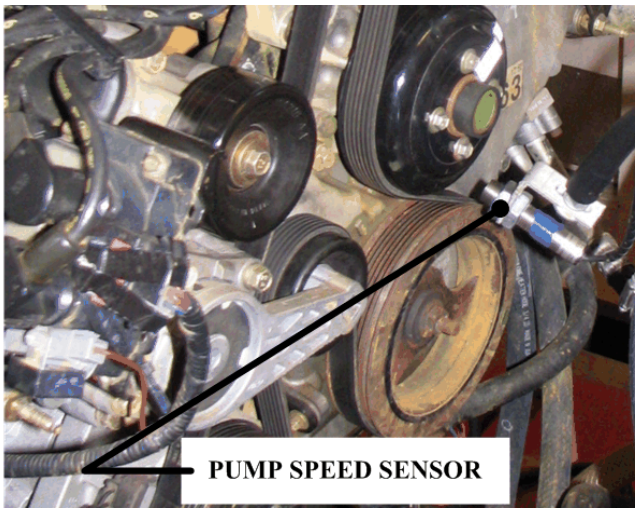

Figure 6.12 On-engine pump speed sensor

The feedback variable in the PI control systems is the engine temperature provided by an embedded engine thermocouple. However, the main purpose for the various feedback signals is to account for thermodynamic action and provide system performance indicators. The pressure sensor feedback from the on-engine pump will provide power consumption comparisons with the off-engine pump pressure drop. The embedded engine thermocouples provide both an estimate of the temperature homogeneity in the engine water jacket and temperature feedback in the PI control algorithms.

Engine Control Console

In this testing, the engine console allow prescribed engine speed through throttle position and torque through water brake as shown in Figure 6.13. The water brake during operation is shown in Figure 6.14.

Figure 6.13 Engine console

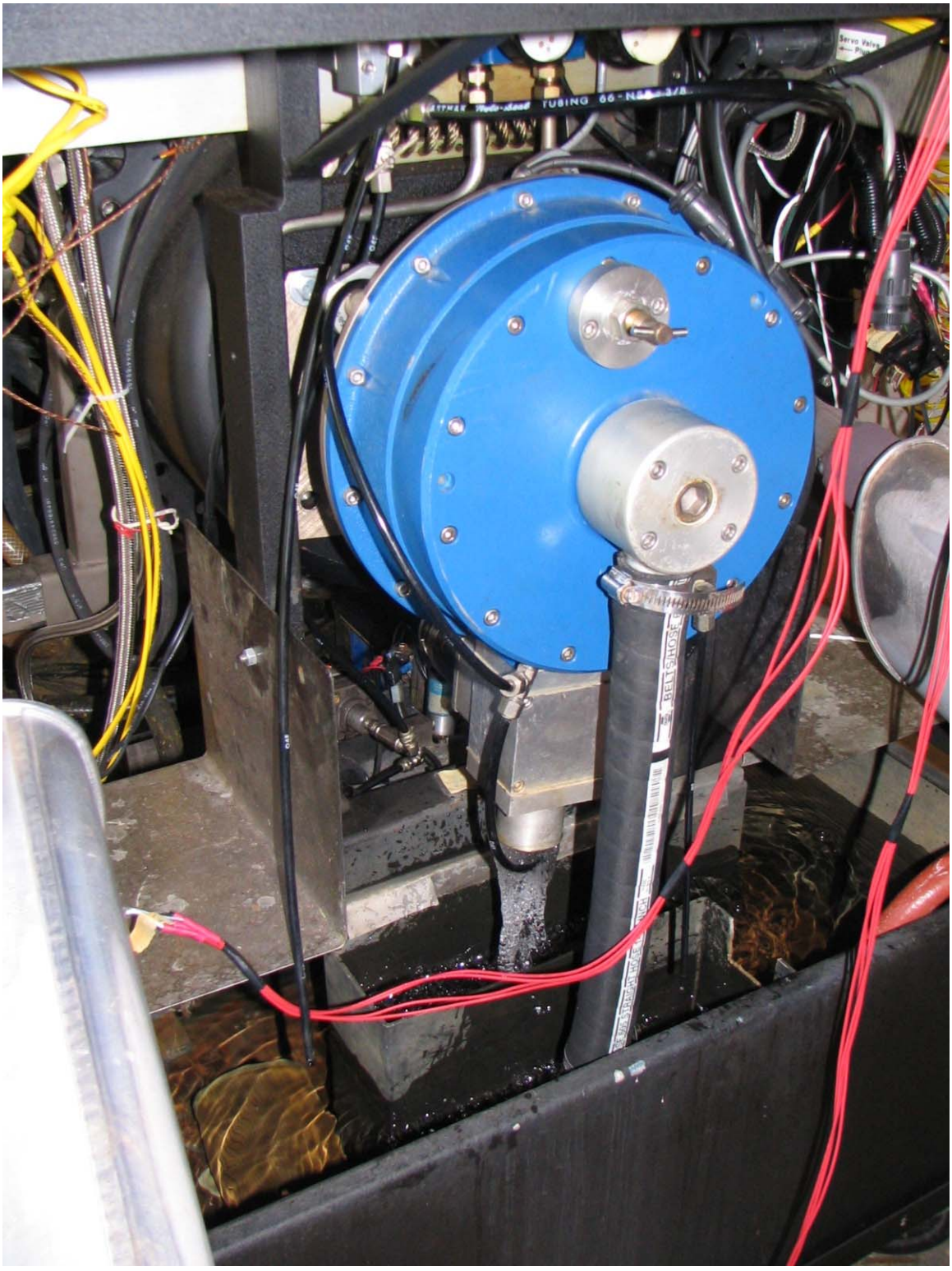

Figure 6.14 Water brake – Superflow 901

Engine Test Results

In Figures 6.15 through 6.18 the engine response to the fourth test configuration and controller combination is presented (Test 4). The temperatures of the left engine bank, T_{lb}, right engine bank, T_{rb}, radiator inlet, $T_{r,i}$, radiator outlet, $T_{r,o}$, and ambient temperature, T_o, are shown versus time, in Figure 6.15. Note that the oscillating temperature response occurs during ram-air conditions accompanied by the larger temperature difference between the radiator, $T_{r,o}$, and the engine, T_{lb}. In Figure 6.16, the temperature error signal is maintained within a ±3ºC neighborhood of zero. This is quite good given an operating threshold of 90ºC. Note that the fan and valve respond immediately to the introduction of a load reduction disturbance at time t=2100 seconds in Figure 6.17. Finally, the accessory loads are presented in Figure 6.18 with the fan, pump and combined power consumptions. It is important to remember that power use will be dependent on the engine displacement. In this case, the 4.6L engine at partial load requires approximately 400 Watts to operate these two components and maintain temperature.

All six tests' time histories are contained in Appendix F.

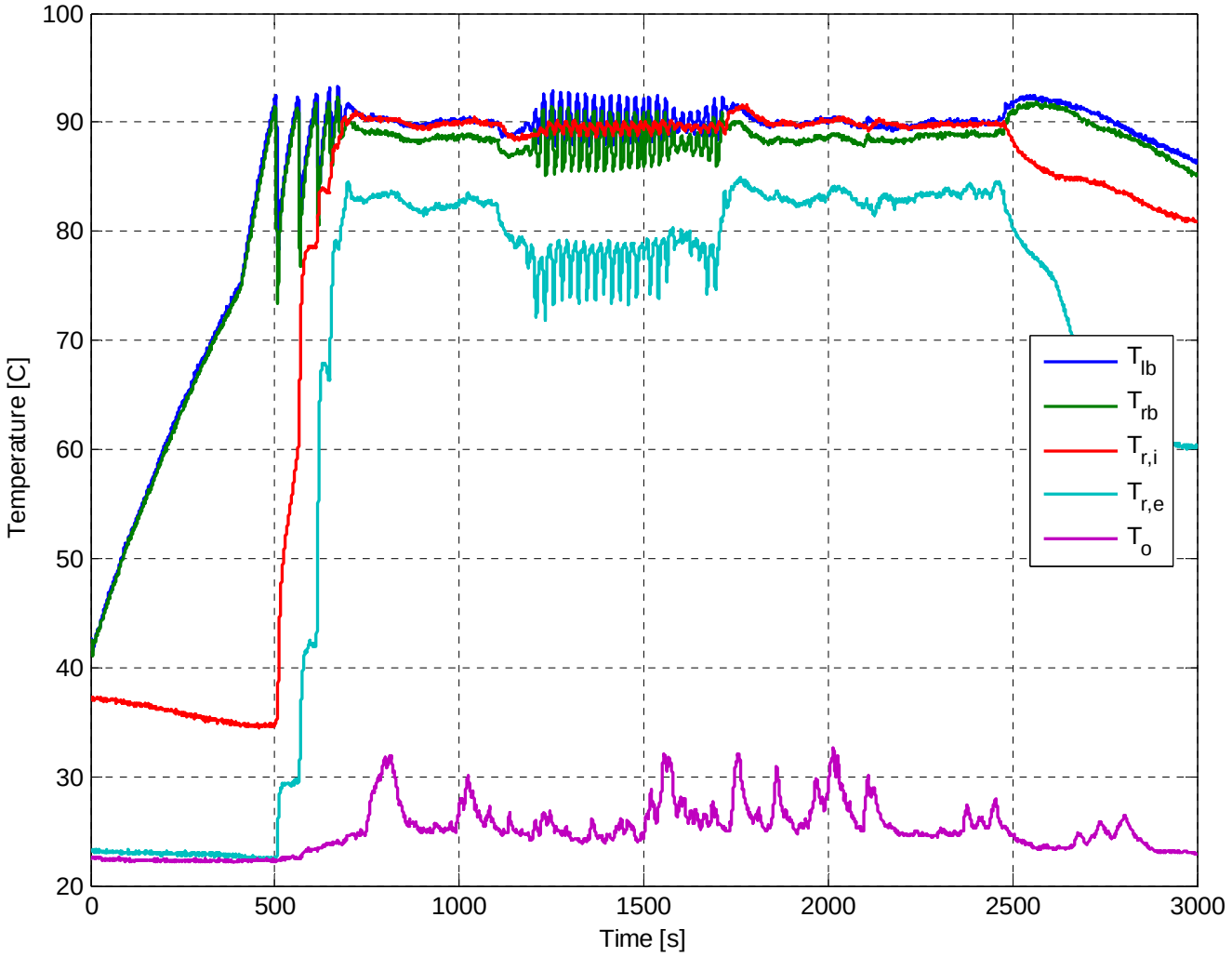

Figure 6.15 Temperature response: Test 4

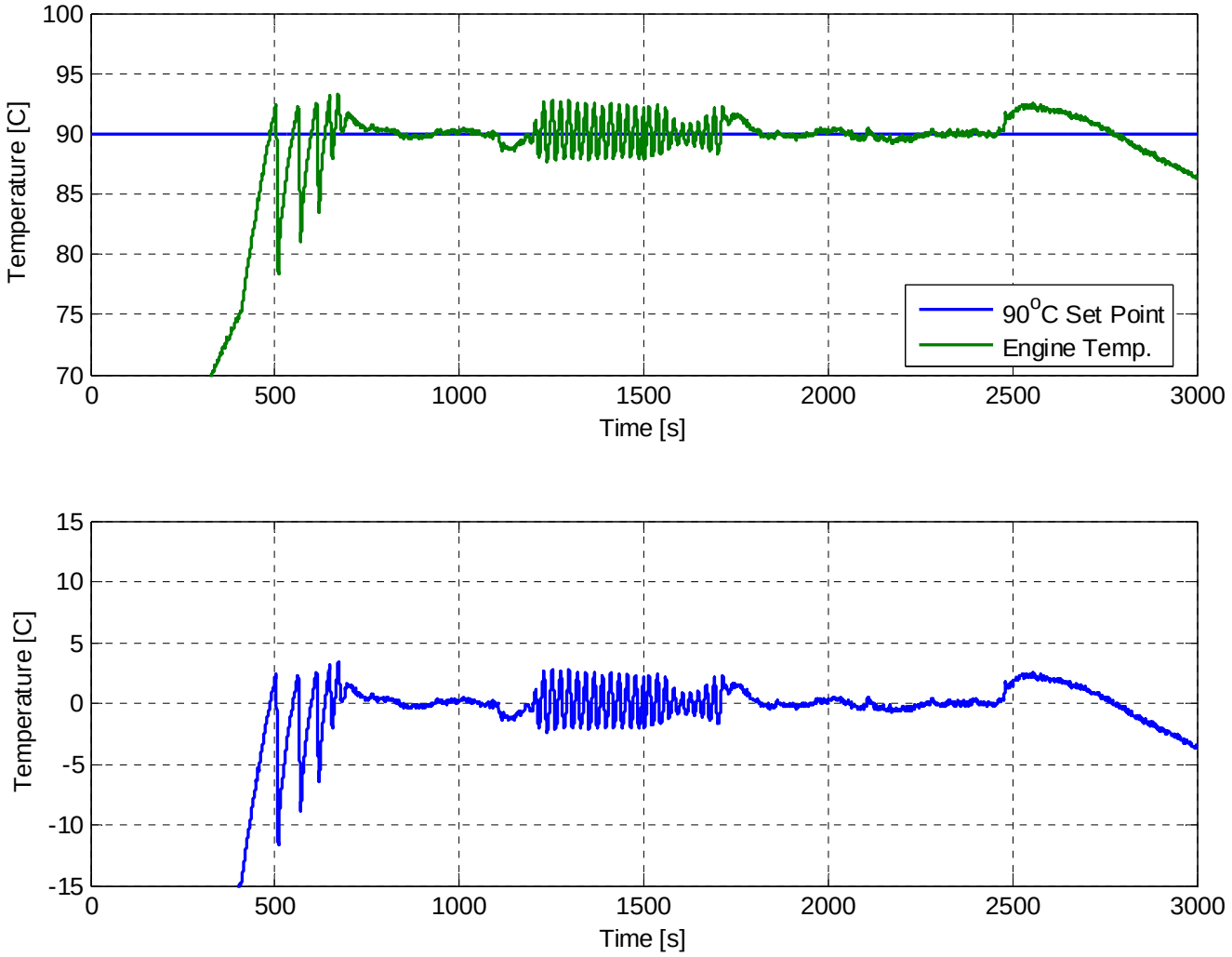

Figure 6.16 Feedback temperature and error signal: Test 4

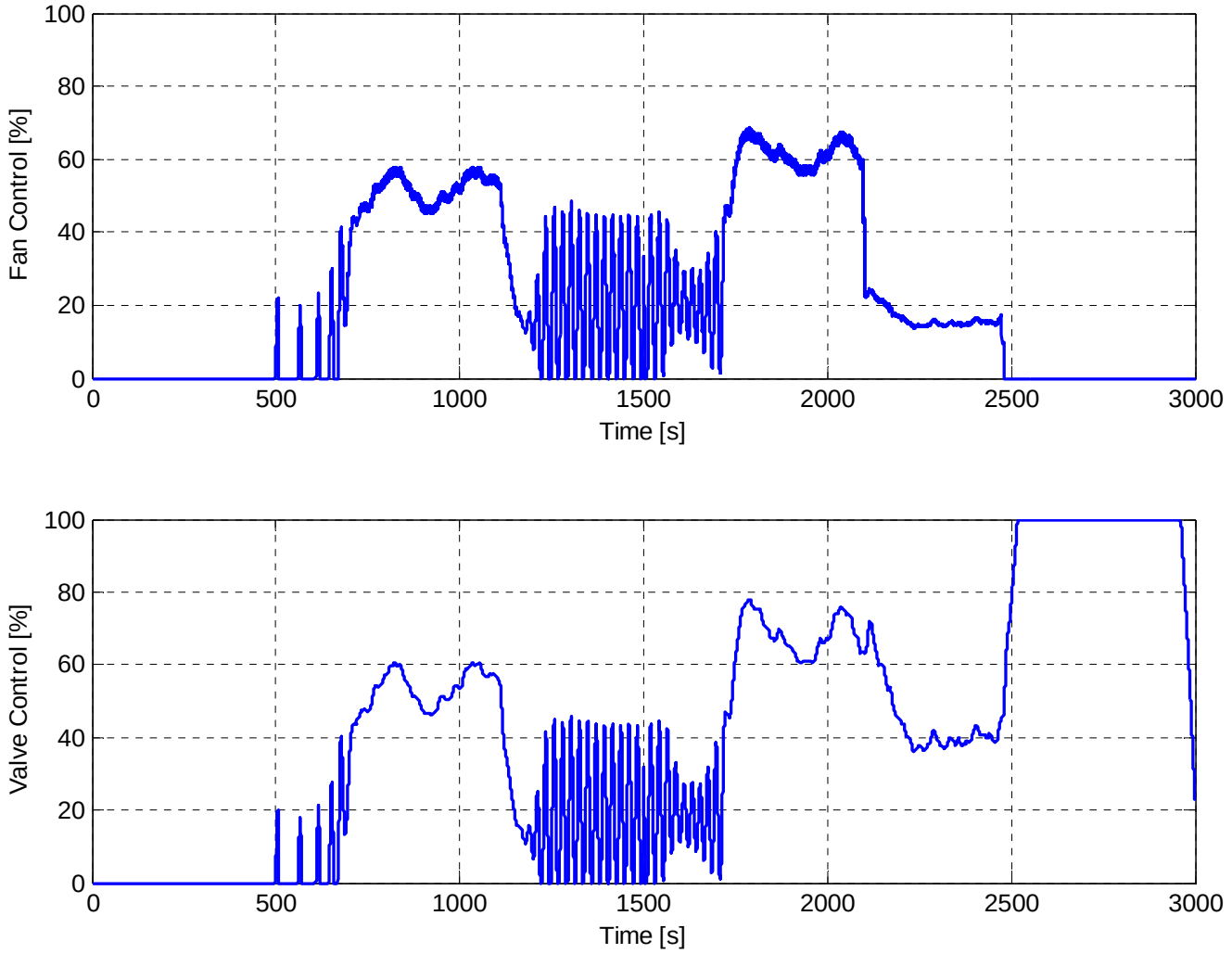

Figure 6.17 Normalized control percentages: Test 4

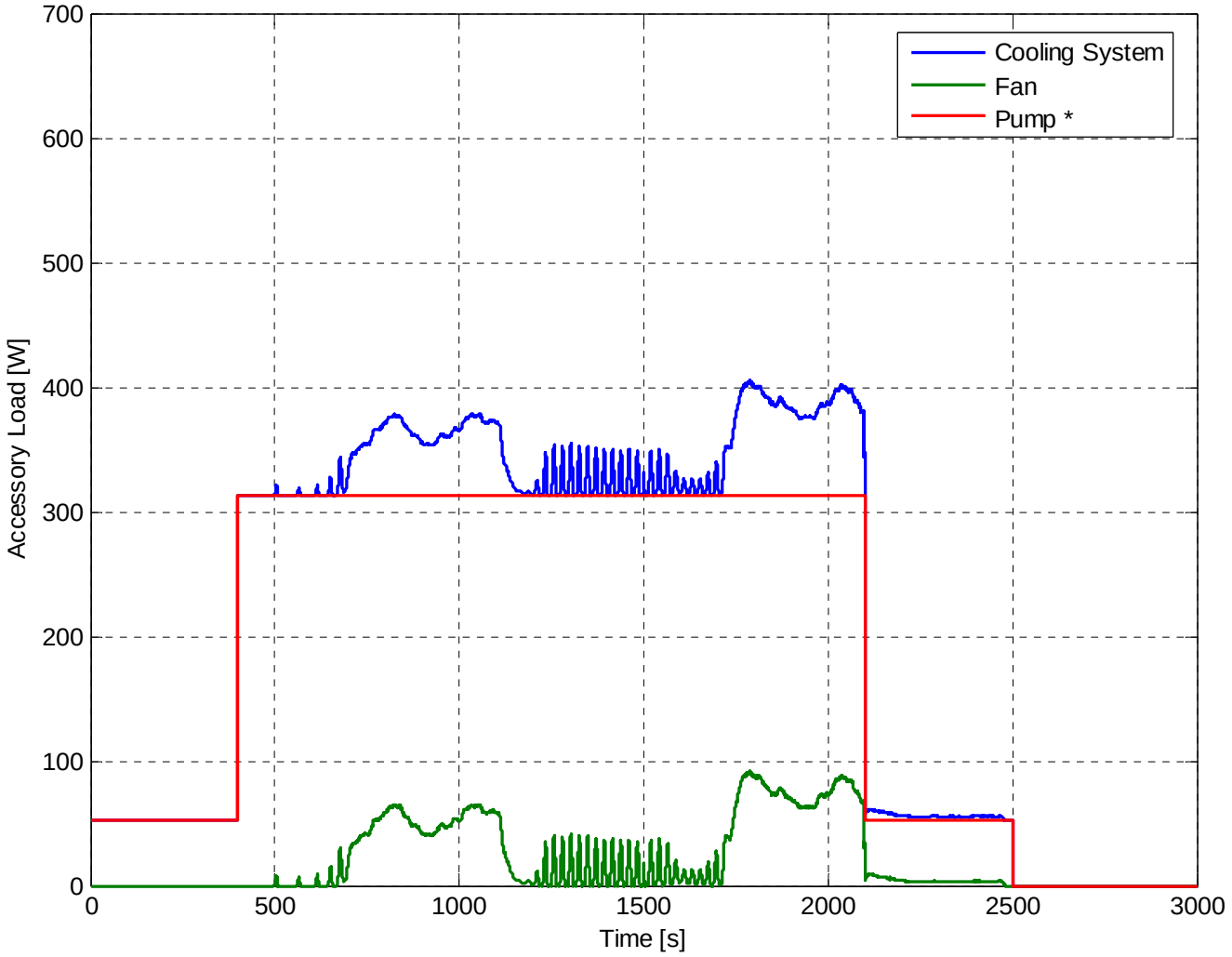

Figure 6.18 Power consumption: Test 4

The temperature tracking results for the six engine tests in Table 6.1 for the profile in Figure 6.4 offer insight into overall cooling system performance. The temperature tracking at the left engine bank at steady state, T_{lb_ss}, and during the transient temperature response, T_{lb_max} and $T_{lb\_min.}$, at the right engine bank, T_{rb_ss}, radiator inlet, T_{r,i_ss}, and radiator outlet, T_{r,e_ss}. In Table 6.2 and 6.3, four of the five key operating condition changes are accounted for: (I) Warm-up transition to operating temperature; (II) Increase in air flow at the radiator known as ram-air; (III) Decrease in air flow at the radiator when a vehicle is at rest; and (IV) Decrease in the engine load when a vehicle is at idle. For the fifth operating condition represents engine key-off shutdown (V) refer to Figure 6.23 which shows the soak characteristics for 3 tests (Tests 2, 5, and 6). Table 6.2 indicates that the wax-based thermostat Tests 1 and 2 do not follow a set point temperature measured at the left engine bank. This is true for both tests even when the fan is controlled. Also, note from this table the radiator outlet temperature is much higher in the controlled valve Tests (3 and 4) and in the controlled pump Tests (5 and 6).

The power consumed by the fan and pump are accounted for in Table 6.3 for all operating conditions. One should note that the pump and fan power were measured using sensors. However, the engine accessory pump was not measured. Instead, it was estimated by the amount of power required to drive the DC driven pump at the same speed, a quantity that was measured during each test, N_p. The steady state power consumption at the pump, P_p, at the fan, P_f, and the peak power load, P_{pl}, from the system are presented. Also contained in this table is the measured radiator flow rate, Q_r. The valve position, $\theta_{v,\%}$, is included in this table where the wax-based thermostat valve never opened above 10% since the engine temperature remained at 90ºC.

Table 6.2 Transient temperature tracking and steady state operation details for six cooling system tests with t_s – settling time, T_{lb} – left bank engine temperature, T_{rb} – right bank engine temperature [ºC], $T_{r,i}$ – radiator inlet temperature, and $T_{r,o}$ – radiator outlet temperature. The subscripts *max*, *min* describe the minimum and maximum temperature during transients and *ss* indicates steady state

I - Warm-Up

Test	t_s	T_{lb_max}	T_{lb_min}	T_{lb_ss}	T_{rb_ss}	T_{r,i_ss}	T_{r,e_ss}
1	174.0	95.6	85.5	91.0	89.0	88.0	40.0
2	327.0	95.5	85.0	90.5	88.5	88.0	45.0
3	350.0	93.0	78.0	90.0	89.0	90.0	85.0
4	235.0	93.0	78.0	90.0	88.4	90.0	83.0
5	375.0	94.8	87.0	90.0	85.0	92.0	83.0
6	565.0	95.0	85.4	90.0	86.0	91.0	84.0

II - Ram-Air On

Test	t_s	T_{lb_max}	T_{lb_min}	T_{lb_ss}	T_{rb_ss}	T_{r,i_ss}	T_{r,e_ss}
1	150.0	91.0	90.0	91.0	89.0	88.0	50.0
2	250.0	91.0	90.0	91.0	89.0	89.0	49.0
3	N/A	93.0	87.0	90.0±2.0	88.5±2.5	89.5±0.5	76±3.0
4	N/A	92.5	87.5	90.0±2.0	88.0±2.0	89.4±0.5	76±2.5
5	225.0	90.0	87.0	90.0	82.5	95.0	70.0
6	325.0	90.0	86.5	90.0	82.5	95.0	70.0

III - Ram-Air Off

Test	t_s	T_{lb_max}	T_{lb_min}	T_{lb_ss}	T_{rb_ss}	T_{r,i_ss}	T_{r,e_ss}
1	100.0	90.5	90.0	90.0	88.5	88.5	45.0
2	100.0	90.5	90.0	90.5	88.5	88.5	45.0
3	200.0	93.0	90.0	90.0	89.0	90.0	85.0
4	125.0	92.0	90.0	90.0	88.5	90.0	83.0
5	250.0	94.8	90.0	90.0	84.0	93.0	83.0
6	>300	96.0	90.0	89.0	86.0	90.0	82.0

IV - Load Decrease

Test	t_s	T_{lb_max}	T_{lb_min}	T_{lb_ss}	T_{rb_ss}	T_{r,i_ss}	T_{r,e_ss}
1	100.0	91.5	89.0	89.0	87.0	87.0	35.0
2	150.0	89.0	89.0	89.0	87.0	82.5	30.0
3	200.0	90.0	86.5	90.0	89.0	90.0	84.0
4	0.0	90.0	90.0	90.0	89.0	90.0	83.0
5	225.0	90.0	86.5	90.0	86.0	92.0	83.0
6	300.0	90.0	87.0	90.0	86.5	92.0	84.0

Table 6.3 Power consumption and system actuation details for six cooling system tests with P_{pl} [W] – peak power load, P_{ssl} – steady state power load, P_p – pump power, P_f – fan power, N_p – pump speed [RPM], $\theta_{v,\%}$ - valve position [% open], and Q_r – radiator flow rate [LPM], * indicates pump power estimate

I - Warm-Up

Test	P_{pl}	P_{ssl}	P_p	P_f	N_p	$\theta_{v,\%}$	Q_r
1	538.0	538.0	313.0*	225.0	2,360	<10.0	<10.0
2	538.0	538.0	313.0*	225.0	2,360	<10.0	<10.0
3	378.0	368.0	313.0*	55.0	2,360	100.0	77.0
4	378.0	373.0	313.0*	60.0	2,360	50.0	52.5
5	350.0	250.0	100.0	150.0	1,060	100.0	30.0
6	240.0	180.0	144.0	36.0	1,700	100.0	50.0

II - Ram-Air On

Test	P_{pl}	P_{ssl}	P_p	P_f	N_p	$\theta_{v,\%}$	Q_r
1	N/A	538.0	313.0*	225.0	2,360	<10.0	<10.0
2	N/A	538.0	313.0*	225.0	2,360	<10.0	<10.0
3	N/A	314.5±2.5	313.0*	5.0 (osc.)	2,360	20.0±20.0	25.0±20.0
4	N/A	333.0±20	313.0*	40.0 (osc.)	2,360	22.0±22.0	25.0±22.0
5	N/A	60.0	45.0	15.0	717	60.0	15.0
6	N/A	60.0	57.0	3.0	717	60.0	15.0

III - Ram-Air Off

Test	P_{pl}	P_{ssl}	P_p	P_f	N_p	$\theta_{v,\%}$	Q_r
1	538.0	538.0	313.0*	225.0	2,360	<10.0	<10.0
2	538.0	538.0	313.0*	225.0	2,360	<10.0	<10.0
3	413.0	368.0	313.0*	55.0	2,360	100.0	77.0
4	403.0	368.0	313.0*	55.0	2,360	70.0	63.0
5	450.0	250.0	250.0	150.0	1,060	100.0	30.0
6	290.0	180.0	180.0	36.0	1,700	100.0	70.0

IV - Load Decrease

Test	P_{pl}	P_{ssl}	P_p	P_f	N_p	$\theta_{v,\%}$	Q_r
1	N/A	277.2	52.2*	225.0	880	<10.0	<10.0
2	N/A	277.2	52.2*	225.0	880	<10.0	<10.0
3	N/A	56.2	52.2*	4.0	880	30.0	15.0
4	N/A	55.2	52.2*	3.0	880	40.0	15.0
5	N/A	45.0	40.5	4.5	717	20.0	9.0
6	N/A	42.0	40.3	1.7	717	20.0	9.0

Observation 1: Fan Control Alone is Insufficient

Test 2 was designed to evaluate the benefits related to fan control. The fan was controlled using a PI controller whose error signal, e, was supplied by the left bank engine temperature, T_{lb}, and a set point defined at T_{sp}=90ºC with $e = T_{lb} - T_{sp}$. This caused the controller to become saturated since fan was not able to affect the engine temperature. The wax-based thermostat valve controls the fluid movement from the engine to the radiator and is controlled in a proportional manner which resulted in allowing a small flow of cooling fluid (Q_r<10 LPM) from the engine to the radiator.

This operating condition can be explained as two reservoirs: one which operates at a high temperature, the engine, $T_{e,e}$≈91ºC; and the other is at a significantly lower temperature, the radiator, $T_{r,e}$≈40ºC. Since the radiator is held to a significantly lower temperature in Tests 1 & 2, only a small flow rate through the radiator is required to maintain set point temperature. This proves to be a very inefficient way to manage the radiator as shown in Figure 6.19 (A) and (C). The first aspect of inefficiency is explained by the effect of coolant flow on the effectiveness of the radiator. As the flow rate increases within the radiator, there is an increase in the number of transfer units, NTU, and, subsequently, an increase in the effectiveness. In Tests 1 and 2, the radiator fan is over exerting during its operation for the given radiator design. Additionally, the second effect that must be considered is the ability for the radiator to exchange heat with the environment through radiation. This radiation effect proves to be an important consideration when controlling the radiator. To take advantage of this effect, the radiator should be operated at a higher temperature as the heat transfer through radiation increases at a rate equal to the emitting surface temperature raised to the fourth power, $T_{r,s}^4$.

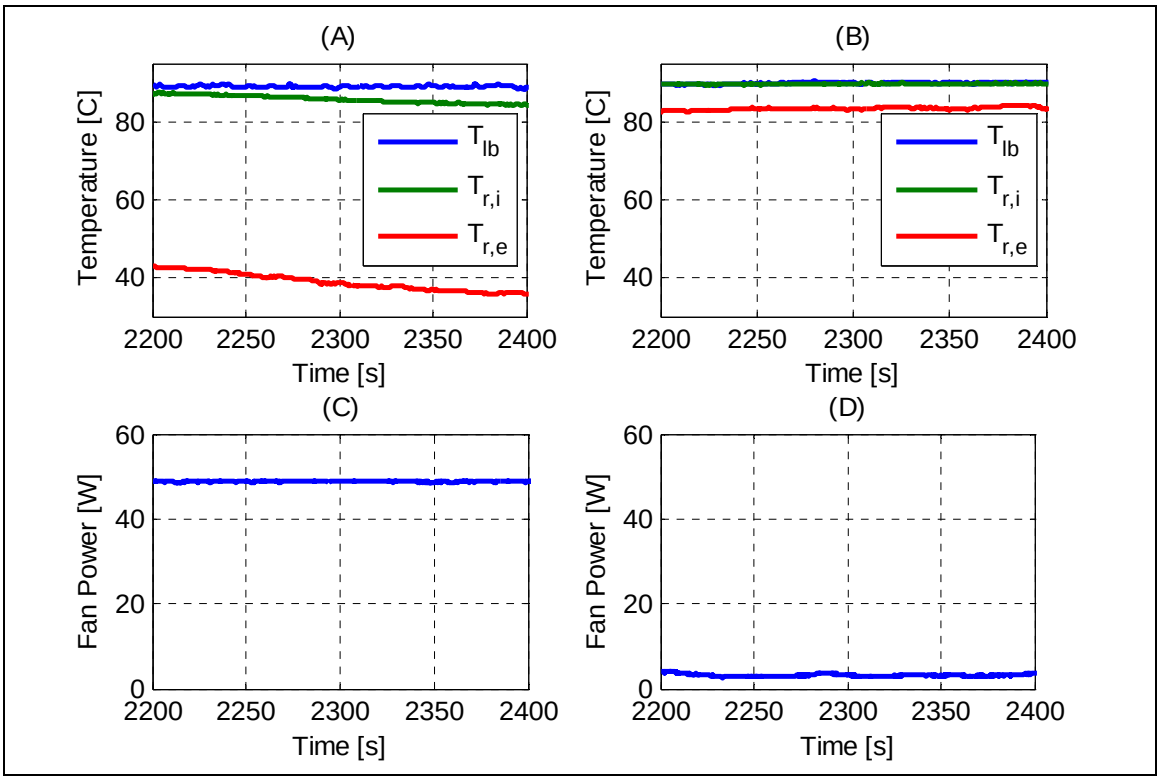

Figure 6.19 System function comparison during idle:
Temperature profiles (A) Test 1 & (B) Test 4
Fan power consumption (C) Test 1 & (D) Test 4

With the current crankshaft driven fan and wax-based thermostat valve cooling system design, the optimum operating point with respect to radiator performance only occurs when the engine is operating at full load. The proper feedback for the fan controller in combination with the wax-based thermostat will not be an engine temperature because this is within the thermostat valve's control authority. To obtain improved radiator performance, an alternative control point temperature must be considered while taking into account latency issues with the fan controller feedback point.

Observation 2: Improved Radiator Function with Fan and Valve Control

Improved radiator function can be revealed by simultaneously controlling both the smart thermostat valve and fan. For example, during engine idle and low load conditions, the fan is able to operate at a lower rate than that prescribed in crankshaft driven fan drives. The reduced fan load can be observed in Figure 6.19 which is a comparison between the baseline system (Test 1, plots A and C) and the valve and fan control configuration (Tests 4, plots B and D) during idle. Observed in Figure 6.19 is the increased radiator outlet temperature from Test 1, $T_{r,e}$≈40ºC, to Test 4, $T_{r,e}$≈84ºC. By implementing a computer controlled valve, the radiator operation can be improved by increasing the flow rate on the coolant side which, in addition, increases coolant heat transfer ability and decreases the magnitude of air flow required. This improvement can be observed in the fan power, P_f, reduction from the baseline results (Test 1) to the controlled valve configuration (Tests 4) in all operating conditions (refer to Table 6.2), with ~45W improvement during idle.

Another improvement due to valve and fan control (Tests 3 & 4) can be observed in the decreased temperature gradient across the engine. This configuration demonstrated that improved temperature homogeneity can be achieved through increased radiator outlet temperature (refer to Table 6.4). In Test 1, the temperature gradient is ΔT_e=1.75 where in Test 4 it is ΔT_e=1.25. Furthermore, the cooling system operates at a temperature closer to the set point temperature as shown by the radiator outlet temperature in Tests 1 and 2, $T_{r,e}$≈40ºC, and in Tests 3 and 4, $T_{r,e}$≈84ºC. It is important to note that the heat transfer rates have not changed between these operating profiles, main operation difference is the radiator flow rate, Q_r, has changed from less than 10 LPM in the baseline configuration (Test 1) to approximately 77 LPM in the PI fan and valve control configuration (Test 3).

Observation 3: Temperature Variations Dependent on Controller Design

The baseline system (Figure 6.20, A) is much less sensitive to changes in operating conditions than the computer controlled configurations T_{lb}=±0.5ºC. However, the controlled valve's deficiency is apparent in the oscillatory temperature response during ram-air conditions (Figure 6.20, B) and increased sensitivity to all operation condition changes. The likely cause of the ±3ºC oscillatory nature of the temperature response is related to the increased pump flow rate which increases the valve's influence. The available fluid flow from the water pump is lower in Test 6 resulting in negligible oscillation in response since the system is less responsive to changes in valve position (Figure 6.20, C). But, the system continued to reveal temperature variations of ±3ºC.

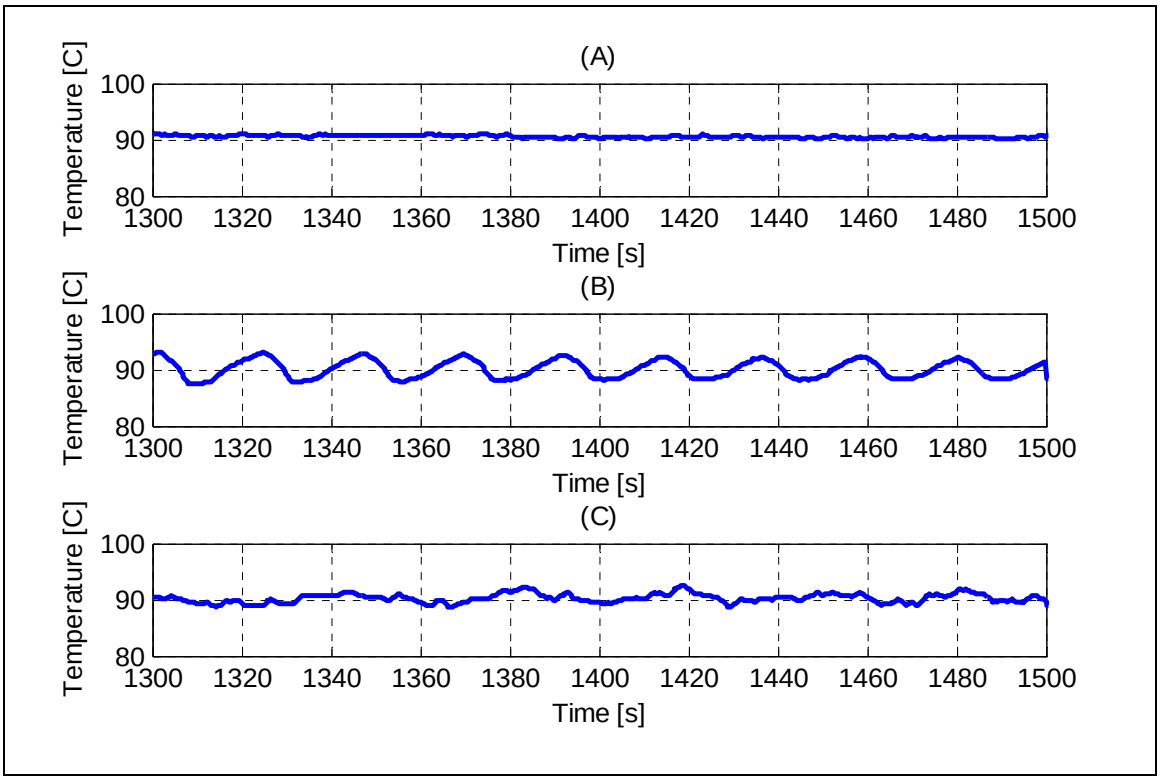

Figure 6.20 Temperature tracking during ram-air: (A) Test 1, (B) Test 3, and (C) Test 6

Observation 4: Cooling System Power Consumption

The balanced control strategy, Equation 6.3, is a more energy efficient cooling system regulation method than the PI structure, Equation 6.2, investigated in this research. The balanced control strategy (Test 6) showed a 70W reduction in power consumption when compared to the PI structure (Test 5) in the full computer controlled configuration (refer to Figure 6.21) due to the efficient proportioning of control magnitude between the fan and pump. The valve is cheapest in terms of power consumption followed by the pump and fan. This efficient proportioning of control reveals that exergy based analysis is the key to efficient control algorithm development (Bejan, 1996, Shinskey, 1978).

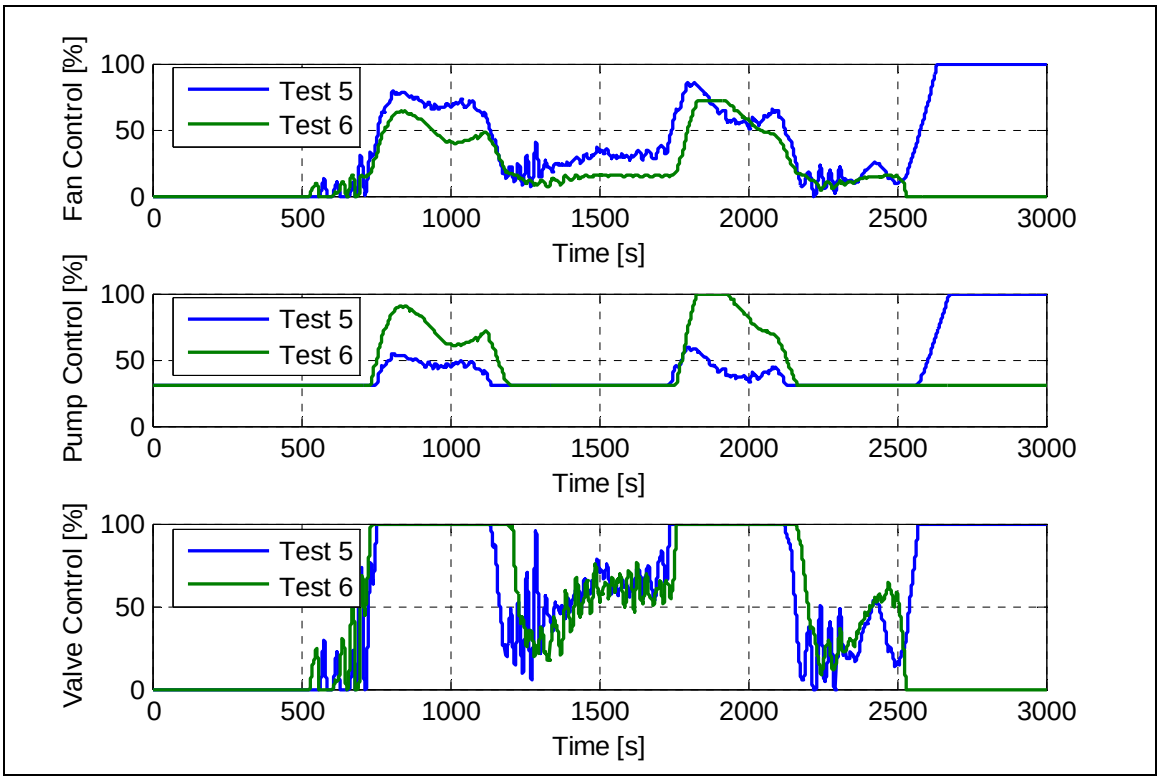

Figure 6.21 Normalized control percentages for Tests 5 & 6

Observation 5: Engine Temperature Homogeneity

The computer controlled pump allows the speed to be decoupled from the engine crankshaft which reduces the power consumption by slowing the fluid flow while maintaining the engine set point temperature. However, the pump control strategies introduce a large temperature gradient across the engine. This gradient is caused by ineffective flow routing and the lower pump flow rates. Figure 6.22 shows the coolant flow rate effect on temperature homogeneity during warm-up for three different tests: (A) Test 2; (B) Test 3; and (C) Test 6.

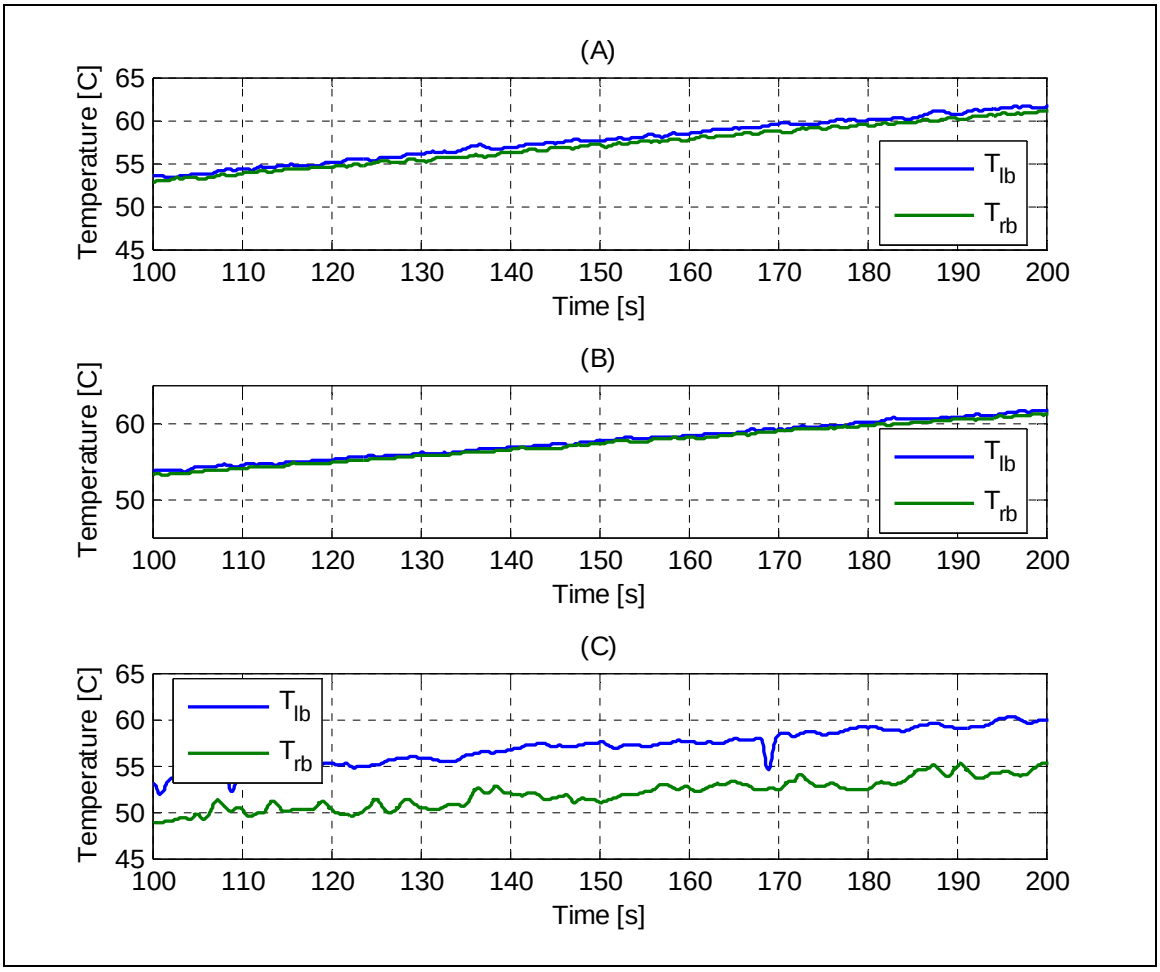

Figure 6.22 Engine temperatures during warm-up:
(A) Test 2; (B) Test 3; and (C) Test 6

Table 6.4 indicates the level of temperature homogeneity while the engine is operated under a load. However, it should be noted that this measure does not indicate the total temperature rise across the engine ($T_{e,e}$-$T_{e,i}$) which can be approximated with knowledge of exact coolant flow rates, $\dot{m}_b$ and $\dot{m}_r$, and temperatures within the engine bypass, $T_{e,e}$, and radiator, $T_{r,e}$. Tests 1 and 2 were conducted using the wax-based thermostat which provides some restriction through the engine bypass and will tend to increase the temperature gradient accompanying the lower flow rate. Additionally, the temperature gradient measured in Tests 3 and 4 showed a slight improvement over Tests 1 and 2 which can be partially attributed to the reduced bypass restriction and increased engine flow rate compare Figure 6.22 (A) and (B). During the loaded condition (refer to Table 6.4), further improvement is caused by the increased radiator operating temperature. Increasing the radiator outlet temperature decreases the impact of the fluids at different temperatures mixing within the engine for Tests 3 and 4.

Table 6.4 Engine temperature gradients during loaded engine condition for six cooling system tests, ΔT_e – Engine temperature gradient as measured by T_{lb} and T_{rb}

Test	$\Delta T_e = T_{lb} - T_{rb}$
1	1.75
2	1.80
3	1.00
4	1.25
5	5.00
6	4.00

Observation 6: Engine Water Jacket Heat Transfer

The transfer of heat from the combustion environment is a function of the heat released during combustion to provide shaft work, exit the cylinder with the combustion gases, and exit through the cylinder walls to the engine coolant. The temperature of the cylinder wall on the coolant side will be higher than the boiling point of the coolant (Kays, 1989). Kays suggests that the main mechanism responsible for heat transfer from the combustion environment is flow boiling which especially occurs at high loads which raise the cylinder wall temperature. Under lower loads, the main mechanism is convective heat transfer. This reveals an important conclusion supported in this work since the heat transfer rate is essentially independent from the coolant flow rate, only the mechanism for this heat transfer is affected and the temperature gradient across the engine, refer to Figure 6.22.

The conclusion that reducing the coolant flow rate will not profoundly reduce warm-up time is further supported by the negligible difference in time to 90ºC. No matter what one does with the flow of coolant, with heat transfer always occurring at similar rates (engine idle) and without reducing the amount of engine block mass, M_e, the amount of time it takes to warm-up the engine does not change. It is an observation that is further supported with an energy balance on the engine control volume (Chapter 5). If the objective exists to improve warm-up time, one must either increase the heat transfer rate in the combustion cylinder (i.e. wider throttle and higher engine loads) or reducing engine mass. For example, a study (Luptowski *et al.*, 2005)) presented a method to decrease warm-up time by increasing exhaust back pressure and thereby increasing engine load. As previously discussed the magnitude of coolant flow through the engine is accounted by the temperature gradient across the engine.

Observation 7: Pump Control for Engine Cool-Down

Pump control after engine key-off provides the only opportunity to reduce the temperature rise within the engine block due to heat soak. Heat soak represents the effect of the high temperature metal of the cylinder walls reaching equilibrium with the coolant in the water jacket after the engine is turned off. Kays (1989) infers that high cylinder wall temperatures are caused by high heat release rates due to increased loads. It is proposed that by decreasing the flow rate within the engine higher wall temperatures will also result which can be corroborated with Ap and Tarquis (2005). Furthermore, when the engine is shut off while operating at this condition, one will observe an increase temperature after engine key-off, heat soak. Observe in Figure 6.23, where two test have been run where the flow rate through the engine is low (Test 5) and where flow rate is high (Test 2) just before turning off the engine. Also, in Figure 6.23, observe Test 6 which through pump control continues to cool the engine for 100 seconds.

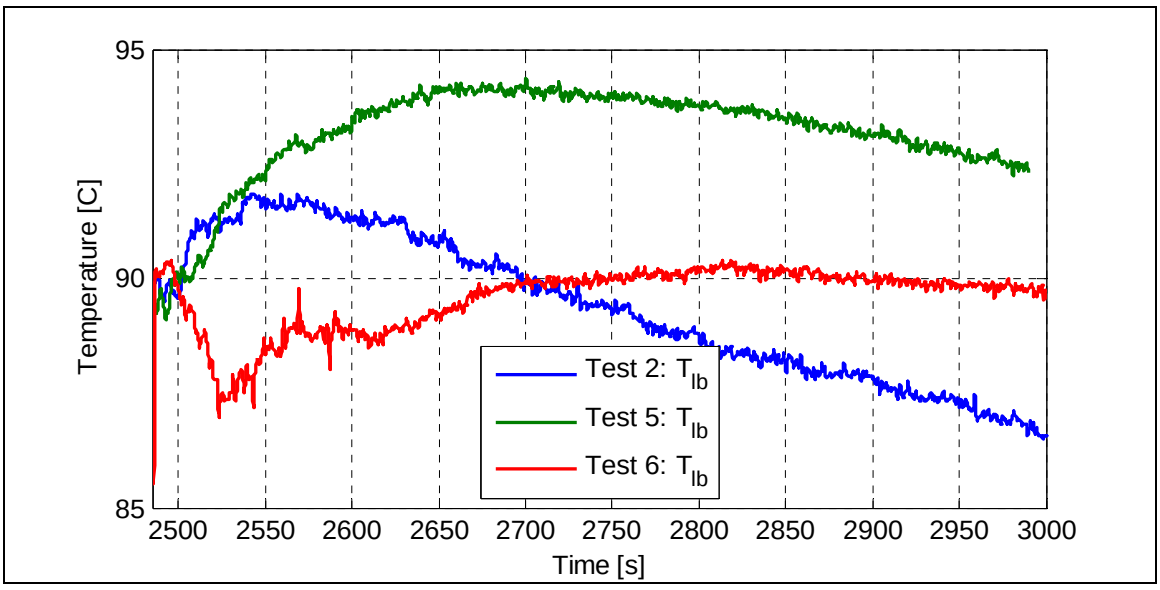

Figure 6.23 Temperature rise due to heat soak at engine key-off

Observation 8: Optimal Cooling System Configuration

The optimal cooling system configuration is the combination of the smart valve and controlled fan drive which reduced parasitic loading by ensuring effective radiator operation and exploiting available ram-air flow. Due to the discussion in Observation 6 and the need to maintain a homogenous engine profile, pump control may not be justified sufficiently. Since pump control is required to keep sufficient flow to maintain engine block temperature uniformity, and not to maintain heat transfer from the combustion cylinder wall, the current engine driven water pump performs well. If the goal exists to always utilize the boiling mechanism for heat transfer under all operating condition and also maintain engine temperature homogeneity, one must break up the engine block into smaller water jackets by redesigning the cooling system on a cylinder-by-cylinder basis, Figure 6.24. This proposed system will allow lower flow rates through each cylinder while minimizing the heat rise of the coolant from the inlet to outlet.

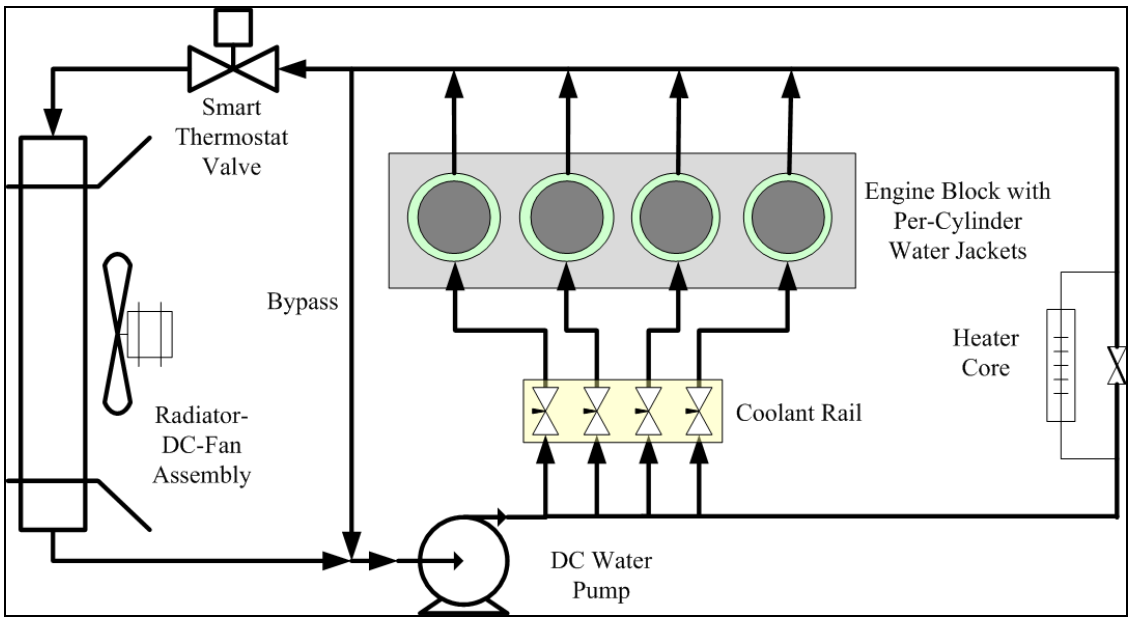

Figure 6.24 Top view of redesigned engine block
with on-demand cylinder dependent cooling system

Overall, controlling the cooling system with DC actuated components provides many observations of importance. The observation of the improved radiator function during low loads provides a benefit by reducing power consumption. However, the operating condition proves to cause unstable temperature tracking during some conditions. This provides a great challenge to a control engineer who is interested in maintaining stable and robust temperature control while running the system under difficult conditions and while consuming the least amount of energy. Meeting these challenges will ultimately lead to a cooling system that can maintain engine temperature during all transient conditions both environmental and engine specific. Over the lifetime of a vehicle, the energy saving will be profound with this type of cooling system and must be considered in all future vehicle designs.

To realize the greatest benefit with minimal design changes, a computer controlled thermostat and controlled fan drive will provide the ability to maintain an efficient radiator function and take advantage of environmental conditions. This is in combination with an engine driven water pump which proves to maintain homogenous engine temperature profiles which can minimize thermal stresses inside the engine water jacket. As discussed, this system will require harmonious control architectures that maintain an engine set point temperature with a minimum cooling power required. While minimizing the amount of temperature variation during transient conditions such as changes in engine load and ambient conditions such as vehicle speed induced air flow, ram-air. Since the changes in the operating conditions occur throughout driving cycles, controller designs and evaluations require considerations for the ever changing environment and driving conditions.

CHAPTER 7

CONCLUSIONS

The cooling of internal combustion engines requires computer controlled system components to meet the demands for temperature tracking and reduced power consumption. The work presented in Chapter 3 details the smart valve design and the position controller for a DC actuated thermostat. Two important conclusions are that this valve should be sized according to application and fast actuation is not required due to the slow thermal system dynamics. Furthermore, the valve size ultimately affects the controllability of the radiator and bypass flow rates. Associated with this is the need for accurate fluid response characteristics of the valve, radiator, pump and water jacket. These components and the radiator heat transfer capacities are empirically modeled in Chapter 4. The results in Chapter 4 offer automotive engineers the component details which are invaluable in system design and controller development activities.

To properly develop system designs and control architectures, a thermodynamic based model was developed. In Chapter 5, this model accurately ($\pm 5^{o}C$ and $\pm 5s$) simulates the temperature tracking for a scale thermal system (refer to Appendix E). In addition to the first law energy balanced method, an exergy based analysis was applied which revealed important system operation tradeoffs. The ability to use this exergy based analysis as a control objective has been utilized in the balanced fan control which improved system function with a reduction in power consumed (Test 5 versus 6).

Chapter 6 discussed the experimental apparatus utilized for the on-engine cooling system configuration and controller testing. This experimental testing showed eight key items: Fan Control Alone is Insufficient; Improved Radiator Function with Fan and Valve Control; Temperature Variations Dependent on Controller Design; Cooling System Power Consumption; Engine Temperature Homogeneity; Engine Water Jacket Heat Transfer; Pump Control for Engine Cool-Down; and Optimal Cooling System Configuration.

This understanding, developed through experimental procedures and careful data evaluation indicates the critical need for controlled radiator fan drives and smart valves. The fan drive technologies which show promise are 48VDC automotive electrical systems (Redfield *et al.,* 2006), controlled viscous coupling fan drives (Bhat *et al.,* 2006) and hydraulically driven fan motors (Frick *et al.*, 2006). Further improvement can be realized with controlled water pumps. However, this benefit negatively affects engine temperature homogeneity which would only be improved with alternative water jacket designs.

The experiments demonstrated that steady state coolant temperature regulation was improved with computer control of the radiator fan, thermostat valve, and coolant pump (Tests 5 & 6) (set point temperature within ±0.5ºC). This system (Test 5 & 6) was able to meet the cooling needs with 60W power consumption. A reduction of 478W parasitic energy use in situations where vehicle ram-air provided a sufficient heat rejection rate when compared to the factory emulation power use of 538W(Test 1). However, with this increased level of control, the system revealed temperature variations of ±3.0ºC in Test 3 versus ±0.1ºC in Test 1 during transient response to ram-air.

APPENDICES

Appendix A Valve Prototype Parts

The valve components were modeled in SolidWorks. The following figures include the detail drawings used to produce the prototype parts.

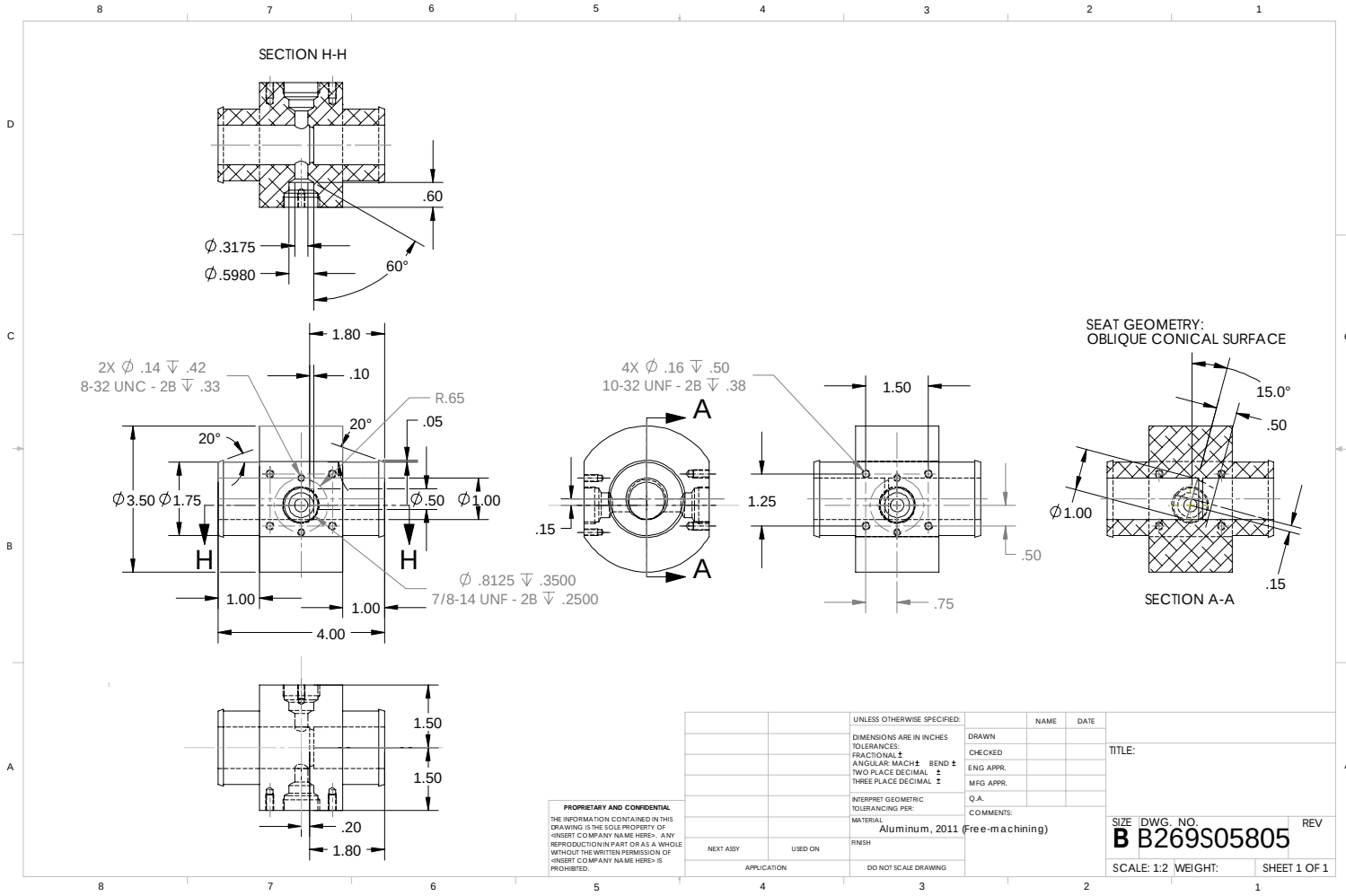

Figure A.1 Detail drawing: Valve body

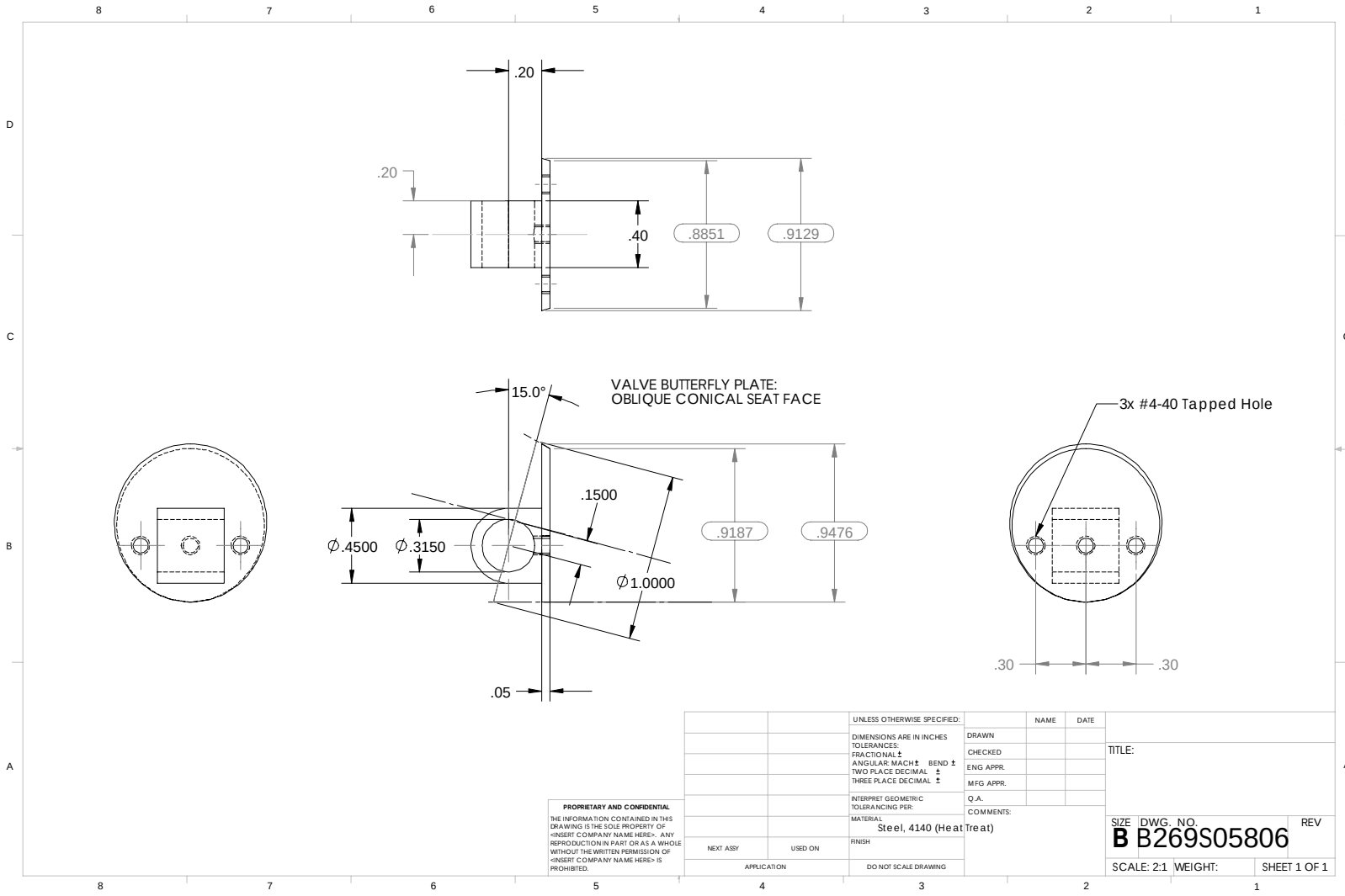

Figure A.2 Detail drawing: Valve flapper

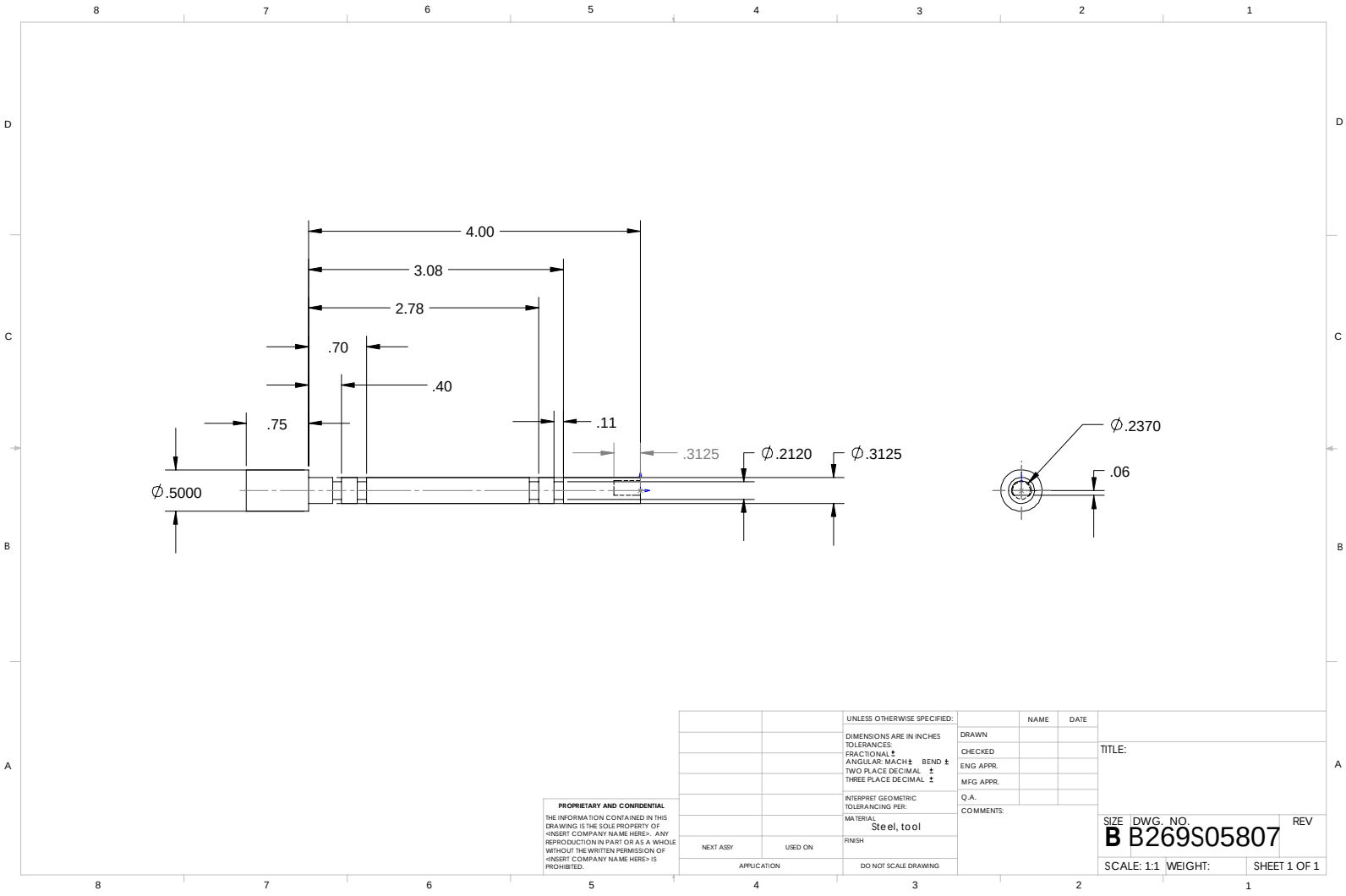

Figure A.3 Detail drawing: Valve pin

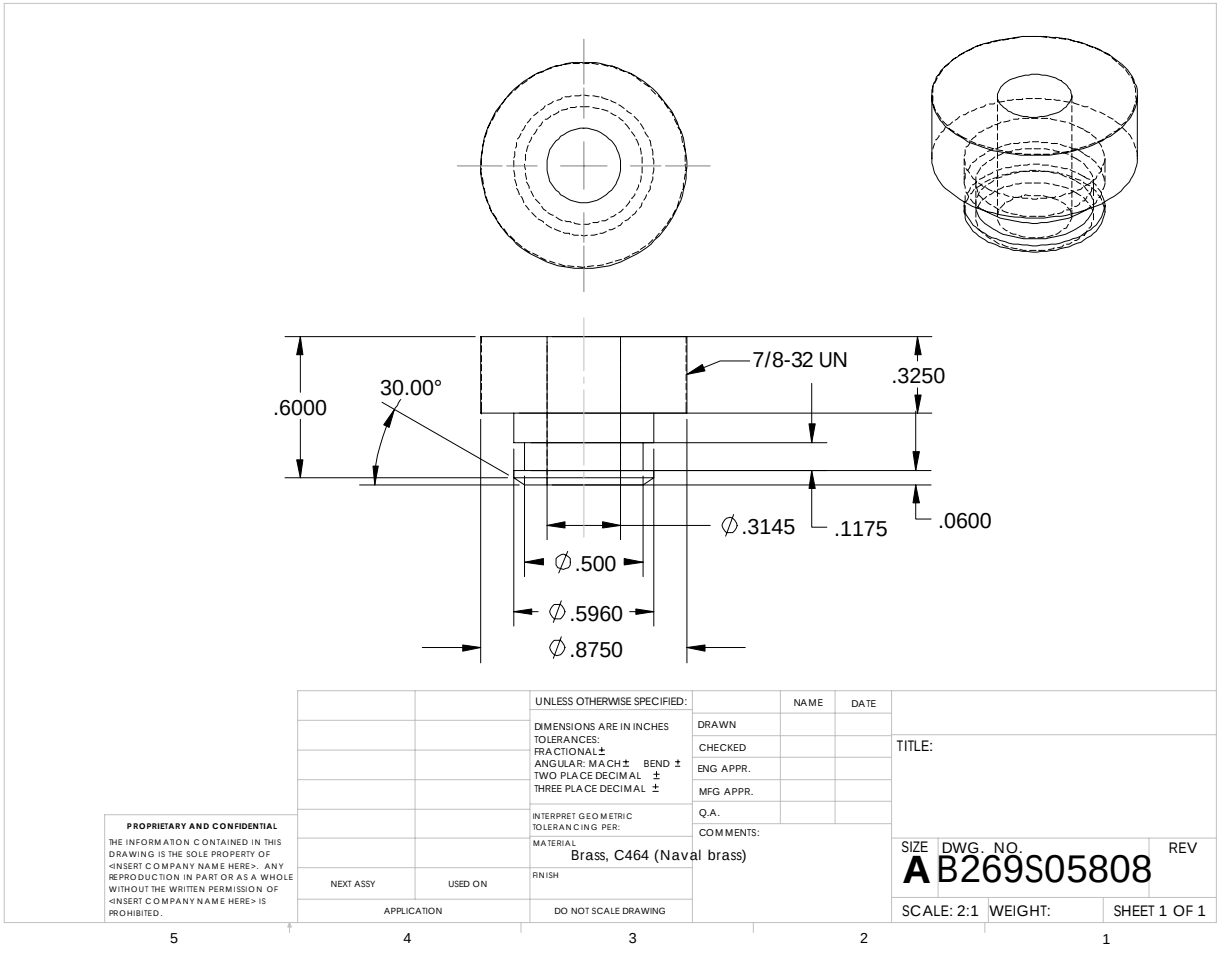

Figure A.4 Detail drawing: Valve seal bushing

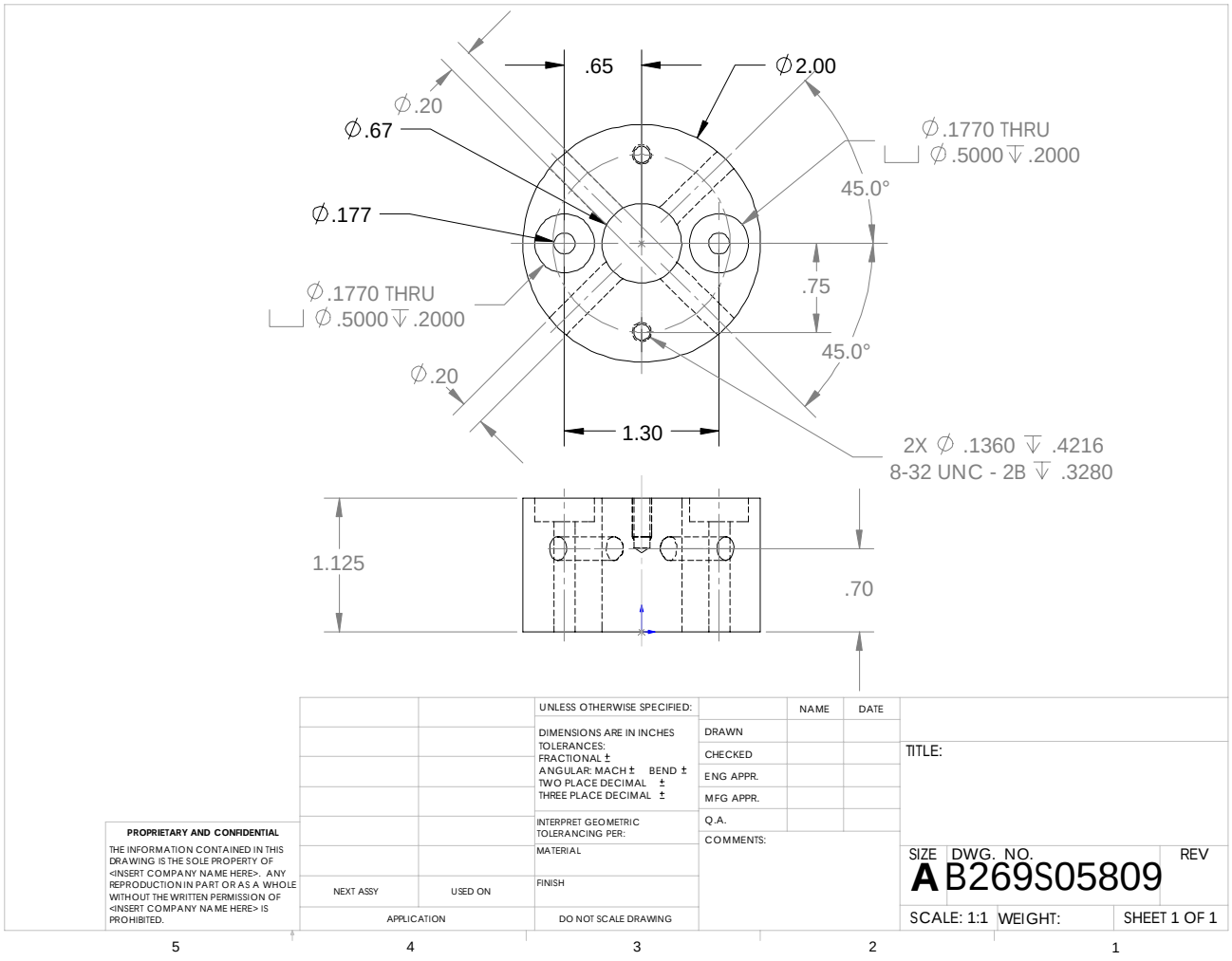

Figure A.5 Detail drawing: Valve/sensor mating plate

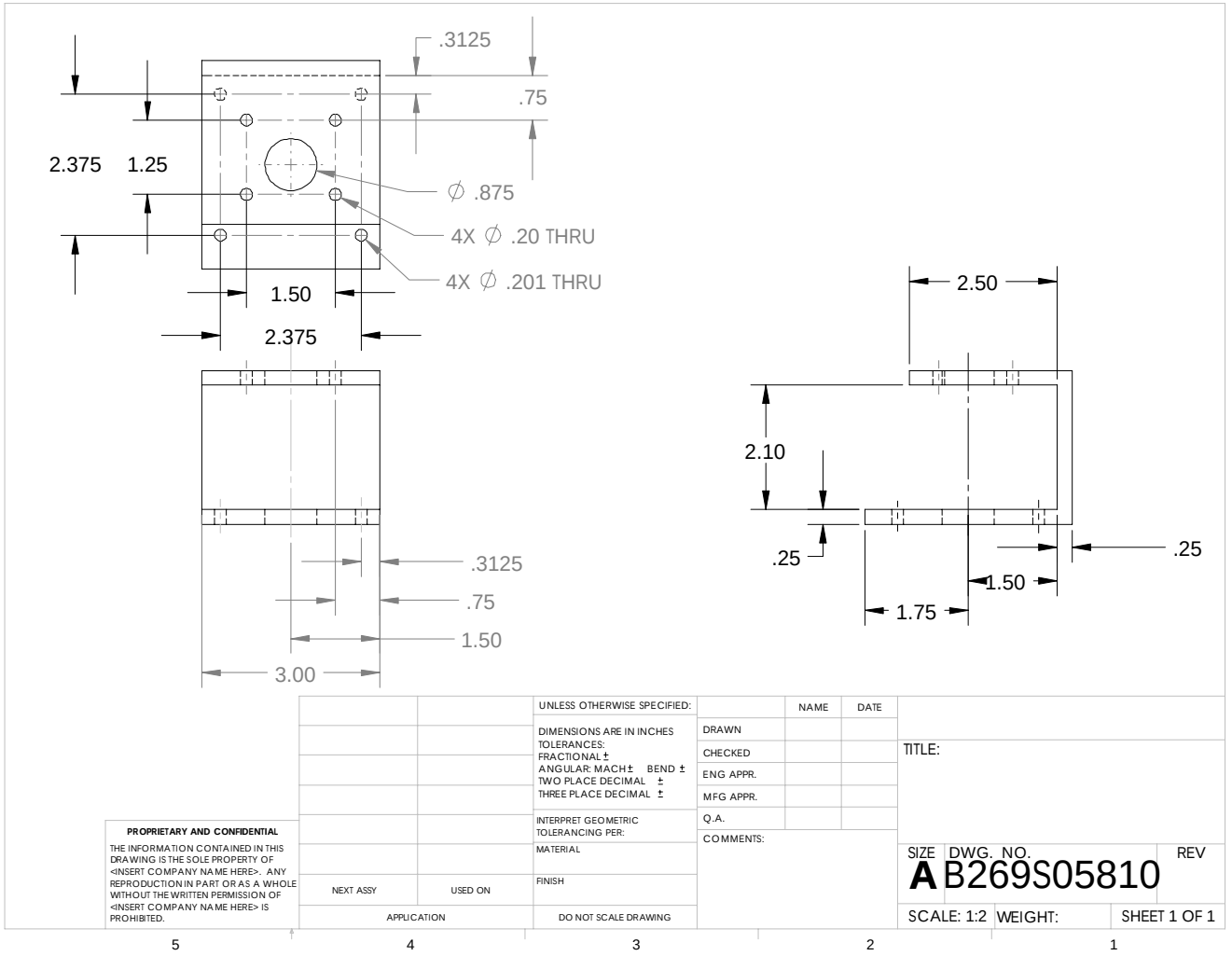

Figure A.6 Detail drawing: Valve/Actuator mounting plate

Appendix B Valve Frequency Response Analysis

The valve frequency response evaluation was facilitated using the time domain data with subsequent analysis in Matlab to determine the transfer function.

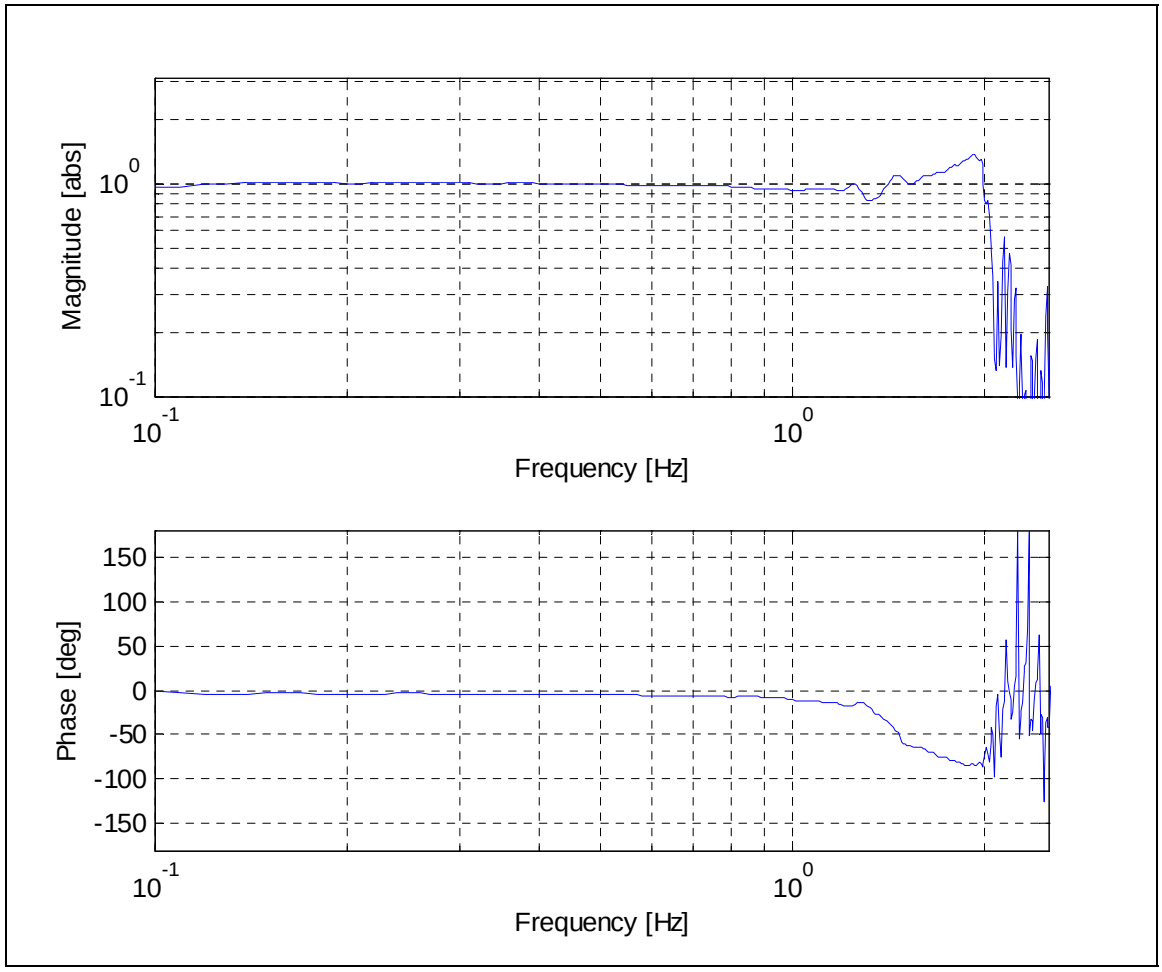

Figure B.1 Smart thermostat valve's transfer function estimate (θ_a / θ_d) for an input signal amplitude of 15º

Matlab Code and Notes

```
clc
close all
clear all

load valvetestchirp14

T=valvetestchirp14.X.Data(1:19500);

X=valvetestchirp14.Y(1,1).Data(1:19500);
Y=valvetestchirp14.Y(1,2).Data(1:19500);


figure
plot(T,X,T,Y)
title('Response to Chirp Signal (0.1 - 1 Hz)')
xlabel('Time (sec.)')
ylabel('\theta (degrees)')
legend('\theta_d', '\theta_a')
grid

[Txy,F]=tfe(Y,X,length(X),100,'linear');  % Transfer Function Estimate


figure
subplot(2,1,1),
loglog(F,abs(Txy))                          % Magnitude of TF
title('Transfer Function:   \theta_a / \theta_d')
grid
axis([.4 10^.7 10^(-2) 10^1.5])
xlabel('Frequency (Hz)')
ylabel('Magnitude (abs)')

for i=1:length(Txy);
    p(i)=angle(Txy(i));
end
                                            % Phase of TF
subplot(2,1,2),semilogx(F,-p*57.3);
axis([.4 10^.7 -180 180])
grid
ylabel('Phase (degrees)')
xlabel('Frequency (Hz)')
```

Appendix C Valve Design Tool and Multi-Pipe Study

The purpose underlying the validation of the valve coefficient is to provide a design tool for this geometric class of butterfly valves. An acceptable valve coefficient for various valve positions allows the following set of equations to determine the required valve size for a given system. The application details necessary are the pressure drop and flow rate ranges. To sufficiently evaluate the valve design tool, a prototype valve of the target design geometry has been produced and tested for pressure head and flow rate ranges. A set of tests are performed to create graphs and empirically derive dimensionless valve coefficients for incremental valve positions. The equation is based on the Darcy-Weisbach equation which relates flow and head by a restriction coefficient (Driskell, 1983)

$$dH = K\frac{V^2}{2g} \tag{C.1}$$

The left hand side represents the pressure head and is equated to some restriction coefficient multiplied by the velocity head, $V^2/2g$. For each valve position there exists a distinct restriction coefficient. The equation used to determine this coefficient is by way of a dimensionless valve coefficient

$$C_d = \frac{V}{\sqrt{2g\Delta H + V^2}} \tag{C.2}$$

$$K = \frac{1}{C_d{}^2} - 1 \tag{C.3}$$

The data is presented with its associated C_d coefficient in Figure C.1. It should be noted in this set of plots, the valve is incremented in steps from 0º to 80º measured from the fully open position.

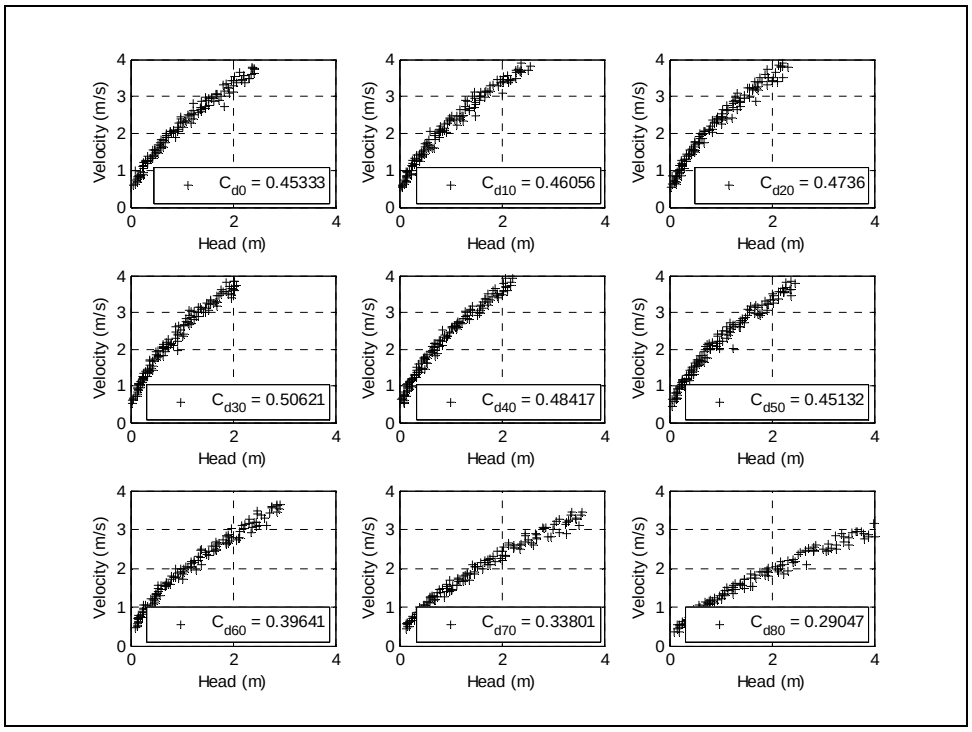

Figure C.1 Dimensionless valve coefficients for specific valve positions

The valve coefficients can then be evaluated for the relationship they have with the valve position. Utilizing a least squares regression, a polynomial has been developed for the relation where this valve coefficient will remain constant for this geometric set of valves. Figure C.2 shows the valve coefficients and the fitted polynomial to the data.

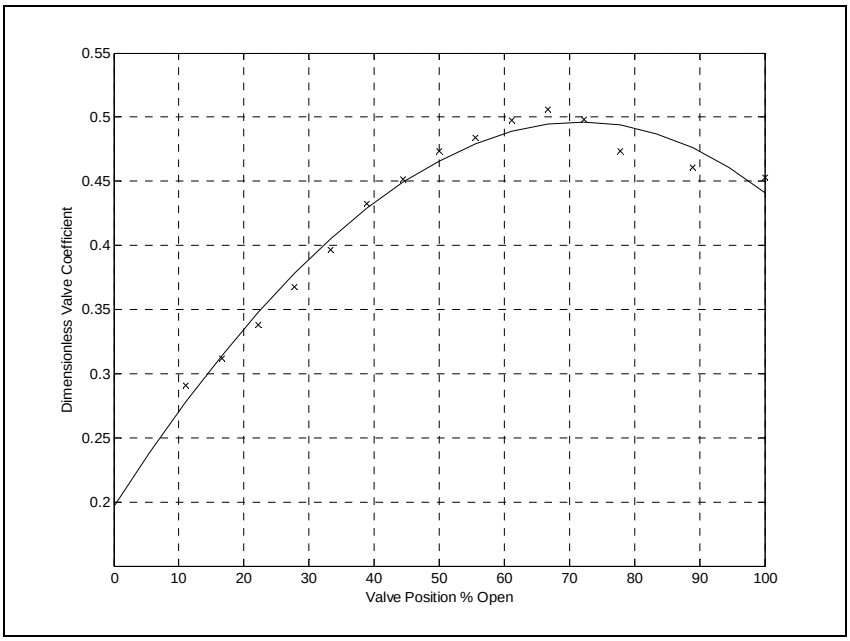

Figure C.2 Valve coefficients and polynomial fit for the valve's operation range

The valve coefficients continue to decrease as the valve closes. Interesting in this data is the trend indicating increased losses at valve positions between 80% and 100% open. This observation though unintuitive, must be attributed to this offset cam valve. Two side view sections are taken from the assembly drawings where the valve is in its 65% and 100% positions as seen in Figure C.3.

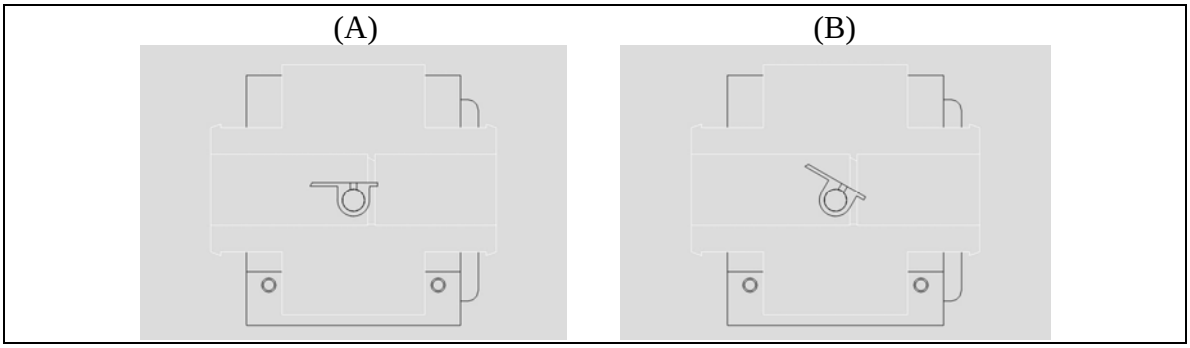

Figure C.3 Valve cross sectional views at (A) 100% and (B) 65% open positions

The resistance coefficient for these calculated valve coefficients are presented in Figure C.4. The minimum in the resistance coefficient does not occur at the fully open condition, though it does occur at the 65% position. The resistance coefficient of this valve offers an excellent manner to show how well the valve controls the fluid flow throughout the valve travel. As shown in Figure C.4, the resistance decreases over the travel up to 65%. Opening the valve more than this would not provide any more controllability. The valve's ability to control flow is presented with the radiator oriented in parallel where they are subjected to the same pressure drop.

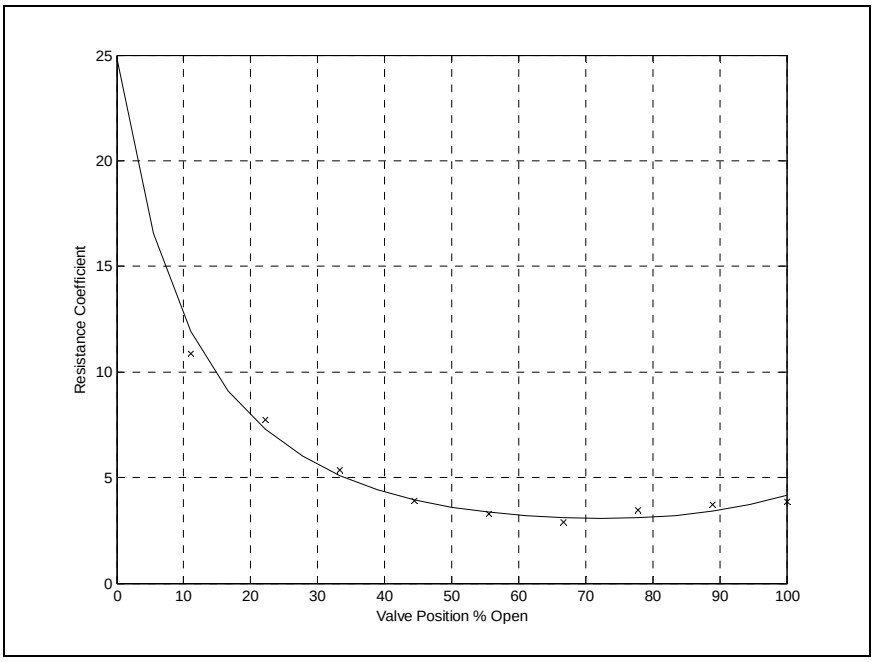

Figure C.4 Valve resistance coefficient

Matlab Code and Notes

The valve coefficient is determined utilizing standards set forth by Driskell (1983). The pressure head and fluid velocity through the valve diameter is used to determine the valve dimensionless coefficient that applies to the valves of this geometric type.

```
clear all
close all
clc

%%%%%%%%%%%%%%
%%%%%%%%%%%%%%

load VPCV00SI

MOH00 = KPAvpcv00*0.10199;                          % METERS OF HEAD
VVI00 = LPMvpcv00*.001/60/(pi*0.0254^2/4);          % VELOCITY INLET VALVE
1.00" VALVE INLET
CD00 = VVI00./(2*9.81.*MOH00+VVI00.^2).^(1/2);      % Dimensionless Valve
Coefficient
K00 = 1./CD00.^2 - 1;                               % Resistance Coefficient K
CD00m = mean(CD00);

figure
plot(MOH00,VVI00,'k+');  legend(num2str(CD00m)); xlabel('Head (m)');
ylabel('Valve Velocity');grid

%%%%%%%%%%%%%%
%%%%%%%%%%%%%%

load VPCV15SI

MOH15 = KPAvpcv15*0.10199;                          % METERS OF HEAD
VVI15 = LPMvpcv15*.001/60/(pi*0.0254^2/4);          % VELOCITY INLET VALVE
1.00" VALVE INLET
CD15 = VVI15./(2*9.81.*MOH15+VVI15.^2).^(1/2);      % Dimensionless Valve
Coefficient
K15 = 1./CD15.^2 - 1;                               % Resistance Coefficient K
CD15m = mean(CD15);


%%%%%%%%%%%%%%
%%%%%%%%%%%%%%


load VPCV10SI

MOH10 = KPAvpcv10*0.10199;                          % METERS OF HEAD
VVI10 = LPMvpcv10*.001/60/(pi*0.0254^2/4);          % VELOCITY INLET VALVE
1.00" VALVE INLET
CD10 = VVI10./(2*9.81.*MOH10+VVI10.^2).^(1/2);      % Dimensionless Valve
Coefficient
K10 = 1./CD10.^2 - 1;                               % Resistance Coefficient K
CD10m = mean(CD10);
```

```
%%%%%%%%%%%%%%
%%%%%%%%%%%%%%

load VPCV15SI

MOH15 = KPAvpcv15*0.10199;                          % METERS OF HEAD
VVI15 = LPMvpcv15*.001/60/(pi*0.0254^2/4);          % VELOCITY INLET VALVE
1.00" VALVE INLET
CD15 = VVI15./(2*9.81.*MOH15+VVI15.^2).^(1/2);      % Dimensionless Valve
Coefficient
K15 = 1./CD15.^2 - 1;                               % Resistance Coefficient K
CD15m = mean(CD15);


%%%%%%%%%%%%%%
%%%%%%%%%%%%%%


load VPCV20SI

MOH20 = KPAvpcv20*0.10199;                          % METERS OF HEAD
VVI20 = LPMvpcv20*.001/60/(pi*0.0254^2/4);          % VELOCITY INLET VALVE
1.00" VALVE INLET
CD20 = VVI10./(2*9.81.*MOH20+VVI20.^2).^(1/2);      % Dimensionless Valve
Coefficient
K20 = 1./CD20.^2 - 1;                               % Resistance Coefficient K
CD20m = mean(CD20);


%%%%%%%%%%%%%%
%%%%%%%%%%%%%%

load VPCV25SI

MOH25 = KPAvpcv25*0.10199;                          % METERS OF HEAD
VVI25 = LPMvpcv25*.001/60/(pi*0.0254^2/4);          % VELOCITY INLET VALVE
1.00" VALVE INLET
CD25 = VVI25./(2*9.81.*MOH25+VVI25.^2).^(1/2);      % Dimensionless Valve
Coefficient
K25 = 1./CD25.^2 - 1;                               % Resistance Coefficient K
CD25m = mean(CD25);


%%%%%%%%%%%%%%
%%%%%%%%%%%%%%


load VPCV30SI

MOH30 = KPAvpcv30*0.10199;                          % METERS OF HEAD
VVI30 = LPMvpcv30*.001/60/(pi*0.0254^2/4);          % VELOCITY INLET VALVE
1.00" VALVE INLET
CD30 = VVI30./(2*9.81.*MOH30+VVI30.^2).^(1/2);      % Dimensionless Valve
Coefficient
K30 = 1./CD30.^2 - 1;                               % Resistance Coefficient K
CD30m = mean(CD30);


%%%%%%%%%%%%%%
%%%%%%%%%%%%%%

load VPCV35SI
```

```
MOH35 = KPAvpcv35*0.10199;                          % METERS OF HEAD
VVI35 = LPMvpcv35*.001/60/(pi*0.0254^2/4);          % VELOCITY INLET VALVE
1.00" VALVE INLET
CD35 = VVI35./(2*9.81.*MOH35+VVI35.^2).^(1/2);      % Dimensionless Valve
Coefficient
K35 = 1./CD35.^2 - 1;                               % Resistance Coefficient K
CD35m = mean(CD35);


%%%%%%%%%%%%%
%%%%%%%%%%%%%


load VPCV40SI

MOH40 = KPAvpcv40*0.10199;                          % METERS OF HEAD
VVI40 = LPMvpcv40*.001/60/(pi*0.0254^2/4);          % VELOCITY INLET VALVE
1.00" VALVE INLET
CD40 = VVI40./(2*9.81.*MOH40+VVI40.^2).^(1/2);      % Dimensionless Valve
Coefficient
K40 = 1./CD40.^2 - 1;                               % Resistance Coefficient K
CD40m = mean(CD40);


%%%%%%%%%%%%%
%%%%%%%%%%%%%

load VPCV45SI

MOH45 = KPAvpcv45*0.10199;                          % METERS OF HEAD
VVI45 = LPMvpcv45*.001/60/(pi*0.0254^2/4);          % VELOCITY INLET VALVE
1.00" VALVE INLET
CD45 = VVI45./(2*9.81.*MOH45+VVI45.^2).^(1/2);      % Dimensionless Valve
Coefficient
K45 = 1./CD45.^2 - 1;                               % Resistance Coefficient K
CD45m = mean(CD45);


%%%%%%%%%%%%%
%%%%%%%%%%%%%


load VPCV50SI

MOH50 = KPAvpcv50*0.10199;                          % METERS OF HEAD
VVI50 = LPMvpcv50*.001/60/(pi*0.0254^2/4);          % VELOCITY INLET VALVE
1.00" VALVE INLET
CD50 = VVI50./(2*9.81.*MOH50+VVI50.^2).^(1/2);      % Dimensionless Valve
Coefficient
K50 = 1./CD50.^2 - 1;                               % Resistance Coefficient K
CD50m = mean(CD50);


%%%%%%%%%%%%%
%%%%%%%%%%%%%

load VPCV55SI

MOH55 = KPAvpcv55*0.10199;                          % METERS OF HEAD
VVI55 = LPMvpcv55*.001/60/(pi*0.0254^2/4);          % VELOCITY INLET VALVE
1.00" VALVE INLET
```

```
CD55 = VVI55./(2*9.81.*MOH55+VVI55.^2).^(1/2);      % Dimensionless Valve
Coefficient
K55 = 1./CD55.^2 - 1;                               % Resistance Coefficient K
CD55m = mean(CD55);


%%%%%%%%%%%%%
%%%%%%%%%%%%%

load VPCV60SI

MOH60 = KPAvpcv60*0.10199;                          % METERS OF HEAD
VVI60 = LPMvpcv60*.001/60/(pi*0.0254^2/4);          % VELOCITY INLET VALVE
1.00" VALVE INLET
CD60 = VVI60./(2*9.81.*MOH60+VVI60.^2).^(1/2);      % Dimensionless Valve
Coefficient
K60 = 1./CD60.^2 - 1;                               % Resistance Coefficient K
CD60m = mean(CD60);


%%%%%%%%%%%%%
%%%%%%%%%%%%%

load VPCV65SI

MOH65 = KPAvpcv65*0.10199;                          % METERS OF HEAD
VVI65 = LPMvpcv65*.001/60/(pi*0.0254^2/4);          % VELOCITY INLET VALVE
1.00" VALVE INLET
CD65 = VVI65./(2*9.81.*MOH65+VVI65.^2).^(1/2);      % Dimensionless Valve
Coefficient
K65 = 1./CD65.^2 - 1;                               % Resistance Coefficient K
CD65m = mean(CD65);


%%%%%%%%%%%%%
%%%%%%%%%%%%%

load VPCV70SI

MOH70 = KPAvpcv70*0.10199;                          % METERS OF HEAD
VVI70 = LPMvpcv70*.001/60/(pi*0.0254^2/4);          % VELOCITY INLET VALVE
1.00" VALVE INLET
CD70 = VVI70./(2*9.81.*MOH70+VVI70.^2).^(1/2);      % Dimensionless Valve
Coefficient
K70 = 1./CD70.^2 - 1;                               % Resistance Coefficient K
CD70m = mean(CD70);


%%%%%%%%%%%%%
%%%%%%%%%%%%%

load VPCV75SI

MOH75 = KPAvpcv75*0.10199;                          % METERS OF HEAD
VVI75 = LPMvpcv75*.001/60/(pi*0.0254^2/4);          % VELOCITY INLET VALVE
1.00" VALVE INLET
CD75 = VVI75./(2*9.81.*MOH75+VVI75.^2).^(1/2);      % Dimensionless Valve
Coefficient
K75 = 1./CD75.^2 - 1;                               % Resistance Coefficient K
CD75m = mean(CD75);


%%%%%%%%%%%%%
```

```
%%%%%%%%%%%%%%

load VPCV80SI

MOH80 = KPAvpcv80*0.10199;                              % METERS OF HEAD
VVI80 = LPMvpcv80*.001/60/(pi*0.0254^2/4);              % VELOCITY INLET VALVE
1.00" VALVE INLET
CD80 = VVI80./(2*9.81.*MOH80+VVI80.^2).^(1/2);          % Dimensionless Valve
Coefficient
K80 = 1./CD80.^2 - 1;                                   % Resistance Coefficient K
CD80m = mean(CD80);


%%%%%%%%%%%%%%
%%%%%%%%%%%%%%

figure
subplot(3,3,1),plot(MOH00,VVI00,'k+'); legend(sprintf('C_d_0 = %0.5g',CD00m),
'Location','SouthEast'); xlabel('Head (m)'); ylabel('Velocity
(m/s)');grid;axis([0 4  0 4])
subplot(3,3,2),plot(MOH10,VVI10,'k+'); legend(sprintf('C_d_1_0 = %0.5g',CD10m),
'Location','SouthEast'); xlabel('Head (m)'); ylabel('Velocity
(m/s)');grid;axis([0 4  0 4])
subplot(3,3,3),plot(MOH20,VVI20,'k+'); legend(sprintf('C_d_2_0 = %0.5g',CD20m),
'Location','SouthEast'); xlabel('Head (m)'); ylabel('Velocity
(m/s)');grid;axis([0 4  0 4])
subplot(3,3,4),plot(MOH30,VVI30,'k+'); legend(sprintf('C_d_3_0 = %0.5g',CD30m),
'Location','SouthEast'); xlabel('Head (m)'); ylabel('Velocity
(m/s)');grid;axis([0 4  0 4])
subplot(3,3,5),plot(MOH40,VVI40,'k+'); legend(sprintf('C_d_4_0 = %0.5g',CD40m),
'Location','SouthEast'); xlabel('Head (m)'); ylabel('Velocity
(m/s)');grid;axis([0 4  0 4])
subplot(3,3,6),plot(MOH50,VVI50,'k+'); legend(sprintf('C_d_5_0 = %0.5g',CD50m),
'Location','SouthEast'); xlabel('Head (m)'); ylabel('Velocity
(m/s)');grid;axis([0 4  0 4])
subplot(3,3,7),plot(MOH60,VVI60,'k+'); legend(sprintf('C_d_6_0 = %0.5g',CD60m),
'Location','SouthEast'); xlabel('Head (m)'); ylabel('Velocity
(m/s)');grid;axis([0 4  0 4])
subplot(3,3,8),plot(MOH70,VVI70,'k+'); legend(sprintf('C_d_7_0 = %0.5g',CD70m),
'Location','SouthEast'); xlabel('Head (m)'); ylabel('Velocity
(m/s)');grid;axis([0 4  0 4])
subplot(3,3,9),plot(MOH80,VVI80,'k+'); legend(sprintf('C_d_8_0 = %0.5g',CD80m),
'Location','SouthEast'); xlabel('Head (m)'); ylabel('Velocity
(m/s)');grid;axis([0 4  0 4])

%%%%%%%%%%%%%%
%%%%%%%%%%%%%%

VP2CD = [ [0 10 20 30 40 50 60 70 80]' [CD00m CD10m CD20m CD30m CD40m CD50m
CD60m CD70m CD80m]' (1./[CD00m CD10m CD20m CD30m CD40m CD50m CD60m CD70m
CD80m].^2-1)'];

[Pcd,Scd,MUcd] = polyfit(VP2CD(:,1),VP2CD(:,2),4);
ValPos = 0:90;
CdFitted = polyval(Pcd, ValPos, Scd, MUcd);

figure
hidden on
plot((90-VP2CD(:,1))*100/90,VP2CD(:,2),'kx',(90-ValPos)*100/90, CdFitted, 'k');
xlabel('Valve Position % Open'); ylabel('Dimensionless Valve Coefficient');
grid

%%%%%%%%%%%%%%
```

```
%%%%%%%%%%%%%

VP2CDd = [ [0 10 20 25 30 35 40 45 50 55 60 65 70 75 80]' [CD00m CD10m CD20m
CD25m CD30m CD35m CD40m CD45m CD50m CD55m CD60m CD65m CD70m CD75m CD80m]'];
save VP2CDd VP2CDd
SUCCESS = xlswrite('C:\Documents and Settings\John Howard Chastain\My
Documents\MS Thesis\Current Research\Radiator Modelling\VP2CDd.xls',VP2CDd)
[Pcdd,Scdd,MUcdd] = polyfit(VP2CDd(:,1),VP2CDd(:,2),3);
ValPos = 0:5:90;
CddFitted = polyval(Pcdd, ValPos, Scdd, MUcdd);
KdFitted = 1./CddFitted.^2 - 1;
figure
plot((90-VP2CDd(:,1))*100/90,VP2CDd(:,2),'kx',(90-ValPos)*100/90,
CddFitted,'k'); xlabel('Valve Position % Open'); ylabel('Dimensionless Valve
Coefficient'); grid

figure
plot((90-ValPos)*100/90, KdFitted,'k',(90-VP2CD(:,1))*100/90,VP2CD(:,3),'xk');
xlabel('Valve Position % Open'); ylabel('Resistance Coefficient'); grid

HeadRange = 0:.25:5;                                    % Meters of Head
for i = 1:length(KdFitted)
    for j = 1:length(HeadRange)
        Velocity(i,j) = sqrt(2*9.81*HeadRange(j)/(KdFitted(i)));
    end
end

figure
surf((90-ValPos)*100/90, HeadRange, Velocity'); xlabel('Valve Position %
Open'); ylabel('Head (m)'); zlabel('Velocity (m/s)')
hold on
plot3((90-AVPvpcv00)/90*100, MOH00, VVI00, 'kx', (90-AVPvpcv10)/90*100, MOH10,
VVI10, 'kx', (90-AVPvpcv20)/90*100, MOH20, VVI20, 'kx', (90-AVPvpcv30)/90*100,
MOH30, VVI30, 'kx', (90-AVPvpcv40)/90*100, MOH40, VVI40, 'kx', (90-
AVPvpcv50)/90*100, MOH50, VVI50, 'kx', ones(size(MOH30))*(90-60)/90*100, MOH60,
VVI60, 'kx', (90-AVPvpcv70)/90*100, MOH70, VVI70, 'kx', (90-AVPvpcv80)/90*100,
MOH80, VVI80,'kx')
hold off
```

The valve has been characterized utilizing a non-dimensional valve coefficient. The pressure-flow relation has been created such that the two way valve prototype can be used as a basis for any valve size within a constrained range (0.5” to 1.5”). The radiator has also been modeled for its pressure and flow characteristics. These two equations, with conservation of mass and equal pressure drop across two components oriented in parallel, provides the ability to solve for flow rates, and pressure drop in both components given a valve position and coolant flow rate. A Newton-Rhapson technique is facilitated to solve the multi-pipe model. The technique simultaneously solves the two pressure-flow relations for the valve and radiator loops as described in the following set of equations

$$h_r = 3.6261 V_r^{\,2} + 1.2476 V_r \tag{C.4}$$

$$h_v = K_d \frac{V_v^{\,2}}{2g} \tag{C.5}$$

$$C_d = 0.5865\left(\theta_v\right)^{0.341} \tag{C.6}$$

$$K_d = \frac{1}{C_d^{\,2}} - 1 \tag{C.7}$$

The solution is constrained by the conservation of mass and equal pressure drop across the radiator and valve. Conservation of mass can be extended to flow rate since constant specific volume is assumed in the incompressible substance model. These conclusions are used to derive

$$Q_c = Q_v + Q_r \tag{C.8}$$

$$h_v = h_r \tag{C.9}$$

These equations comprise the functions to be minimized through iteration. Each iteration will evaluate the sensitivity coefficients to be used in determining the changes to be made on the fluid velocities in the valve and radiator. The functions are described as follows

$$f_1 = h_v - h_r \tag{C.10}$$

$$f_2 = Q_c - \left(a_r V_r + a_v V_v\right) \tag{C.11}$$

where a_r is the radiator coolant flow area and a_v is the valve flow area.

The sensitivity coefficients are the partial derivatives of the velocities with respect to the functions. In order to determine the amount by which the velocities should be changed, one must take the first order terms from a Taylor series expansion of the nonlinear equations. Individual partial derivatives are substituted as

$$\frac{\partial f_1}{\partial V_v} = a_{11}, \frac{\partial f_1}{\partial V_r} = a_{12} \tag{C.12}$$

$$\frac{\partial f_2}{\partial V_v} = a_{21}, \frac{\partial f_2}{\partial V_r} = a_{22} \tag{C.13}$$

The changes must be simultaneously considered by solving the set of equations for each function and the necessary adjustments for velocities. The following equation is suggested by the Newton Rhapson technique and is comprised of the first order terms in the Taylor Series expansion of a non-linear equation

$$\begin{aligned} f_1\left(V_r, V_v\right) \approx\ & f_1\left(V_{r,c}, V_{v,c}\right) + \left[\frac{\partial f_1\left(V_{r,c}, V_{v,c}\right)}{\partial V_{r,c}}\right]\left(V_r - V_{r,c}\right) \\ & + \left[\frac{\partial f_1\left(V_{r,c}, V_{v,c}\right)}{\partial V_{v,c}}\right]\left(V_v - V_{v,c}\right) \end{aligned} \tag{C.14}$$

Putting these equations in matrix forms allows efficient solution in Matlab. Matlab is capable of solving for the velocity changes for each subsequent iteration $(\Delta V = V_x - V_{x,c})$ evaluating the solution of this linear set of equations represented as

$$\begin{bmatrix} a_{11} & a_{12} \\ a_{21} & a_{22} \end{bmatrix} \begin{Bmatrix} \Delta V_v \\ \Delta V_r \end{Bmatrix} = \begin{Bmatrix} f_1 \\ f_2 \end{Bmatrix} \tag{C.15}$$

To facilitate solution, initial guesses must be formed and solution tolerance must be implemented. This model is programmed in Matlab and can be implemented as an embedded Matlab function in Simulink. The output of this function is the pressure head across the components and the flow rates in each component given the overall system flow rate and valve position. This will now function as the multi-pipe model and can be used in valve sizing studies and simulations. The multi-pipe model is implemented in the scale bench simulation and has provided improved matching with experimental data.

Matlab Code and Notes

The algorithm mpipeSim.m is an embedded Matlab function that utilizes a Newton-Raphson solution technique to solve for head loss, volumetric flow rates, based on coolant flow rate and valve position.

```
function [dP, Qrad, Qv] = mpipeSim(Qc, ValPos)

if ValPos > 75;                                %% linear interpolate to zero
    Qrl = Qc; Qvl = 0;                         %% valve flow when closed
    [dP, Qrad2, Qv] = mpipeNR(Qc,75);
    Qrad = (Qrad2-Qrl)*(90-ValPos)/15 + Qrl;
    Qv = (Qv-Qvl)*(90-ValPos)/15;
else
    [dP, Qrad,Qv] = mpipeNR(Qc,ValPos);        %% Newton Rhapson Solution
end

%%%%%%%%%%%%%%%%%%%%%%%%%%%%%%%%%%%%%%%%%%%%%%%%%%%%%%%%%%
%%%%%%%%%%%%%%%%%%%%%%%%%%%%%%%%%%%%%%%%%%%%%%%%%%%%%%%%%%
%%%%%%%%%%%%%%%%%%%%%%%%%%%%%%%%%%%%%%%%%%%%%%%%%%%%%%%%%%


function [dP, Qrad, Qv] = mpipeNR(Qc, ValPos)  %% Newton Rhapson Solution


a = 2.032*10^(-3)-2*(.5*10^-5);         %%%%%%%%%%%%%%
b = 5.715*10^(-2)-2*(.5*10^-5);         %  Radiator  %
Acsc = (38*a*b);                        %  Flow Area %
                                        %%%%%%%%%%%%%%


%%%%%%%%%%%%%%%%%%%%%%%%%%%%%%%%%%%%%%%%
%%%%  Newton-Raphson Solution 2 NL  %%%%
%%%%                                %%%%
%%%%  Hr = 3.6261 Vr^2 + 1.2476 Vr  %%%%
%%%%                                %%%%
%%%%                                %%%%
%%%%  Hv = Kd * Vv^2/(2*g)          %%%%
%%%%%%%%%%%%%%%%%%%%%%%%%%%%%%%%%%%%%%%%

%%%%%%%%%%%%%%%%%%%%%%%%%%%%%%%%%%%%%%%%
%%%%    f1 = hv - hr                %%%%
%%%%    f2 = Q - (Vr*ar + Vv*av)    %%%%
%%%%%%%%%%%%%%%%%%%%%%%%%%%%%%%%%%%%%%%%

%%%%%%%%%%%%%%%%%%%%%%%%%%%%%%%%%%%%%%%%
%%%%      df1/dVv = Kd * Vv / g     %%%%
%%%% df1/dVr = 2(3.6261)Vr + 1.2476 %%%%
%%%%%%%%%%%%%%%%%%%%%%%%%%%%%%%%%%%%%%%%

%%%%%%%%%%%%%%%%%%%%%%%%%%%%%%%%%%%%%%%%
%%%%          df2/dVv = -av         %%%%
%%%%          df2/dVr = -ar         %%%%
%%%%%%%%%%%%%%%%%%%%%%%%%%%%%%%%%%%%%%%%
```

```
%% Conversion factors
av = (.001/60/(pi*0.0254^2/4))^(-1);    % Conversion factor for cons. of mass
                                        % (note incompressible/constant
density)
                                        % allows the volumetric flow rate to be
                                        % conserved.

ar = (.001/60/Acsc)^(-1);               % Conversion factor for cons. of mass
                                        % (note incompressible/constant
density)
                                        % allows the volumetric flow rate to be
                                        % conserved.

%%%%%%%%%%%%%%%%%%%%%%%%%%%%%%%%%%%%%%%%
%%%%  Kd = fcn(\theta_v_a_l_v_e)    %%%%
%%%%%%%%%%%%%%%%%%%%%%%%%%%%%%%%%%%%%%%%

Valperc = (90-ValPos)/90;               % Defining Valve Position
Cd = 0.5865*(Valperc)^0.341;            % Valve Coefficient
Kd = 1./Cd.^2 - 1;                      % Friction Factor

%%%%%%%%%%%%%%%%%%%%%%%%%%%%%%%%%%%%%%%%
%   First guess for Qs,  50/50 Qr/Qv   %
%%%%%%%%%%%%%%%%%%%%%%%%%%%%%%%%%%%%%%%%
    htv = 1;                            % initial pressure head guess
    htr = 1;                            % initial pressure head guess
    Vtv = (Qc * .5) / av;               % initial valve flow velocity guess
    Vtr = (Qc * .5) / ar;               % initial radiator flow velocity guess
    tol = 1;                            % setting tol as a loop variable
%%%%%%%%%%%%%%%%%%%%%%%%%%%%%%%%%%%%%%%%%%%%%
%   Newton Rhapson While Loop tol = 10^-5   %
%%%%%%%%%%%%%%%%%%%%%%%%%%%%%%%%%%%%%%%%%%%%%
while tol > 10^(-5);
    htv = Kd * Vtv^2 / (2*9.81);           % Valve Head (m)
    htr = (3.6261)*Vtr^2 + 1.2476*Vtr;     % Radiator Head (m)
            f1 = htv - htr;                % Minimize Head Error
            f2 = Qc - (ar*Vtr + av*Vtv);   % Minimize Conservation Error
            F = [   f1;
                    f2];
            a11 = Kd * Vtv / 9.81;
            a21 = -av;
            a12 = 2*(3.6261)*Vtr + 1.2476;
            a22 = -ar;
            A = [   a11     a21 ;          % A matrix for linear equation
                    a21     a22 ];         % solution
            dV = inv(A)*F;                 % Solving for changes in Flow
                                           % Velocity changes that minimize f1
                                           % and f2
            Vtv = Vtv - dV(1);
            Vtr = Vtr - dV(2);
            tol = max(F);
end

    dP = htv/(.101);        % DeltaP kPa
    Qrad = Vtr*ar;          % Radiator Flow Rate
    Qv = Vtv*av;            % Valve/Bypass Flow Rate
```

Appendix D Radiator Loss Model

Various losses within the thermal management system must be accounted for and evaluated in the total effectiveness of the system. The radiator pressure drop must be considered in calculating the total radiator effectiveness since some pumping power is used to overcome this friction. Evaluating the radiator pressure drop begins with the calculation of hydraulic diameter which is the ratio of four times the cross sectional area to the wetted perimeter. Using this hydraulic diameter as well as properties of the fluid, and fluid velocity, the Reynold's number is calculated as

$$D_h = \frac{4ab}{2a+2b} \tag{D.1}$$

$$\mathrm{Re}_{D_h} = \frac{D_h V \rho}{\mu} \tag{D.2}$$

The calculation of the friction factor for the radiator tube is possible using the following equation which is derived from the parallel-plate friction law and shows great agreement with experimental data. Friction for turbulent cases, $\mathrm{Re}_{D_h} \geq 2000$, is calculated by

$$\frac{1}{f^{1/2}} = 2.0\log\left(0.64\,\mathrm{Re}_{D_h}\, f^{1/2}\right) - 0.8 \tag{D.3}$$

and in all other cases it is calculated by

$$f = \frac{96}{\mathrm{Re}_{D_h}} \tag{D.4}$$

Important to the evaluation of system losses due to friction is quantify the pressure drop at the radiator. The calculation of the head loss and the pressure drop, suggested by White (2003), is accomplished with

$$h = f\left(\frac{L}{D_h}\right)\left(\frac{V^2}{2g}\right) \tag{D.5}$$

$$\Delta P = \rho g h \tag{D.6}$$

Radiator pressure drop has been experimentally modeled with pressure measurements and flow rates. Utilizing this information, the theoretical model has been validated against the experimental data. For completeness, an alternative model utilizing Colebrook's equation for friction factors has been used as well (White, 2003). Both models represent the experimental data very well with minimal errors across the flow range representative in system operation which can be observed in Figure D.1.

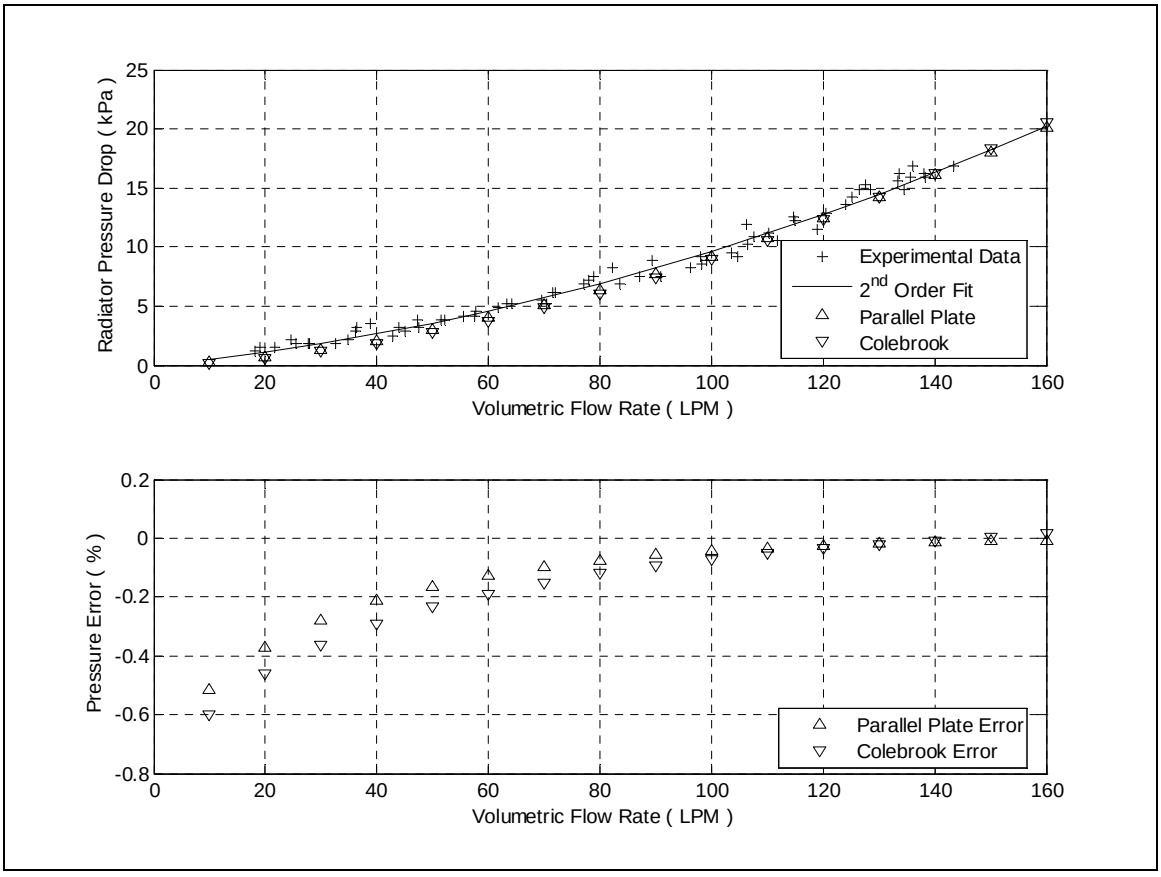

Figure D.1 Radiator theoretical pressure loss model with experimental data

A parallel plate based theoretical friction evaluation provides the best model of the experimental data and will be further evaluated with an uncertainty analysis. This uncertainty analysis calculates the error in the pressure drop related to errors in the evaluation of geometrical properties of the flow passages and measurement of flow rate.

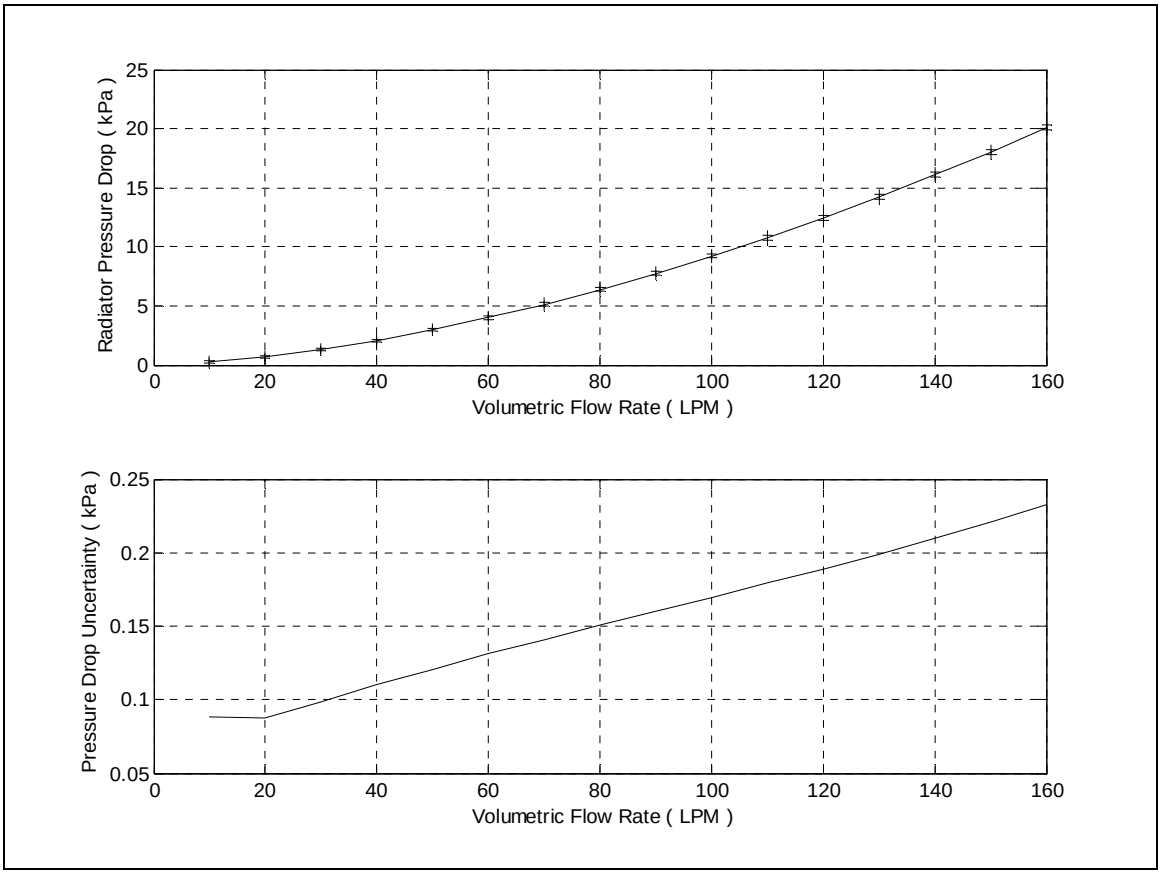

Figure D.2 Radiator pressure drop with uncertainty

Since the uncertainty resides within 0.1 kPa in the flow range, the use of this model in conjunction with a paddlewheel type flow meter to estimate pressure drop at the radiator is acceptable. The use of the friction factor equation derived from the parallel plate theory will suffice for the real-time measurement of pressure drop with a volumetric flow rate measurement. This volumetric flow rate measurement in application may not

be possible which may require special considerations. One consideration may be the use of an empirical model of the fluid dynamic behavior of the thermal management system. The basis of such an empirical model must reflect the flow rate in the radiator as a function of coolant system operating condition (Chastain and Wagner, 2006).

The end goal of such a pressure measurement is to determine the lost power at the radiator due to friction losses. This can be accomplished utilizing a calculation for water power which is a function of head loss and flow rate. The power loss at the radiator and calculation error is plotted in Figure B.3 and is calculated by

$$P_w = \rho g h Q \tag{D.7}$$

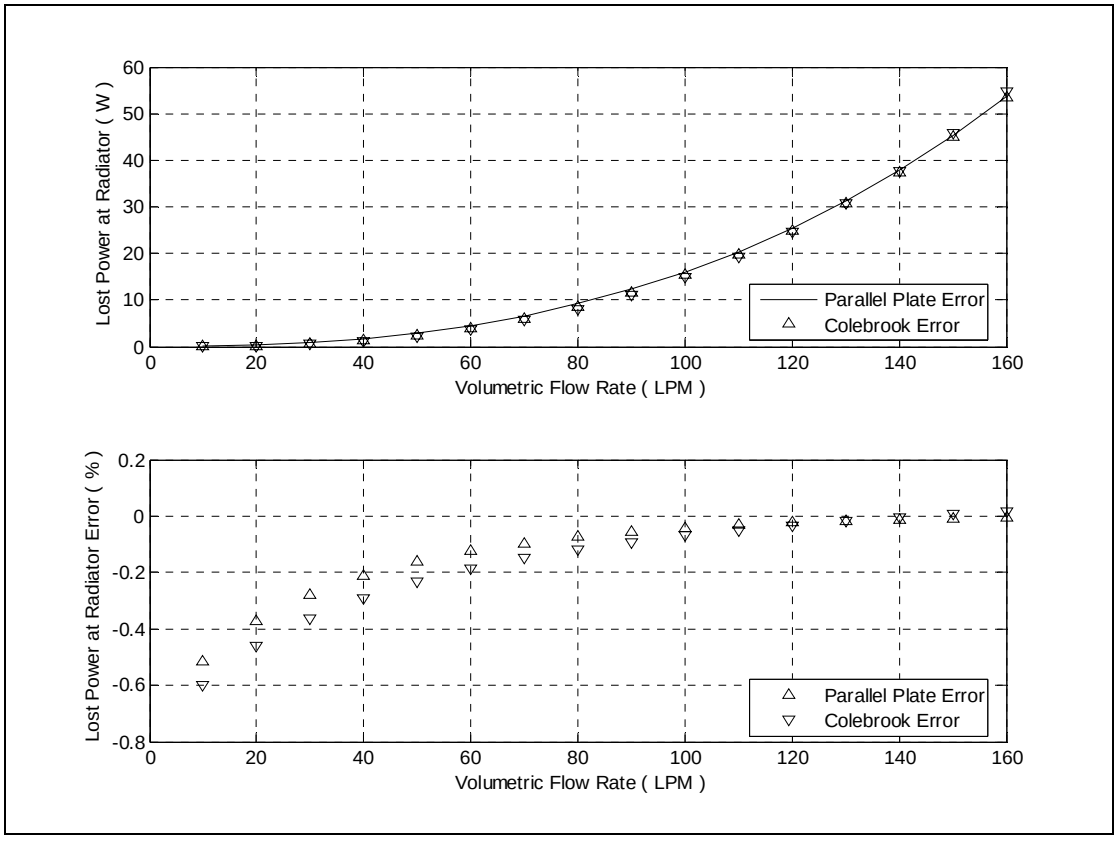

Figure D.3 Radiator power loss due to fluid friction

Matlab Code and Notes

Radiator friction loss model is based on the solution of a parallel plate theory derived relation for friction factor and is solved utilizing an iteration routine. The model relies on determination of the dimensions of the radiator flow passage, properties of water and temperature in order to calculate the Reynold's number of the water flow in the radiator passage. The relation for the friction factor is applicable for turbulent flows and is assumed to apply in the laminar range as well.

```
clear all
close all
clc

%%% water properties from Incropera and Dewitt
WTP =[      280     1       4.198   1422    582 10.26;
            290     0.999   4.184   1080    598 7.56;
            300     0.997   4.179   855     613 5.83;
            310     0.993   4.178   695     628 4.62;
            320     0.989   4.18    577     640 3.77;
            330     0.995   4.184   489     650 3.15;
            340     0.979   4.188   420     660 2.66;
            350     0.974   4.195   365     668 2.29;
            360     0.967   4.203   324     674 2.02;
            370     0.961   4.214   289     679 1.8];

[P1, S1, MU1] = polyfit(WTP(:,1),WTP(:,2),3);        % Density curve fit
[P2, S2, MU2] = polyfit(WTP(:,1),WTP(:,3),3);        % Specific heat curve fit
[P3, S3, MU3] = polyfit(WTP(:,1),WTP(:,4),3);        % Viscosity
[P4, S4, MU4] = polyfit(WTP(:,1),WTP(:,5),3);        % Thermal conductivity
[P5, S5, MU5] = polyfit(WTP(:,1),WTP(:,6),3);        % Prandtl number
T = 25+273;
rhoc = polyval(P1,T,S1,MU1)*1000;   % density           kg/m3
Cpc = polyval(P2,T,S2,MU2);         % specific heat     kJ/kgK
muc = polyval(P3,T,S3,MU3)*10^(-6); % viscosity         N-s/m2
kc = polyval(P4,T,S4,MU4)*10^(-3);    % th. cond.         W/mK
Prc = polyval(P5,T,S5,MU5);         % Prandtl           NonD

%%% Indicative Flow Rates

Q = 10:10:160; %LPM

a = 2.032*10^(-3)-2*(.5*10^-5);  % Height
b = 5.715*10^(-2)-2*(.5*10^-5);  % Width
Acsc = (38*a*b);                 % 38 tubes with cross section

%%%%%%%%%  Uncertainty Analysis  %%%%%%%%%%%%%%%
%% FP5100 with FP5310BR -> pipe ID = 1.009" = 0.0256 m
%% +/- 0.2 ft/s accuracy and +/- 0.5 ft/s repeatability
%% +/- 0.061 m/s accuracy and +/- 0.152 m/s repeatability
%% Q = AV = pi*D^2/4 V
```

```
D = 0.0256;               % Radiator Tube Diameter
A = pi*D^2/4;             % Radiator Tube Area

UQa = 0.061*A;            % Uncertainty in area
UQr = 0.152*A;            % Uncertainty to velocity

UQ = sqrt(UQa^2+UQr^2)*1000*60; % Flow measure uncertainty

%% Caliper measurements of Radiator Cross Section
%% Ul = +/-1.27*10^-5 m
%% Uacs = sqrt((Ul*a)^2 + (Ul*b)^2)

Ul = 1.27e-5;                          % Sensitivity to Length
Uacs = sqrt((Ul*a)^2 + (Ul*b)^2);      % Area measure uncertainty


%% Hydraulic Diameter Error
%% Using Sequencial Perturbation
Dhcp = 4*(a+Ul)*b/(2*(a+Ul)+2*b);
Dhcm = 4*(a-Ul)*b/(2*(a-Ul)+2*b);

UDhc = sqrt(2*((Dhcp-Dhcm)/2)^2);      % Uncertainty in Diameter measurement


%%%%   Radiator Dimensions
for i = 1:length(Q);

%% Velocity in Radiator Passage
thetaQ = 1/(60*1000*Acsc);       % Sensitivity of velocity to Flow measure
thetaA = -Q(i)*Acsc^(-2)/(60*1000);     % Sensitivity of area to flow measure

                                                    % Propagation of
UVc(i) = sqrt((thetaQ*UQ)^2 + (thetaA*Uacs)^2);     % Measurement uncertainty
                                                    % Velocity measurement
Vc(i) = Q(i)/60*.001/Acsc;
Dhc = 4*a*b/(2*a+2*b);                        % Hydraulic Diameter
ReDh(i) = Dhc*Vc(i)*rhoc/muc;                 % Reynold's Number

f0 = 0.04;                          % initial friction estimate

g = 9.81;           %m/ss
L = .828675;        %m


%% Reynold's Number Error

thetaReD(i) = Vc(i)*rhoc/muc;           % Sensitivity to Diameter
thetaReV = Dhc*rhoc/muc;                % Sensitivity to Velocity

UReDh(i) = sqrt((thetaReD(i).*UDhc).^2 + (thetaReV*UVc(i))^2);
                  % Error propagation Uncertainty in Reynold's number

% if ReDh(i) >= 2000             % Solving implicit equation through iteration
    for j=1:5                    % five loops is enough
            f0= ((2*log10(0.64*ReDh(i)*sqrt(f0)))-.8)^(-2);
    end
%     else
%       f0=96/ReDh(i);
% end
f0p = 0.04;                      % Solving another implicit equation through
    for j=1:5                    % iterating for five loops
            f0p = ((2*log10(0.64*(ReDh(i)+UReDh(i))*sqrt(f0p)))-.8)^(-2);
    end
```

```
f0m = 0.04;
    for j=1:5              % another implicit equation solution with
                           % worst case uncertainties
            f0m = ((2*log10(0.64*(ReDh(i)-UReDh(i))*sqrt(f0m)))-.8)^(-2);
    end

Uf0(i) = (f0p-f0m)/2;

fC = 0.04;
e = .00004;
    for j = 1:5            % another implicit equation solution with
                           % worst case uncertainties
            fC =(-2.0*log10((e/Dhc)/3.7 + 2.51/(ReDh(i)*sqrt(fC))))^(-2);
    end

% fCp = 0.04;
%     for j=1:5
%           fCp =(-2.0*log10((e/(Dhc)/3.7 +
2.51/((ReDh(i)+UReDh(i))*sqrt(fCp))))^(-2);
%     end
%
% fCm = 0.04;
%     for j=1:5
%           fCm =(-2.0*log10((e/Dhc)/3.7 + 2.51/((ReDh(i)-
UReDh(i))*sqrt(fCm))))^(-2);
%     end
%
% UfC(i) = (fCp-fCm)/2;

h2(i) = f0*L/Dhc*Vc(i)^2/(2);          % head through radiator coolant side
h3(i) = fC*L/Dhc*Vc(i)^2/(2);          % head through radiator coolant side

%% head loss error
thetahf(i) = L/Dhc*Vc(i)^2/(2);  % Sensitivity of head loss to friction factor
thetahL(i) = f0/Dhc*Vc(i)^2/(2); % Sensitivity of head loss to Length measure
thetahVc(i) = fC*L/Dhc*Vc(i)^3/(6);% Sensitivity of head loss to velocity

Uh2(i) = sqrt((thetahf(i)*Uf0(i))^2 + (thetahL(i)*Ul)^2 +
(thetahVc(i)*UVc(i))^2);         % error propagation head uncertainty

delp2(i) = rhoc * g * h2(i)./1000;      % pressure in kPa
thetadP = rhoc * g /1000;               % sensitivity to head measure
UdP2(i) = sqrt((thetadP * Uh2(i))^2);   % I trust tables no error in density
delp(i) = 0.0005*Q(i)^2 + 0.0464*Q(i);  % Empirical Pressure loss
delp3(i) =  rhoc * g * h3(i)./1000;     % Third Pressure for comparison

end                % end of a big loop
                   % Now beginning to plot the data

QDPdata = xlsread('radqdp','sheet1','a2:b66');

figure
subplot(2,1,1),plot(QDPdata(:,1),QDPdata(:,2),'+k',Q,delp,'k',Q,delp2,'k^',Q,de
lp3,'kV');legend('Experimental Data','2^n^d Order Fit','Parallel
Plate','Colebrook','Location','SouthEast');grid
xlabel('Volumetric Flow Rate ( LPM )');ylabel('Radiator Pressure Drop ( kPa
)');

% figure
% plot(Q,(delp-delp2),'^',Q,(delp-delp3),'V');legend('Parallel Plate
Error','Colebrook Error');grid
% xlabel('Volumetric Flow Rate ( LPM )');ylabel('Pressure Error ( kPa )');
```

```
subplot(2,1,2),plot(Q,(delp2-delp)./delp,'k^',Q,(delp3-
delp)./delp,'kV');legend('Parallel Plate Error','Colebrook
Error','Location','SouthEast');grid
xlabel('Volumetric Flow Rate ( LPM )');ylabel('Pressure Error ( % )');

h = delp*0.101998;
CMS = Q*.001/60; %cubic meter per second
WHP = CMS.*rhoc.*9.81.*h;        % Water power calculations
WHP2 = CMS.*rhoc.*9.81.*h2;      % using head loss and flow rate
WHP3 = CMS.*rhoc.*9.81.*h3;      % using head loss and flow rate

figure
subplot(2,1,1),plot(Q,WHP,'k',Q,WHP2,'k^',Q,WHP3,'kV');grid;xlabel('Volumetric
Flow Rate ( LPM )');ylabel('Lost Power at Radiator ( W )')
legend('Parallel Plate Error','Colebrook Error','Location','SouthEast')

subplot(2,1,2),plot(Q,(WHP2-WHP)./WHP,'k^',Q,(WHP3-
WHP)./WHP,'kV');grid;xlabel('Volumetric Flow Rate ( LPM )');ylabel('Lost Power
at Radiator Error ( % )')
legend('Parallel Plate Error','Colebrook Error','Location','SouthEast')

figure
subplot(2,1,1),plot(Q,(delp2+UdP2),'k+',Q,(delp2-
UdP2),'k+',Q,(delp2),'k');grid;xlabel('Volumetric Flow Rate ( LPM
)');ylabel('Radiator Pressure Drop ( kPa )')
subplot(2,1,2),plot(Q,UdP2,'k');grid;xlabel('Volumetric Flow Rate ( LPM
)');ylabel('Pressure Drop Uncertainty ( kPa )')
```

Appendix E Thermodynamic Simulation: Application and Validation

The combination of embedded function allows the simulation of the scale thermal bench. Adding pipe segments improves the transient accuracy of the simulation tool. Each pipe bases the thermal lag on pipe length and is variable effectively with the mass flow rate in the system. The temperature response show increased lag with slower flow rates and decreases with faster flow rates. Further improvements to the simulation include the implementation of the multi-pipe model. This dynamic model considers the interaction of the coolant flow and valve position in the bypass and radiator. The model is theoretically based and experimentally verified at room temperature. The entire simulation is based around the incompressible substance model where specific heat and specific volume are independent from temperature. Critical to the multi-pipe model is that the fluid has constant specific volume. Also in the multi-pipe model, transients in fluid flows are not modeled. Transients that drive this simulation are mainly observed in the temperatures and driven by the coolant mass in the system. At specific system nodes, radiator and engine, temperature transients are due to their masses and will only show in the coolant temperature responses. The materials surrounding the coolant also increase the thermal lag by the effects of thermal conductivity. Experiments are undertaken on the scale thermal bench to provide the comparison basis for model tuning.

The scale thermal bench, utilizing a bank of six heaters, is capable of 12kW in 2kW increments. The experiments utilize a model free PID controller which is used in conjunction with a feed-forward technique to control the pump and fan actuators. The fan and pump models are implemented in the simulation and have been considered to have a linear response between flow rate and control voltage. Transport delays are

implemented to account for the material conduction induced lag at the radiator. The model uses a transport delay in order to imitate the warming and cooling of the radiator tubes. However, a dynamic radiator model would much more rigorously model the transient behavior of the heat transfer at the radiator.

Overall, the model deficiencies can be attributed to some of the linear approximations for the system actuators and some of the neglected aspects of the heat transfer process. Further, the pump and fan exhibit a second order relationship between the actuator's speed and device's generated pressure head. These deviations can be observed in Figure E.1 where some of the temperatures, as well as actuator responses do not match between the two sets of data.

Figure E.1 displays the reactions of the system's response to temperature, which vary across the system as shown by the main system nodes at the radiator and engine at their inlet and outlet. The distributed nature of the model, where there exist individual pipe elements, allows the model to match the experimental temperature trajectories. Also shown in Figure E.1, the actuator responses have been controlled under identical structure in both the simulation and experiment. The actuator were modeled as linear elements and tuned to match the experimental results. The valve actuator trajectory is plotted along with the fan and pump control efforts.

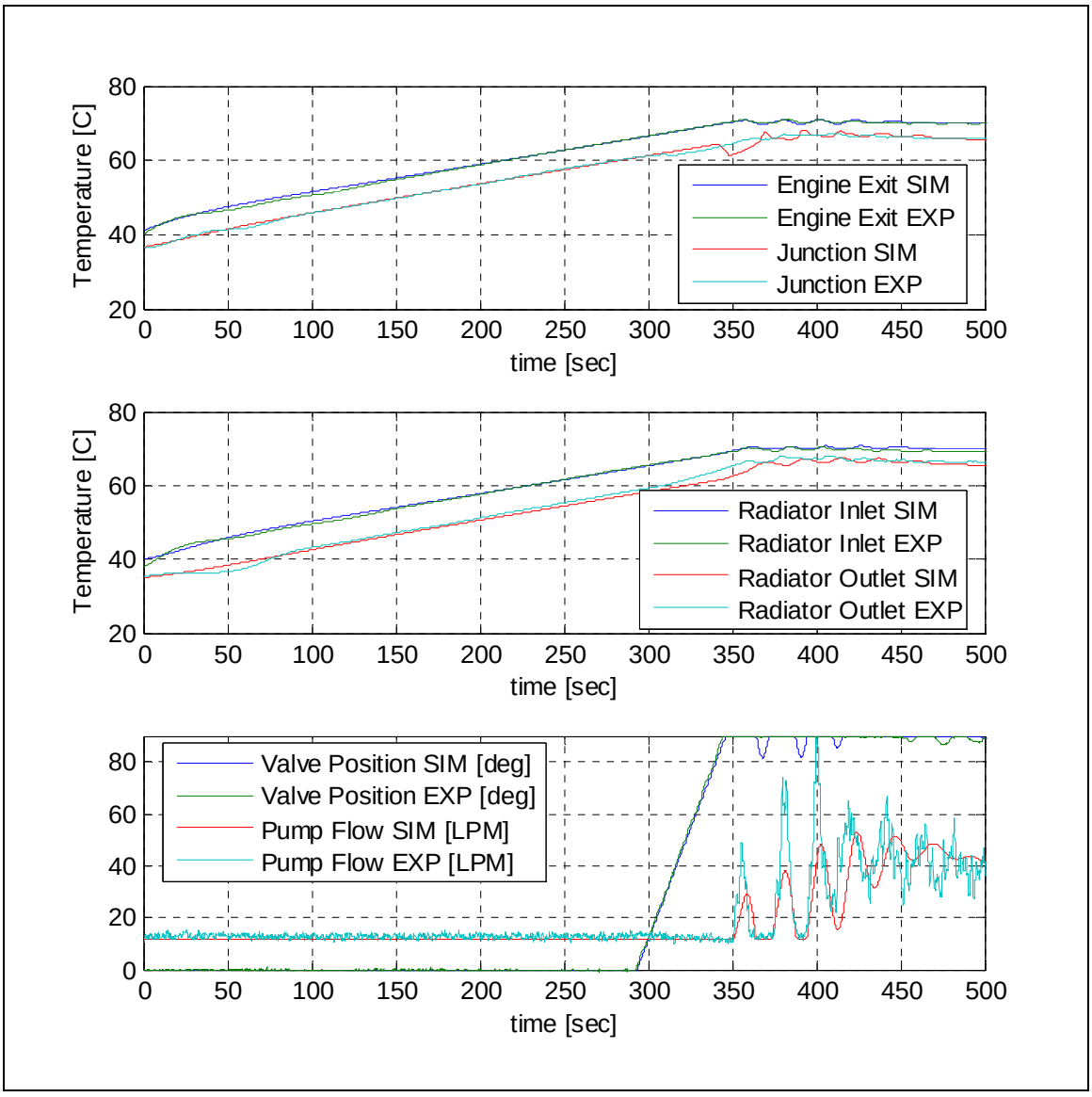

Figure E.1 Scale thermal bench theoretical and experimental response

The pump dynamic interaction with the system effectively denotes a time lag in the response of the actuator voltage and the flow rate. If this actuator behavior is modeled as a constant lag, the model may be tuned. Note that a rigorous accounting requires modeling the pump and system interaction based on conservation of momentum (Doebelin, 1998).

The radiator dynamic interaction with the environment/air-stream is also represented as a time lag. Again, this lag was tuned to match the experimental data. This lag can be explained by the radiator materials in causing heat transfer lags due to conduction.

It should be mentioned that the tuning of the thermal capacitances in this model is quite time consuming. The thermal capacitance initial estimates according to the amount of fluid contained in each node require some adjustment to represent the experimental data. Further efforts could apply on line model identification procedures to tune various model parameters.

This thermodynamic modeling takes place within the Matlab/Simulink environment. The two files presented here are used to evaluate the entropy generation and the thermodynamic model. The thermodynamic model implements the equations to be solved in the Simulink environment. The values and inherent structure is based on the experimental thermal scale bench

Matlab Code and Notes

TdotSim.m is an embedded Matlab function that represents the unsteady first law energy balances for system nodes. This model has eight nodes distributed in the system: three main nodes for the engine, radiator and junction; and five secondary pipe nodes which vary in length according to experimental system layout.

```
function [T1d,T2d,T5d,T6d,T7d,T8d,T9d,T10d] =
TdotSim(m_a,m_c,m_r,m_v,T1,T2,T5,T6,T7,T8,T9,T10)

Qe = 12;        % Heat Rejection Rate at Engine
eff = 0.30;     % Radiator Effectiveness
ca = 1.005;     % Air Specific Heat
Ta = 25;       % Ambient Air Temperature
cc = 4.217;     % Specific Heat of Coolant (Water)
me = 9.7;      % Mass of Coolant   : Engine
mr = 8.9;       %                   : Radiator
mj =  0.05;     %                   : Junction
mp1 = 1.0;      %                   : Pipe 1
mp2 = 1.0;      %                   : Pipe 2
mp3 =  3.0;     %                   : Pipe 3
mp4 =  1.2;     %                   : Pipe 4
mp5 =  14;      %                   : Pipe 5

%%%%%%%%%%%%%%%%%%%%%%%%%%%%%%%%%%%%%%%%%%%%%%%%%%%%%%%%%%%%%%%%%%%%%%%%%
%%
%%%%%%  First Law Energy Balance Equations for Thermal Simulation
%%%%%%%
%%%%%%           All Temperatures in Kelvin
%%%%%%%
%%%%%%%%%%%%%%%%%%%%%%%%%%%%%%%%%%%%%%%%%%%%%%%%%%%%%%%%%%%%%%%%%%%%%%%%%
%%

T1d = 1/(me*cc)*(Qe + m_c*cc*(T10-T1));
T2d = 1/(mp1*cc)*(m_c*cc*(T1-T2));
T5d = 1/(mp2*cc)*(m_r*cc*(T2-T5));
T6d = 1/(mr*cc)*(m_r*cc*(T5-T6) - eff*m_a*ca*(T5-Ta));
T7d = 1/(mp4*cc)*(m_r*cc*(T6-T7));
T8d = 1/(mp3*cc)*(m_c*cc*(T2-T8));
T9d = 1/(mj*cc)*(m_r*cc*T7 + m_v*cc*T8 - m_c*cc*T9);
T10d = 1/(mp5*cc)*(m_c*cc*(T9-T10));
```

Also implemented in the simulation tool is SGEN.m. This program takes the system parameters and conditions to calculate the entropy generation rate during simulations and controller evaluations.

```
function [Sgj,Sgr,Sge,Sgtot] =
SGEN(dPm,dPe,m_a,m_c,m_r,m_v,T1,T2,T5,T6,T7,T8,T9,T10)

Qe = 12;        % Heat Rejection Rate at Engine
Tec = 400;      % Temperature of Cylinder Wall
Ta = 298;       % Ambient Air Temperature
cc = 4.217;     % Specific Heat of Coolant (Water)
vc = 1/956.8;   % Specific Volume of Coolant (Water)
ca = 1.005;     % Air Specific Heat
eff = 0.3;     % Radiator Effectiveness
Pa = 101*10^3;  % Atmospheric Pressure (Pa)
Tao = Ta + eff*((T5+273)-Ta);
asdp = 1.0728*m_a^2+.6112*m_a; %Pa
R = 8.314/28.97;

Pa2 = (Pa-asdp)/Pa;     % bar
Pa1 = 1;                %bar
%%%%%%%%%%%%%%%%%%%%%%%%%%%%%%%%%%%%%%%%%%%%%%%%%%%%%%%%%%%%%%%%%%%%%%%%%%%%%%%%
%%
%%%%%%  Exergy Balance Equations To Compute Entropy Generation
%%%%%%%
%%%%%%            All Temperatures in Kelvin
%%%%%%%
%%%%%%%%%%%%%%%%%%%%%%%%%%%%%%%%%%%%%%%%%%%%%%%%%%%%%%%%%%%%%%%%%%%%%%%%%%%%%%%%
%%

Sgj = m_v*cc*log((T9+273)/(T8+273)) + m_r*cc*log((T9+273)/(T7+273)) +
m_v*vc*dPm/Ta;
Sgr = m_r*cc*log((T6+273)/(T5+273)) + m_r*vc*dPm/Ta +
m_a*ca*log(Tao/Ta) - m_a*R*log(Pa2/Pa1);
Sge = m_c*cc*log(T1/T10) + (1-Ta/Tec)*Qe/Ta + m_c*vc*dPe/Ta;

Sgtot = Sgj + Sgr + Sge;
```

Appendix F Engine Test - Time Histories

The proceeding set of figures document the time histories as recorded during cooling system configuration testing. Refer to Table 6.1 for a description of the tests that were conducted and Tables 6.2 and 6.3 for a summary of the results. The C-code on the dSPACE board runs at f=1000 Hz where the data was acquired at f=10 Hz. This is accomplished in the acquisition software, dSPACE Control Desk, by sampling after every 100 samples which was required due to the long test times and data logging limitations. The data was processed and plotted utilizing Matlab.

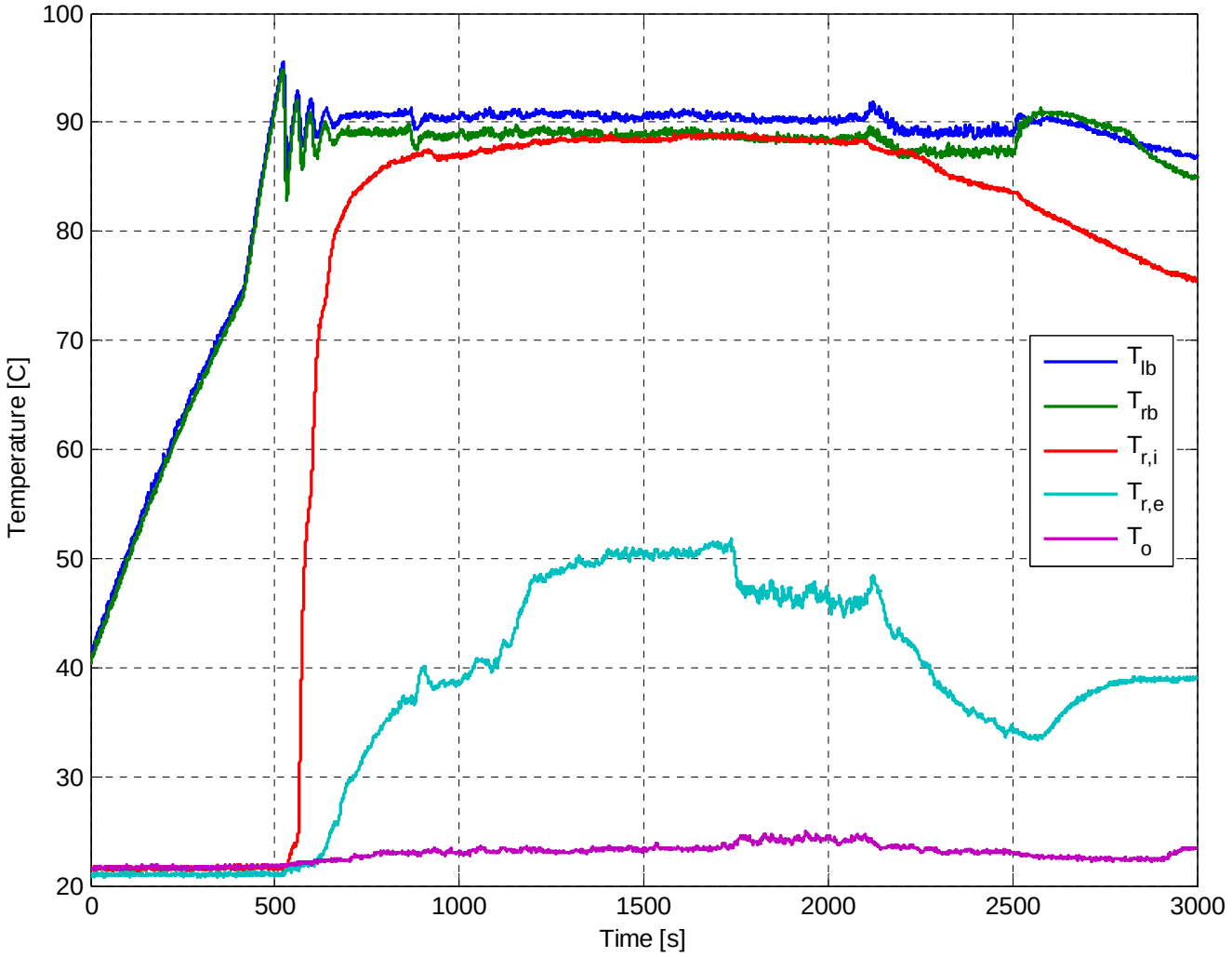

Figure F.1 Temperature response: Test 1

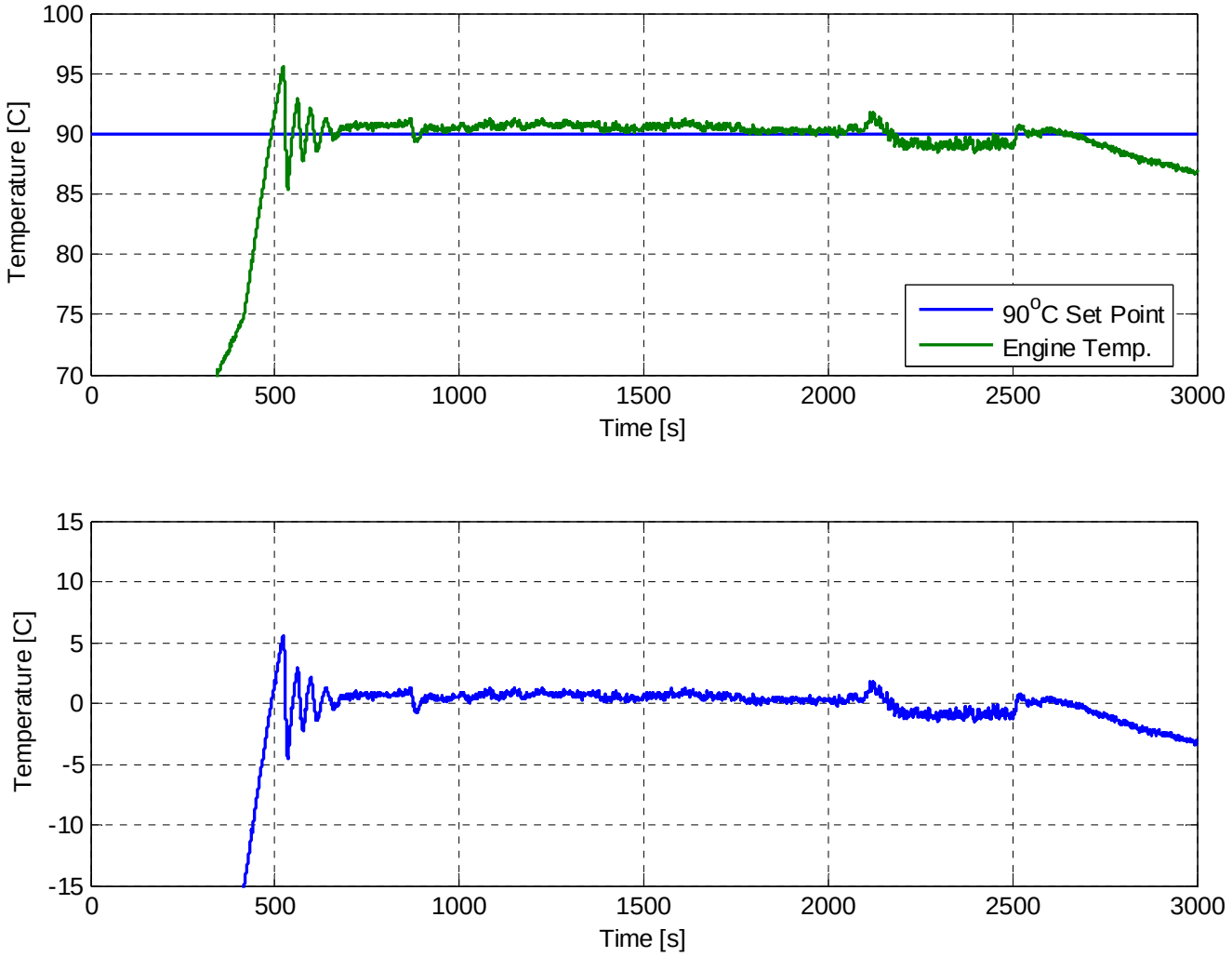

Figure F.2 Feedback temperature and error signal: Test 1

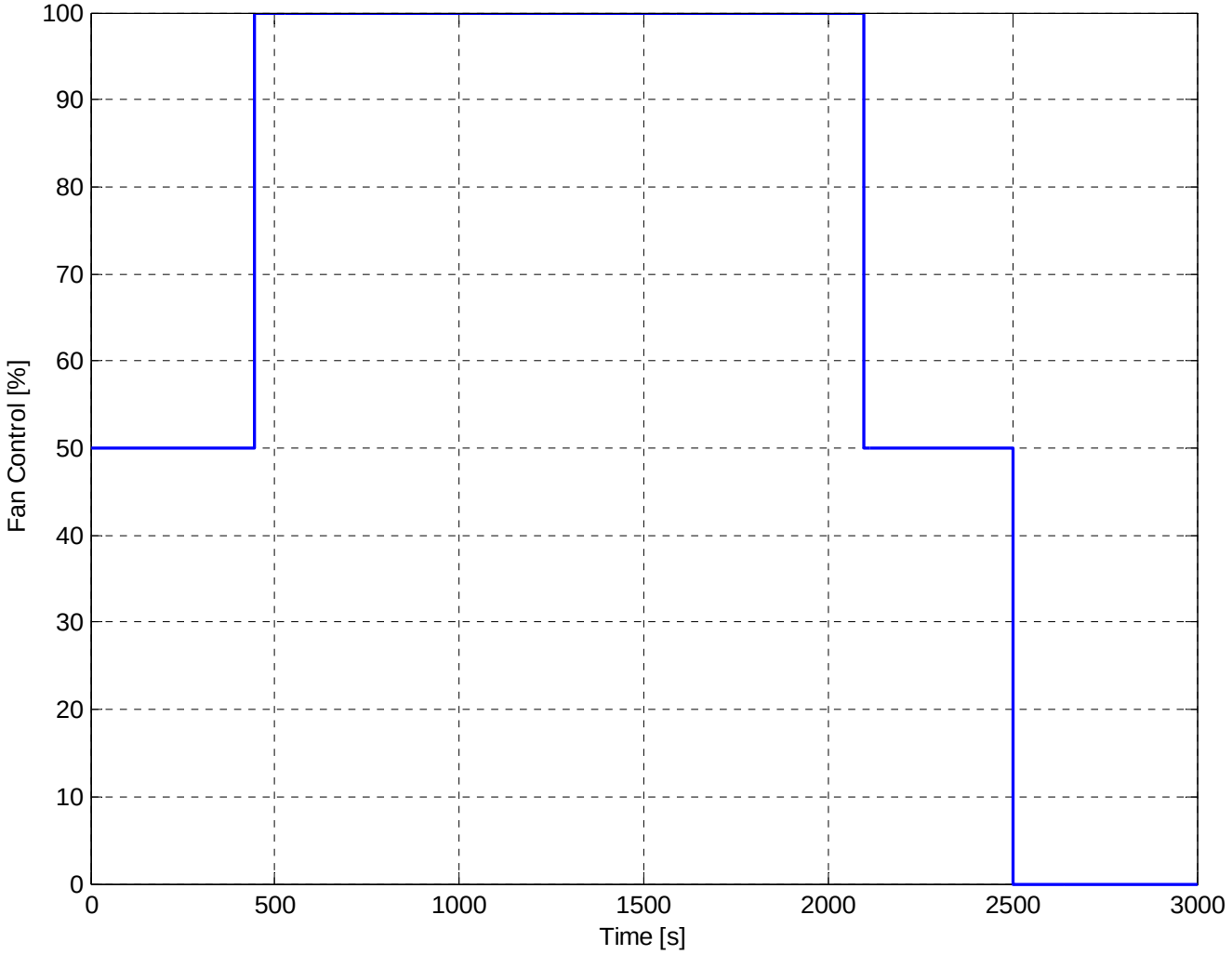

Figure F.3 Normalized control percentage: Test 1

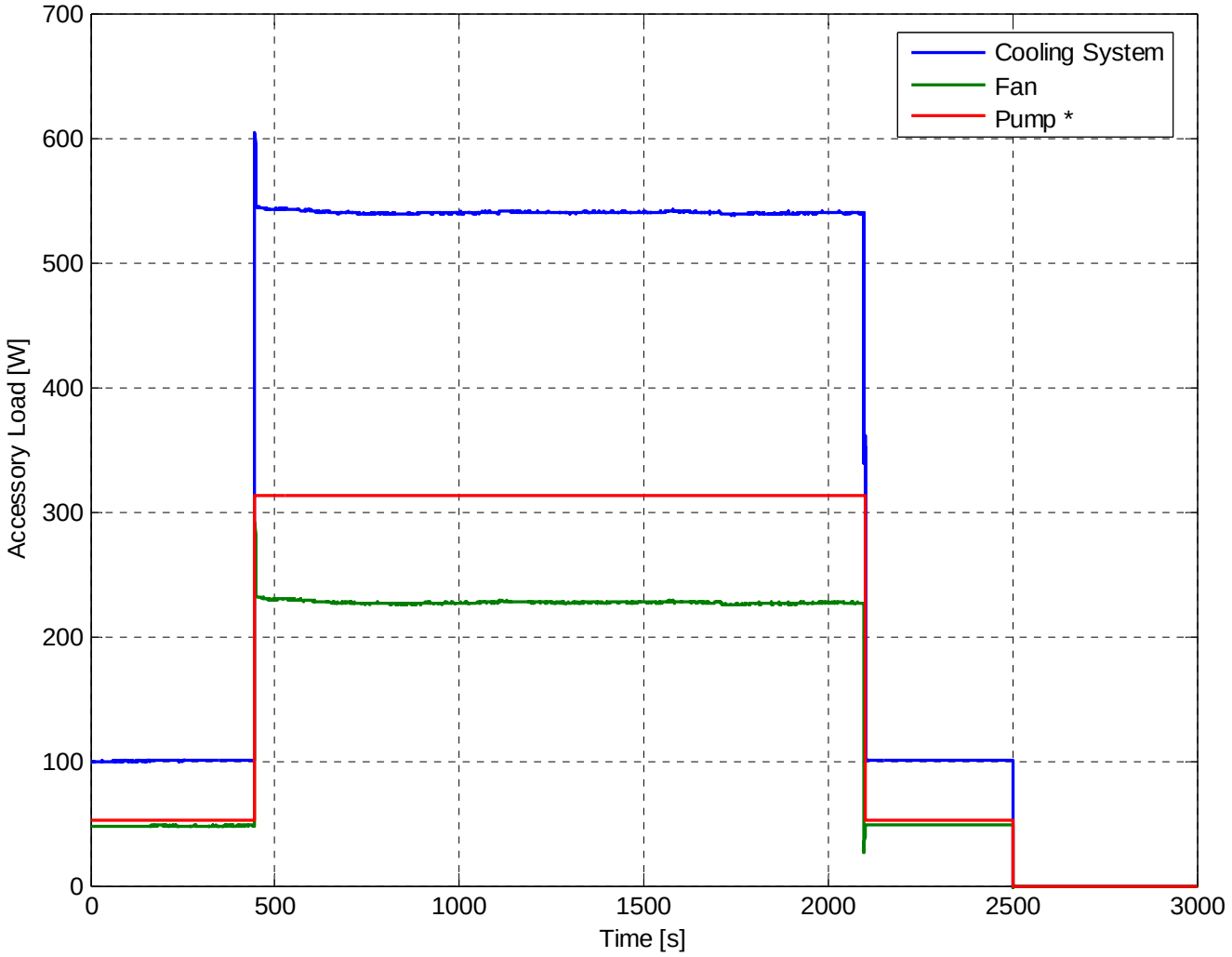

Figure F.4 Power consumption: Test 1

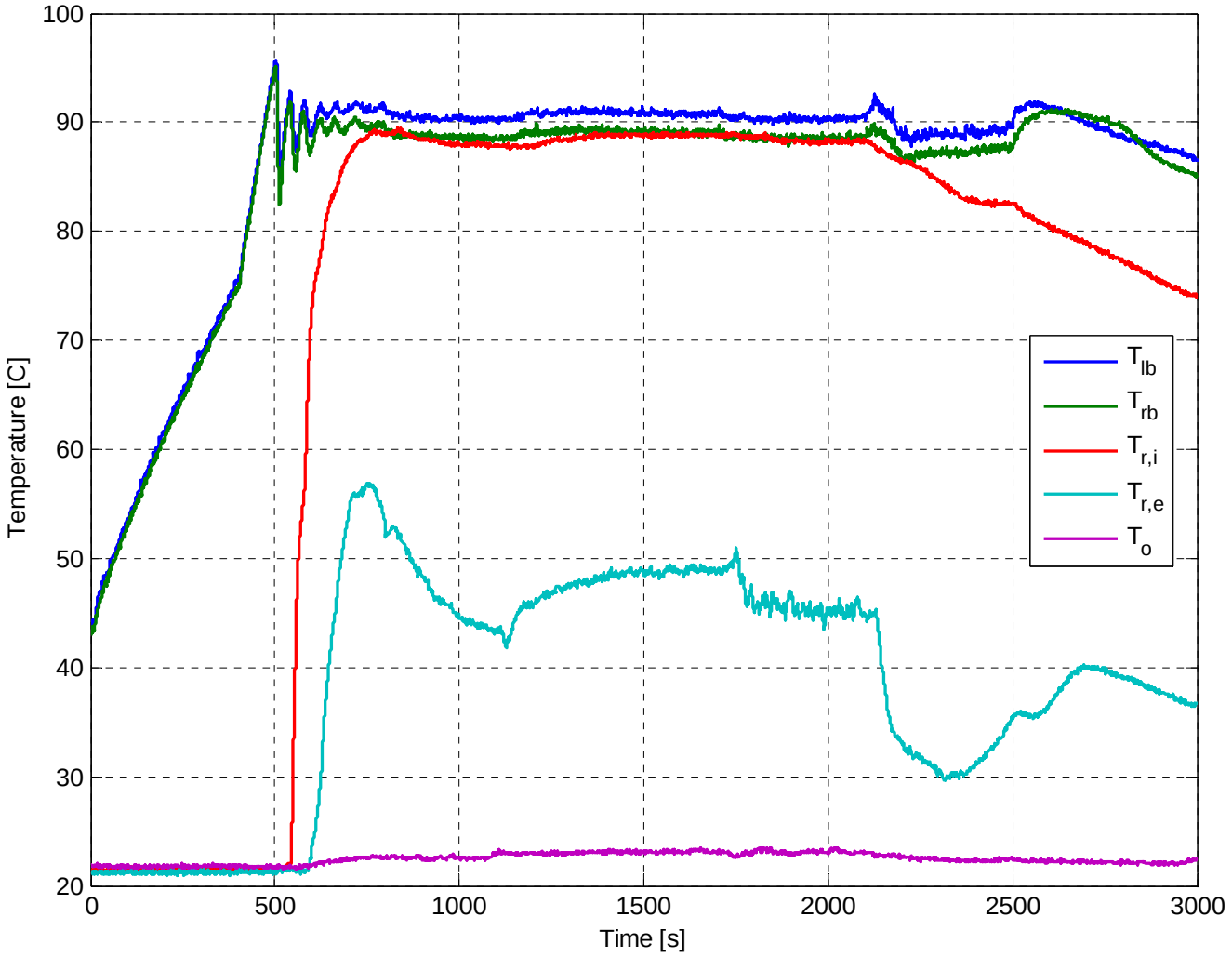

Figure F.5 Temperature response: Test 2

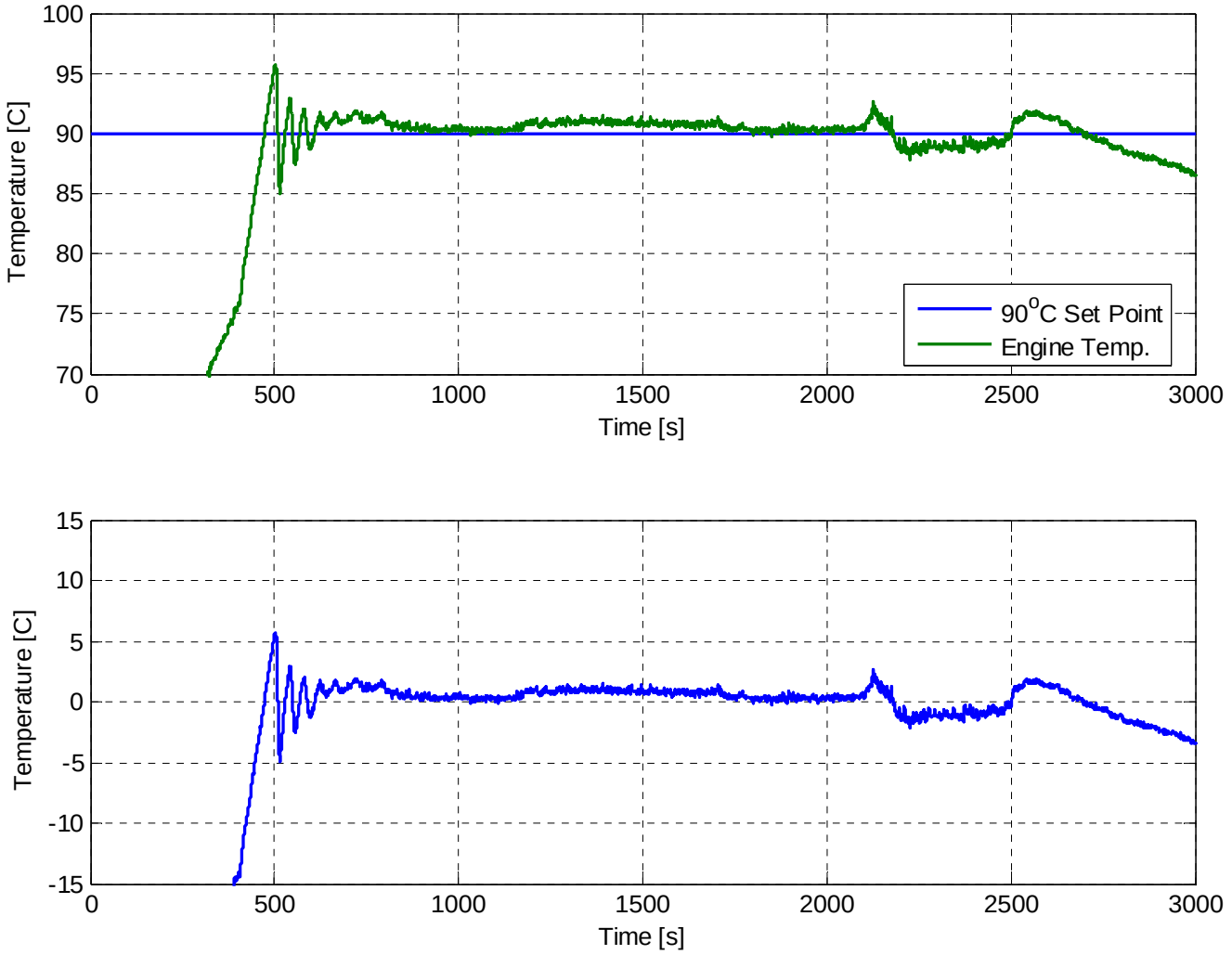

Figure F.6 Feedback temperature and error signal: Test 2

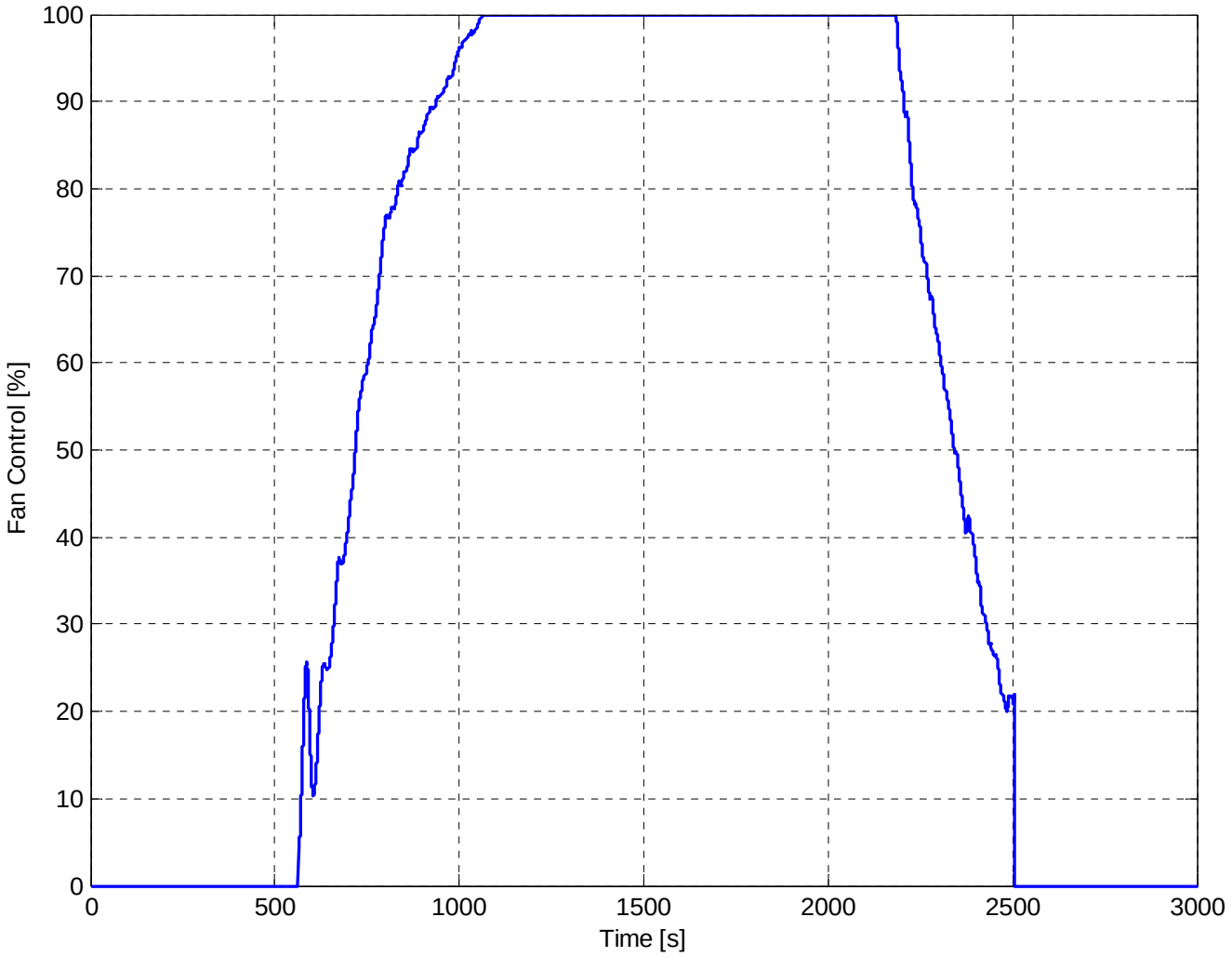

Figure F.7 Normalized control percentage: Test 2

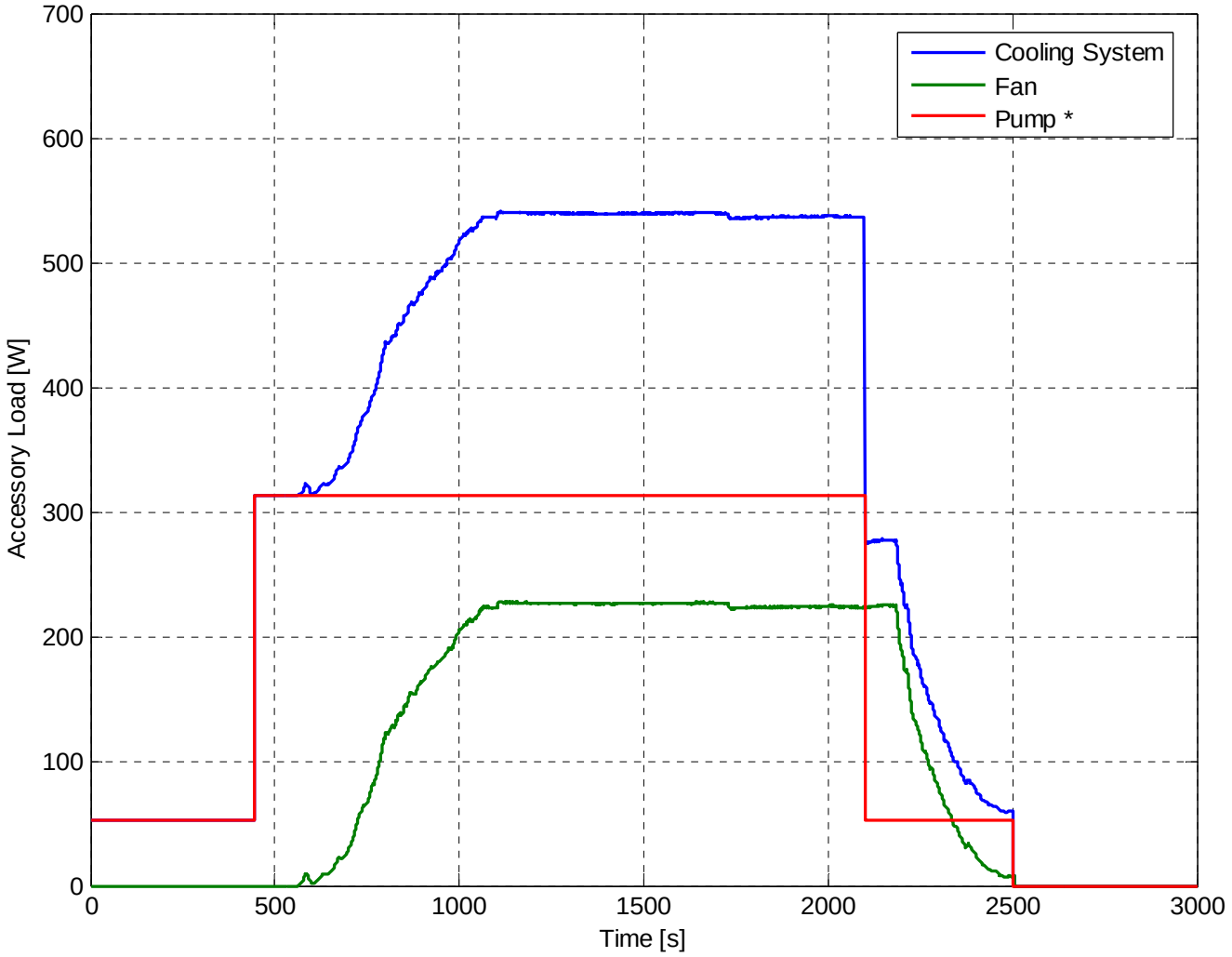

Figure F.8 Power consumption: Test 2

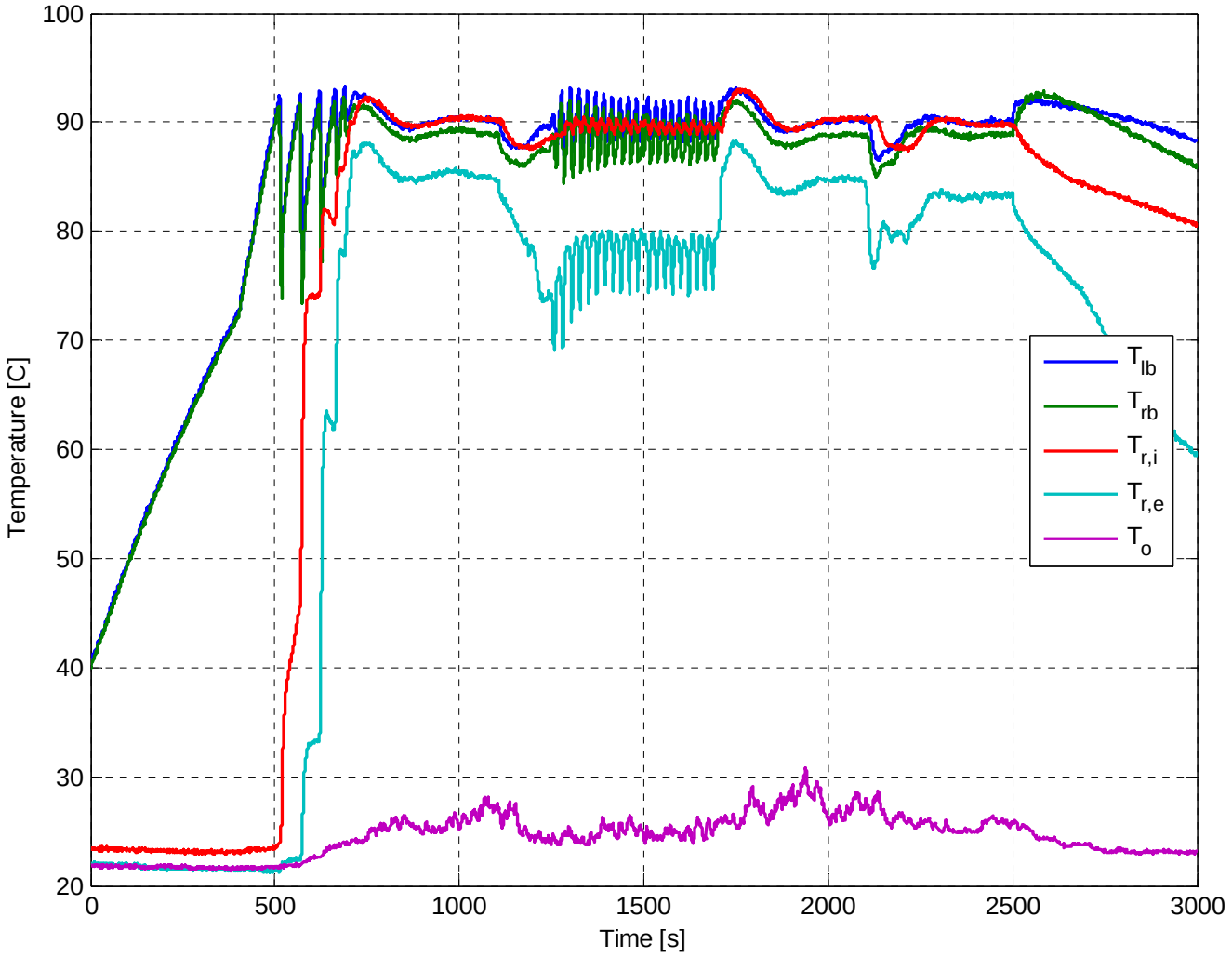

Figure F.9 Temperature response: Test 3

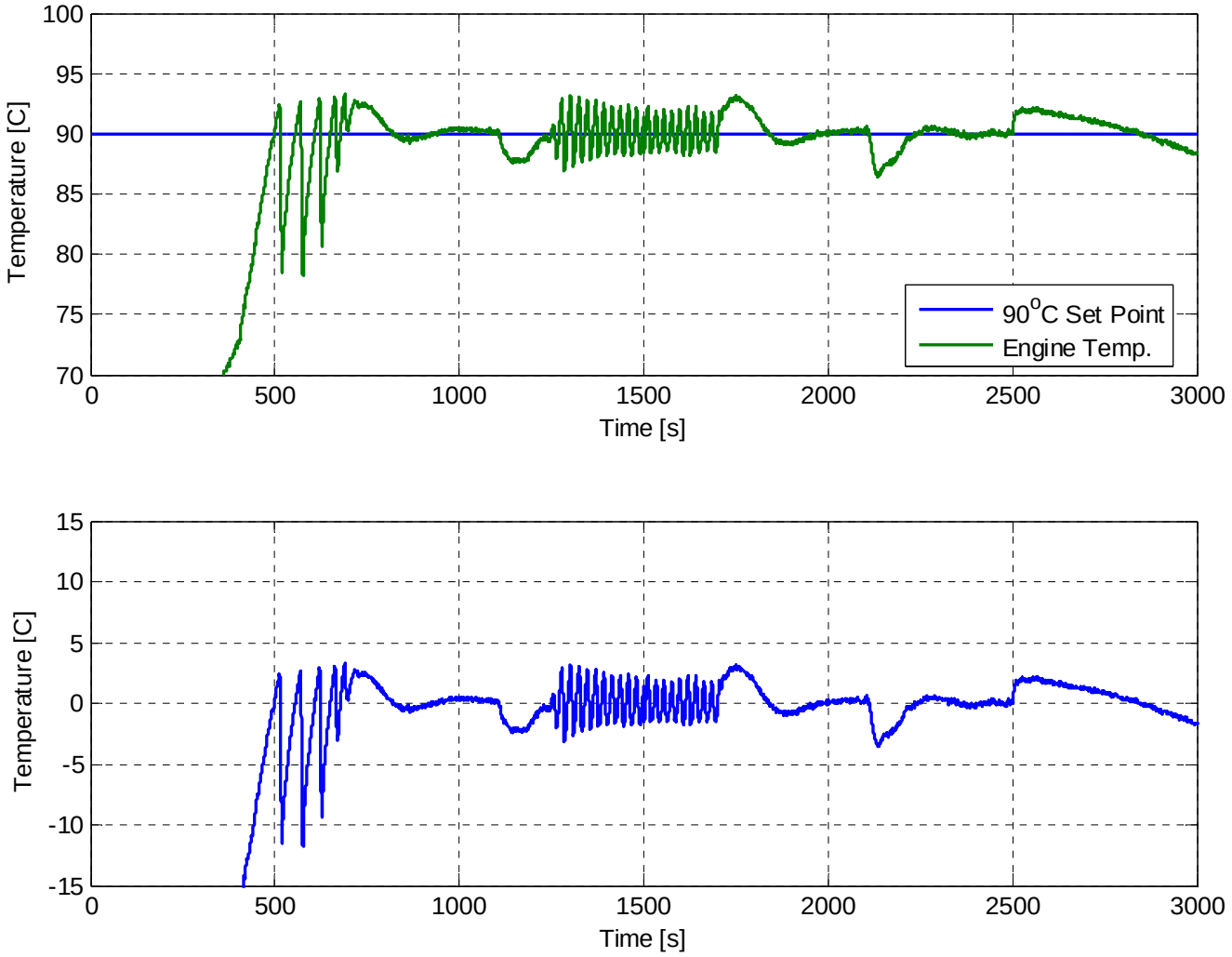

Figure F.10 Feedback temperature and error signal: Test 3

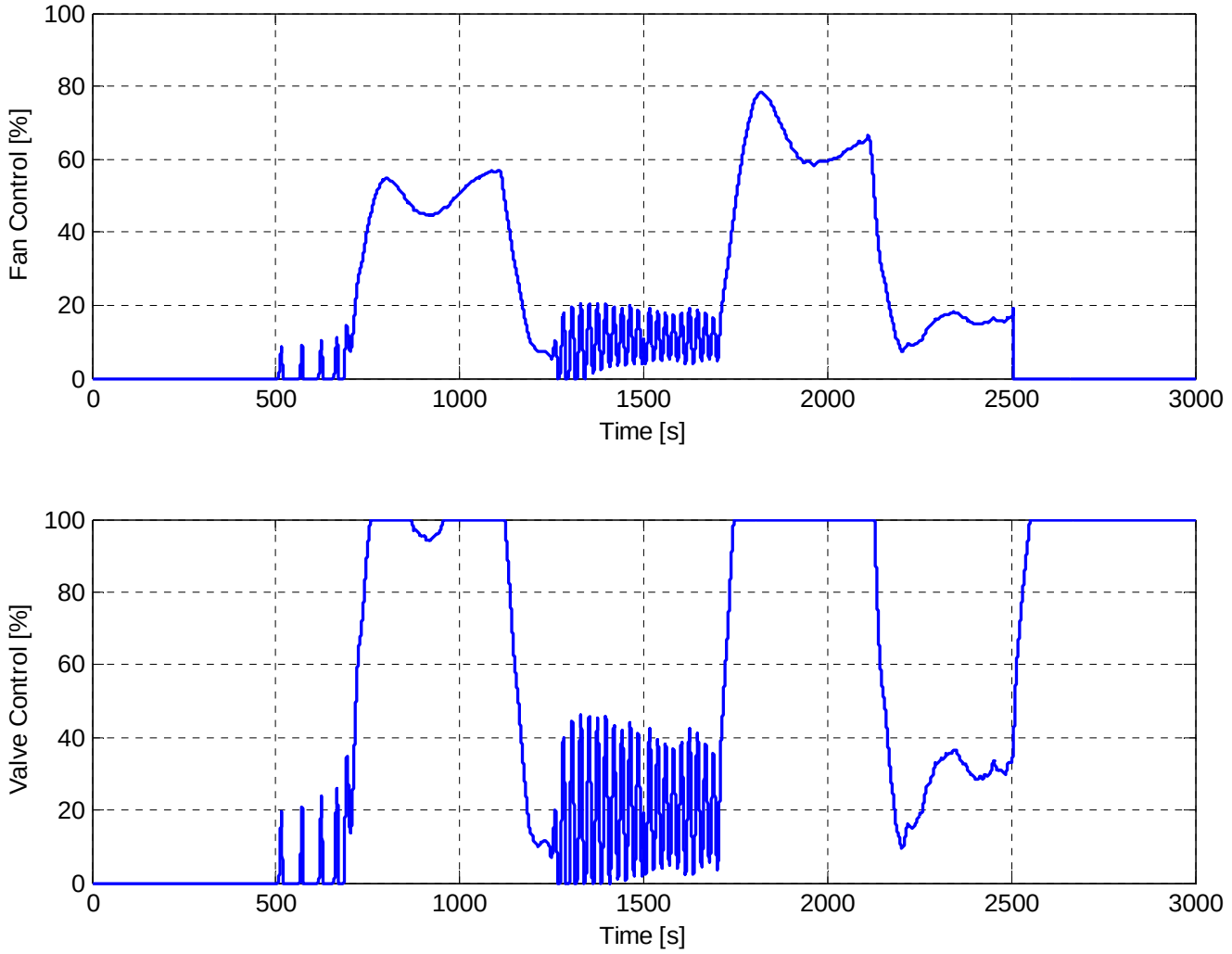

Figure F.11 Normalized control percentages: Test 3

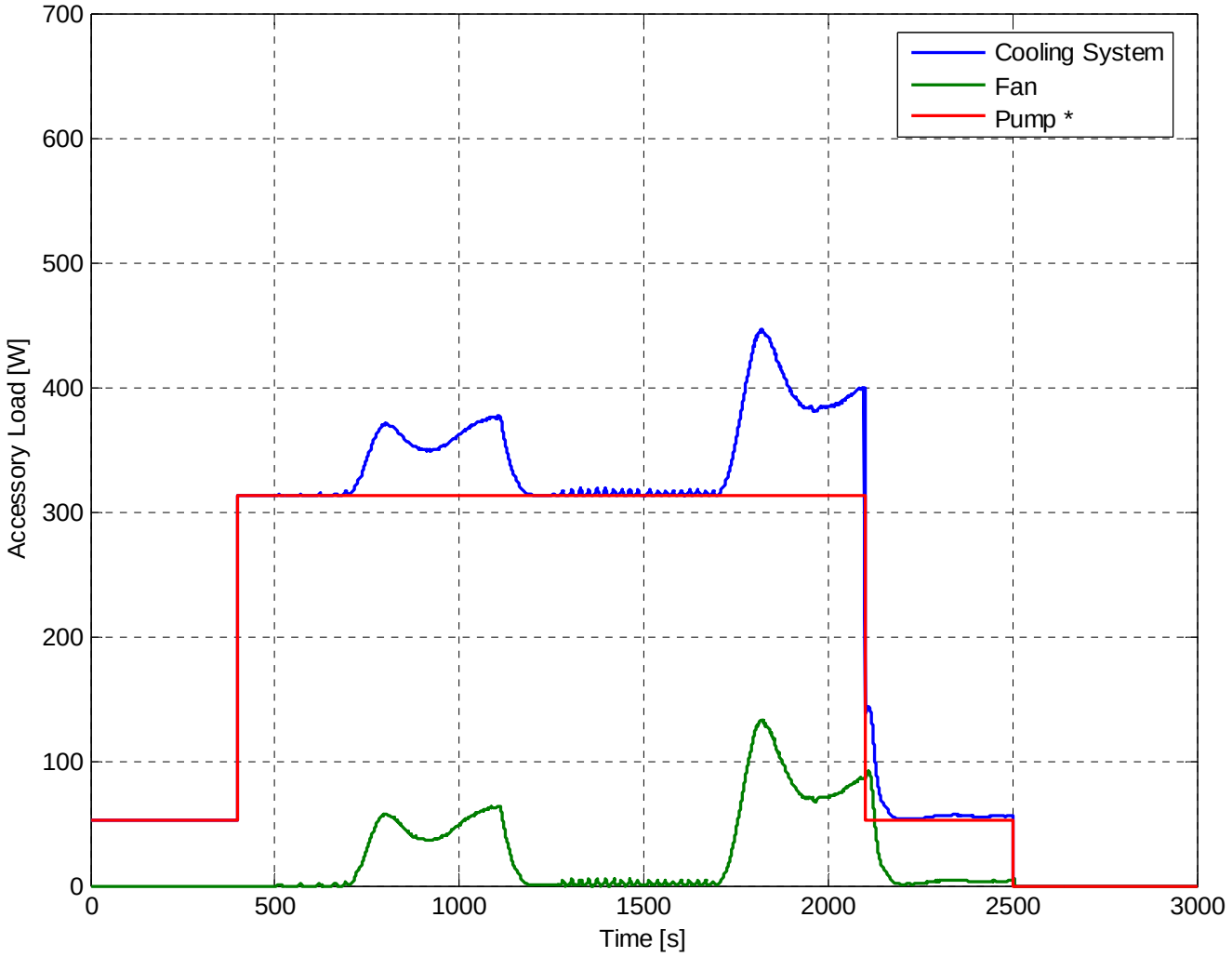

Figure F.12 Power consumption: Test 3

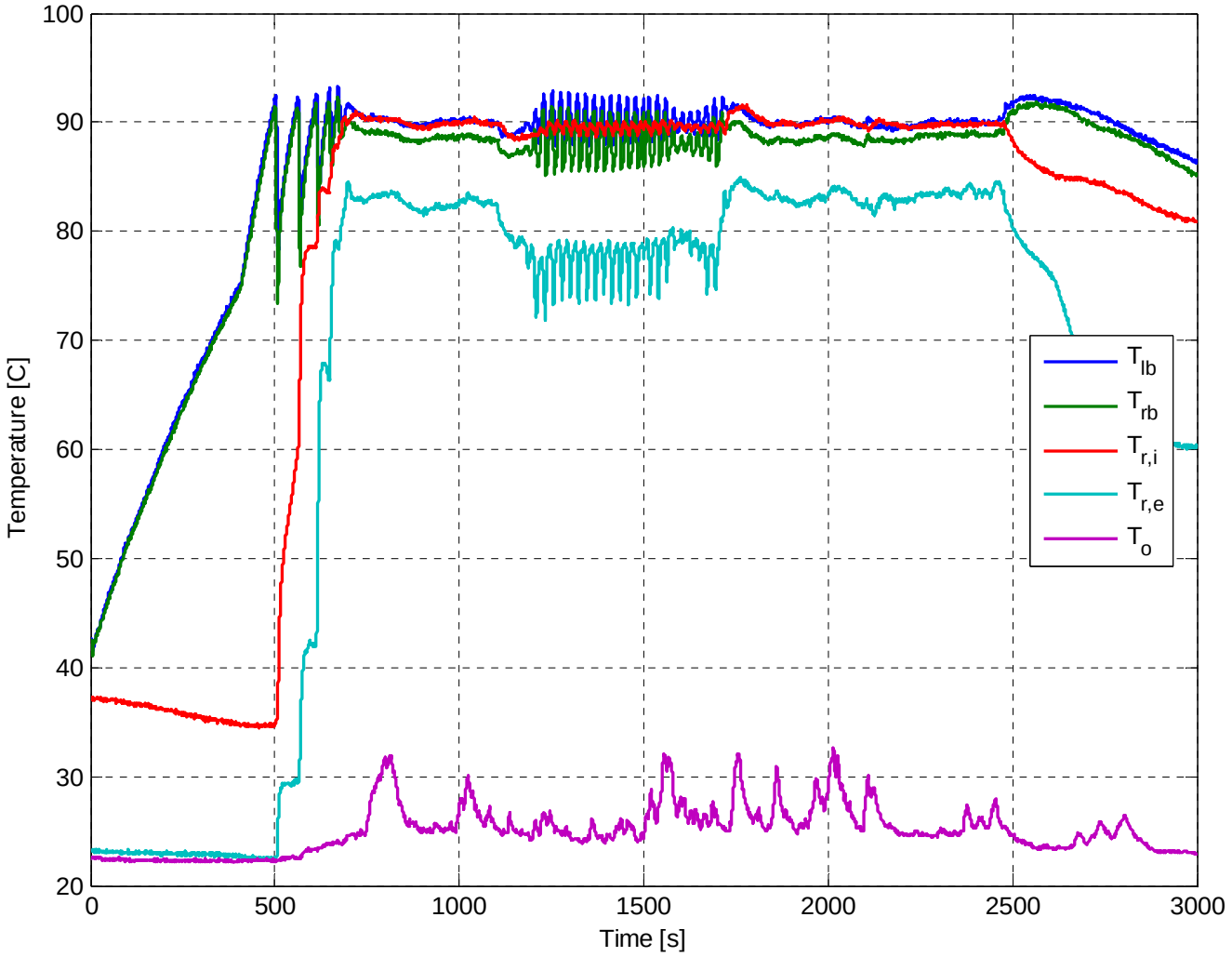

Figure F.13 Temperature response: Test 4

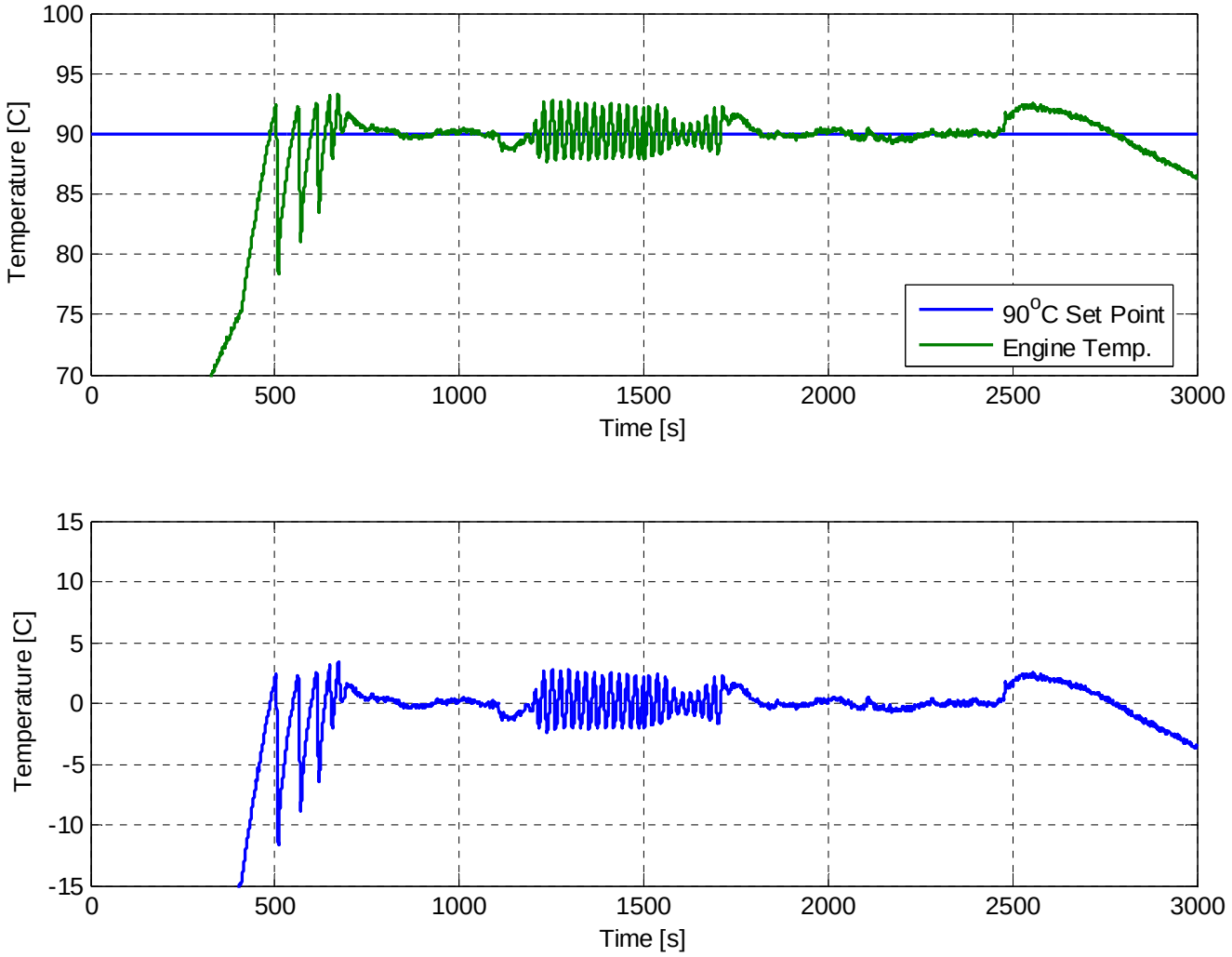

Figure F.14 Feedback temperature and error signal: Test 4

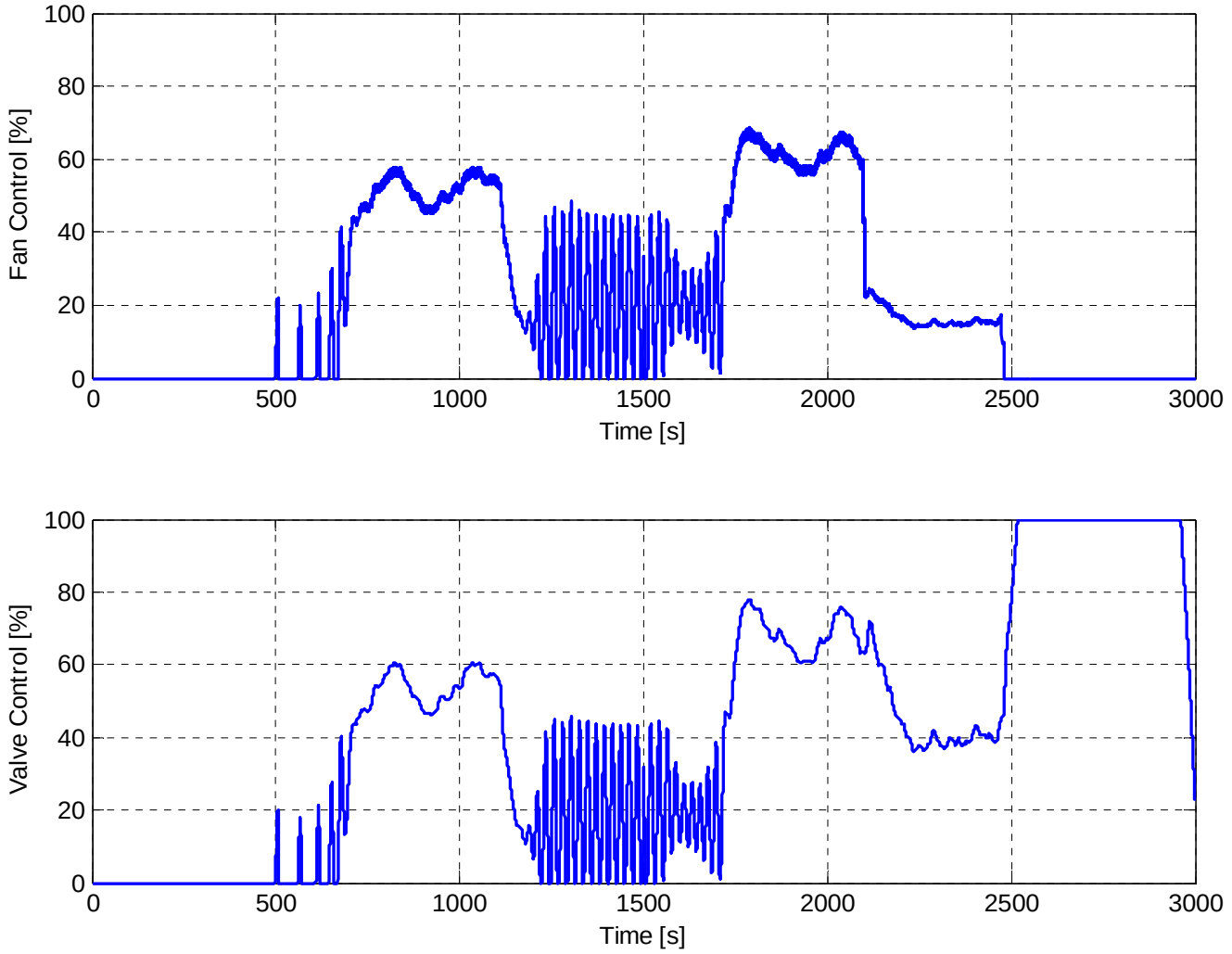

Figure F.15 Normalized control percentages: Test 4

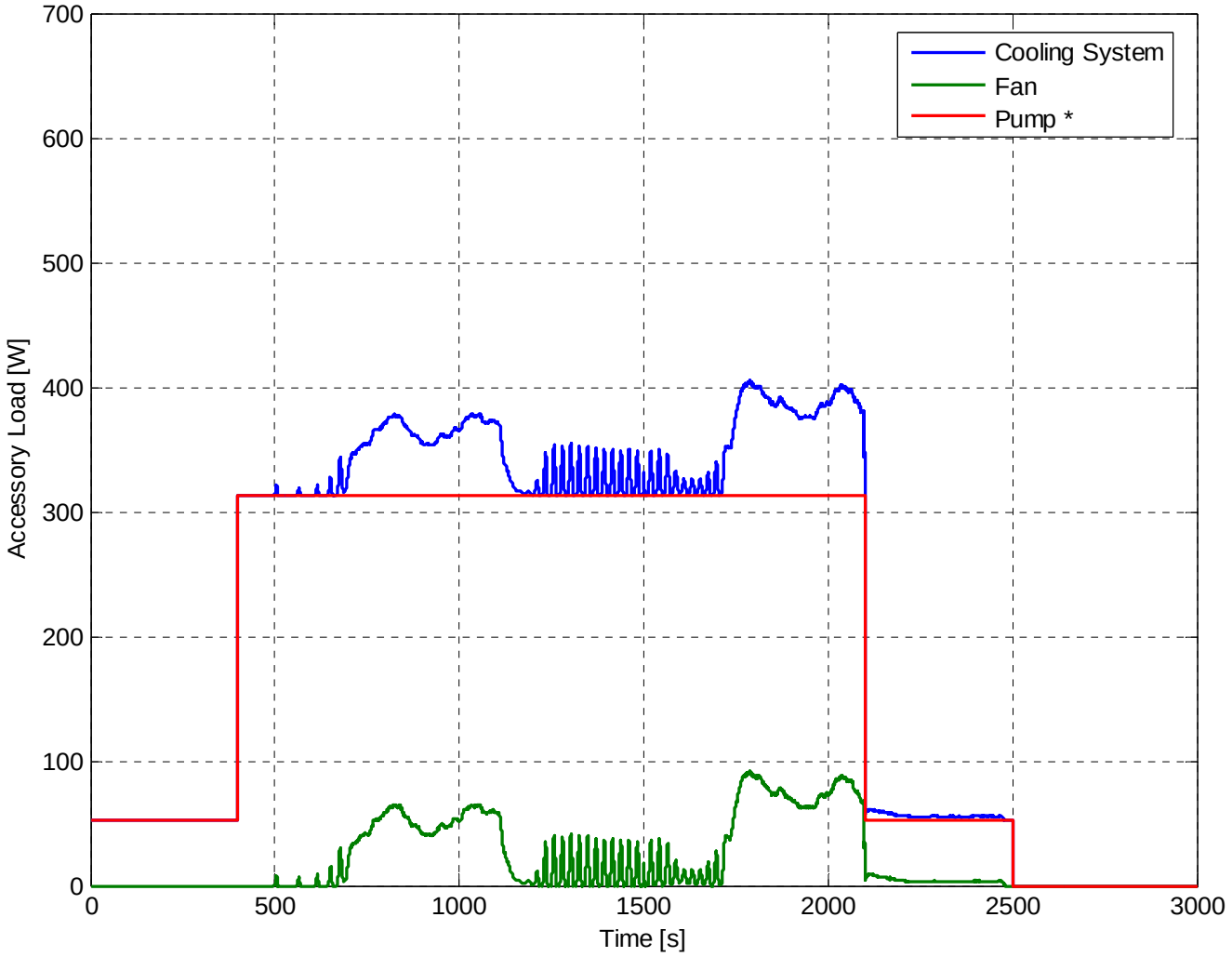

Figure F.16 Power consumption: Test 4

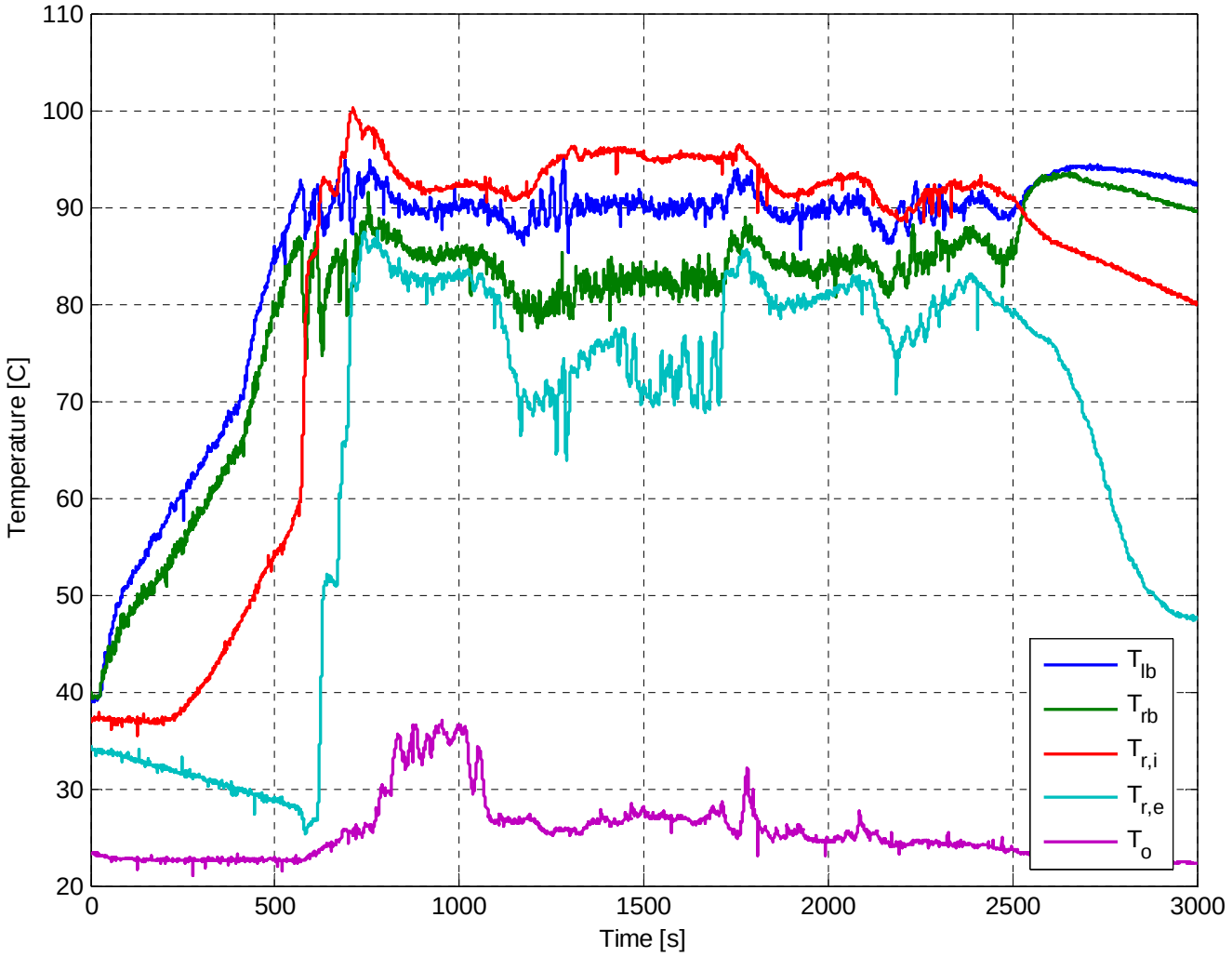

Figure F.17 Temperature response: Test 5

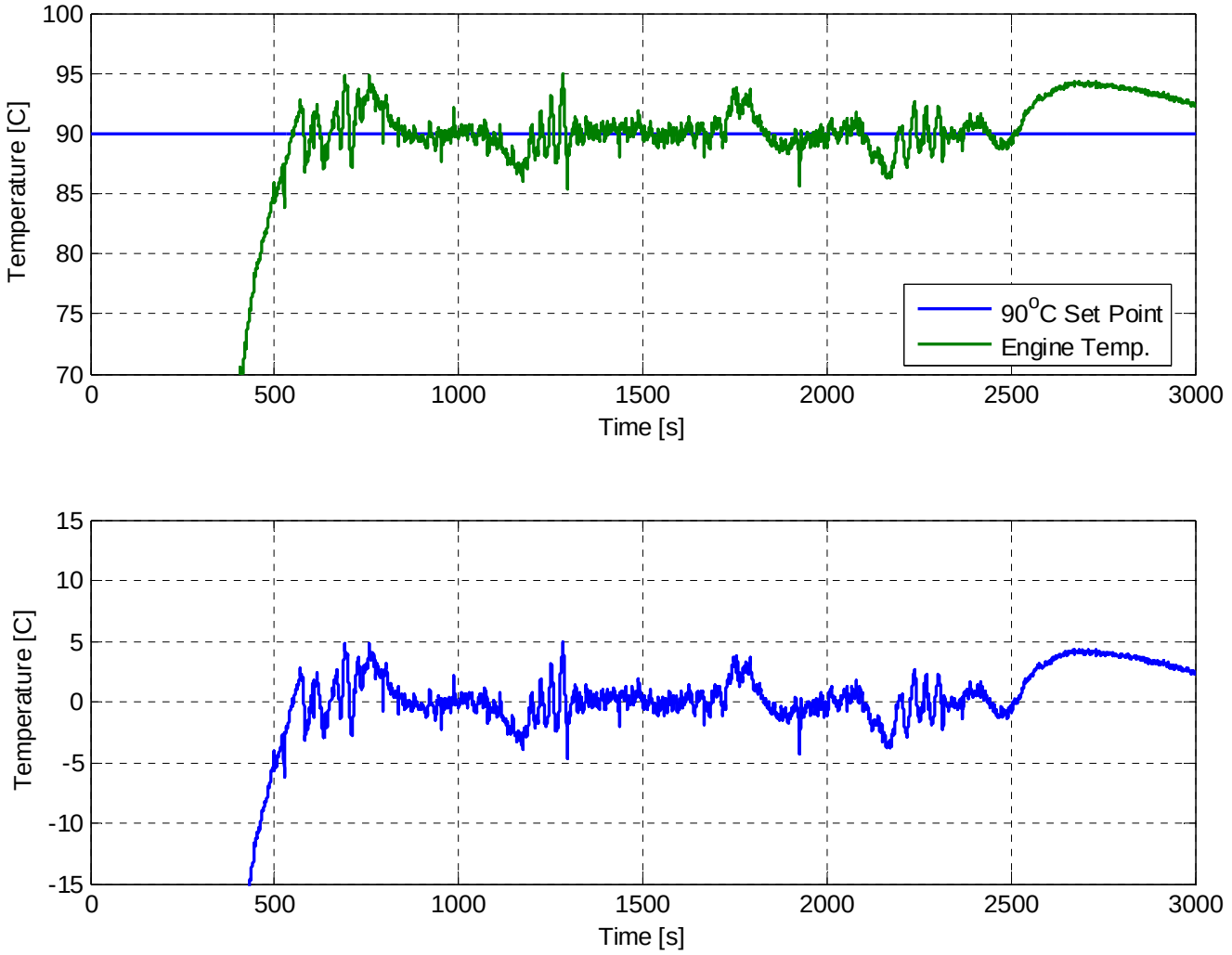

Figure F.18 Feedback temperature and error signal: Test 5

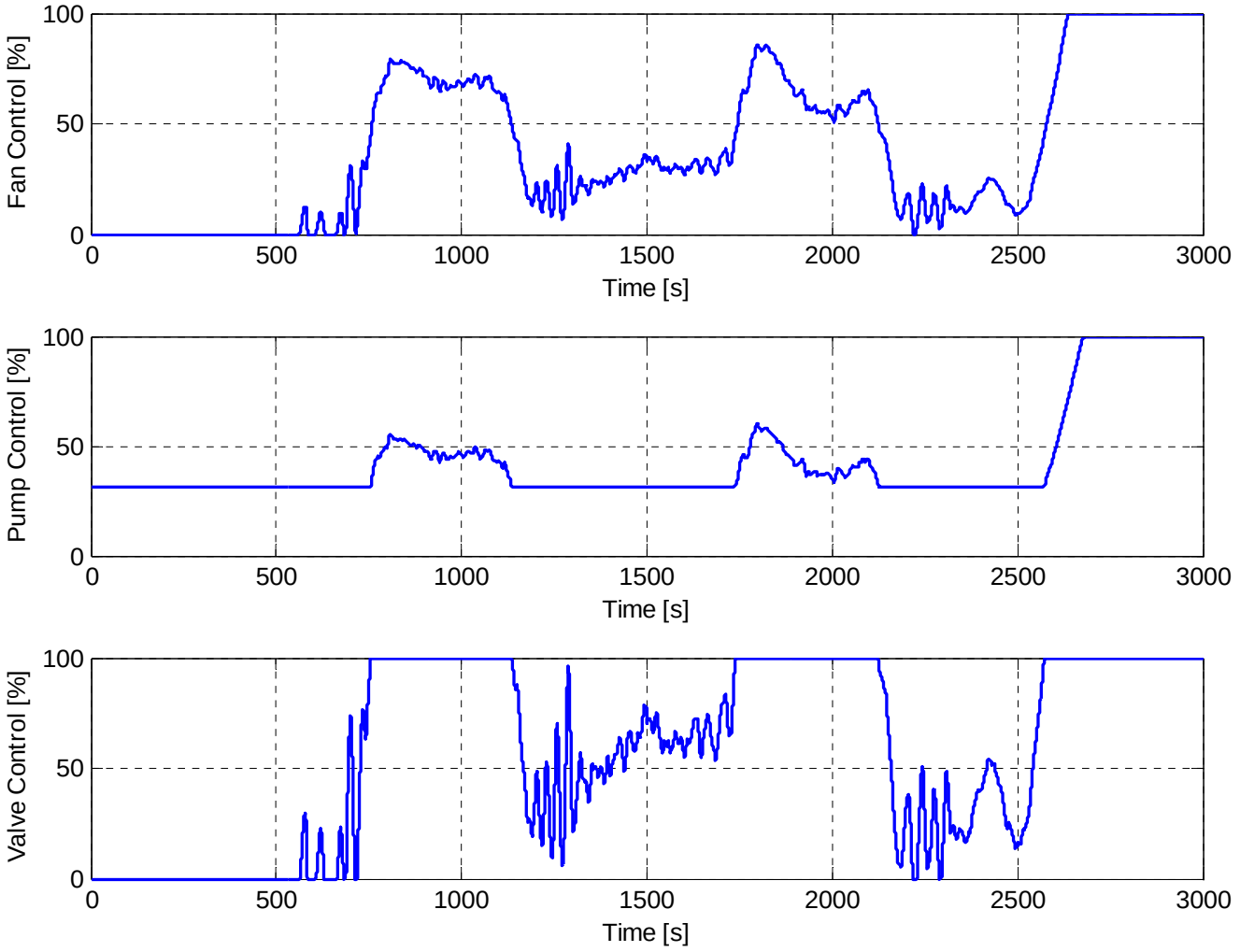

Figure F.19 Normalized control percentages: Test 5

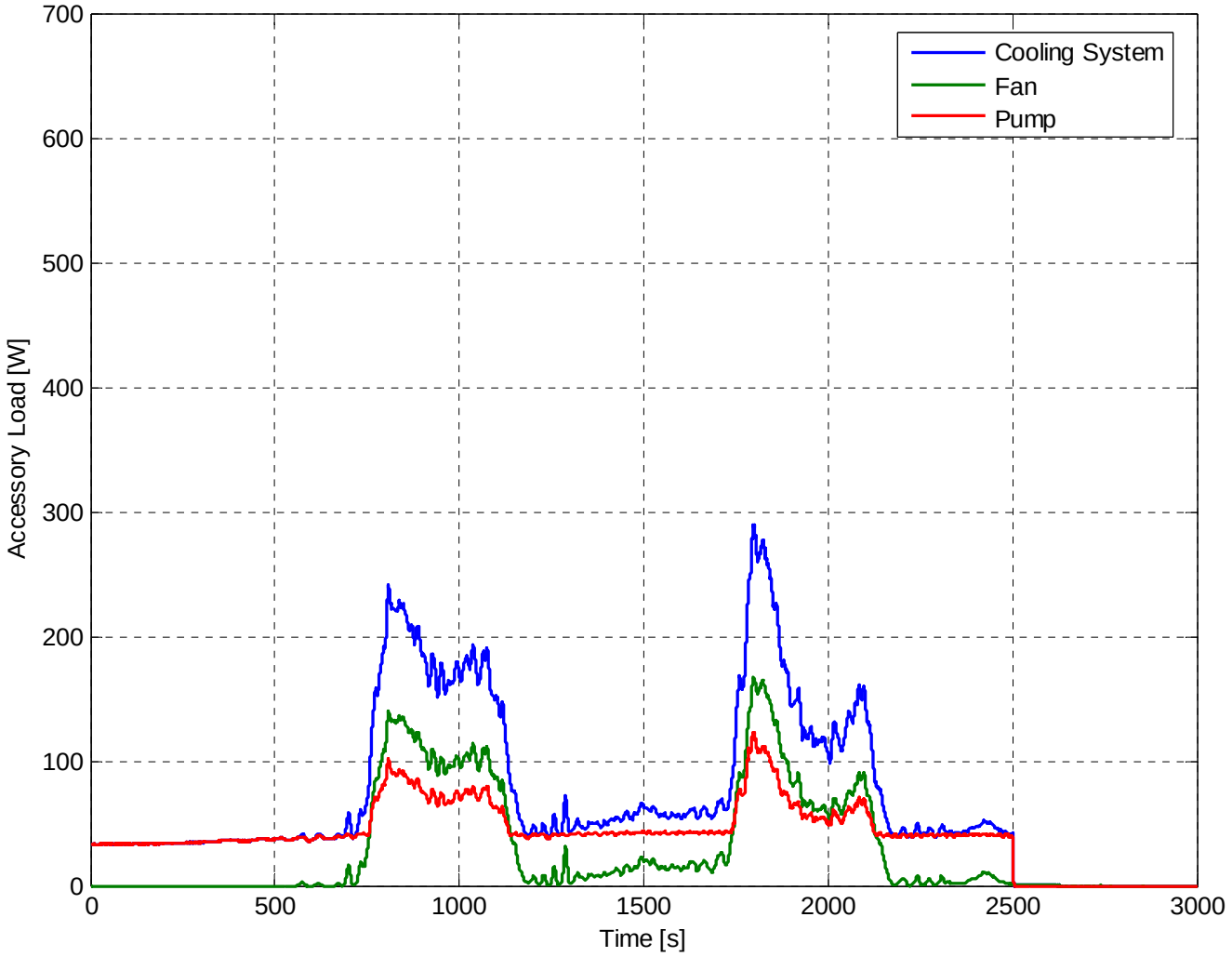

Figure F.20 Power consumption: Test 5

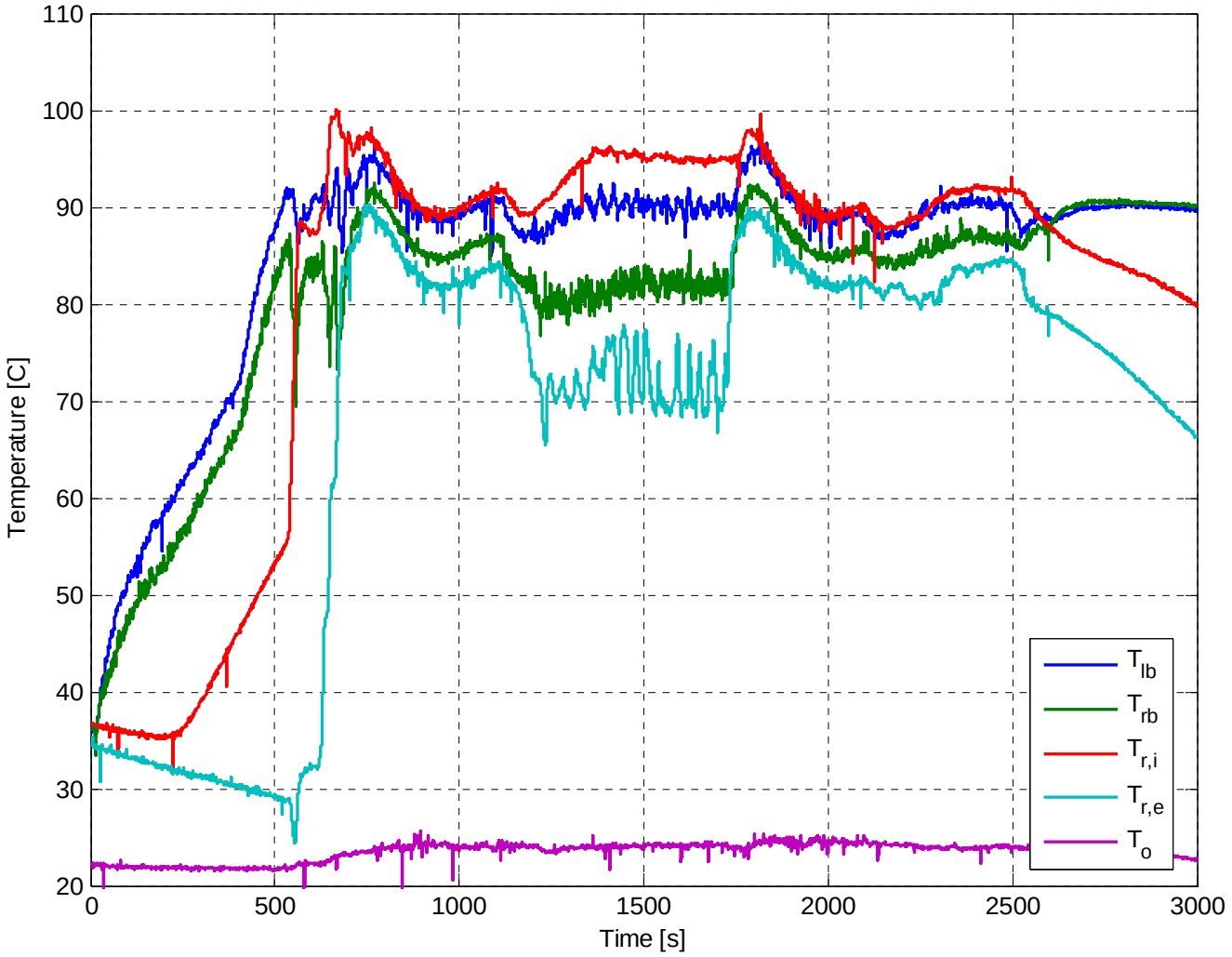

Figure F.21 Temperature response: Test 6

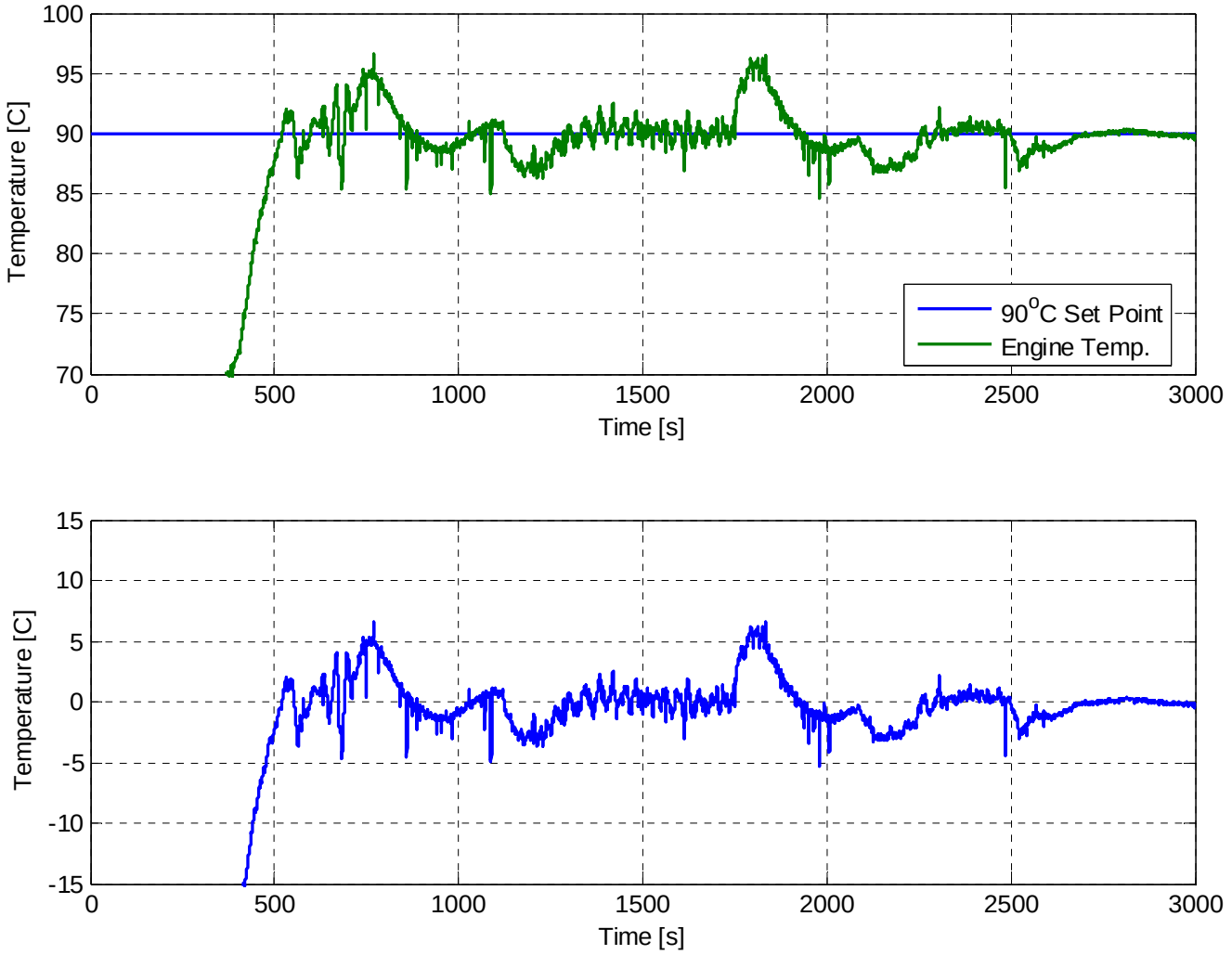

Figure F.22 Feedback temperature and error signal: Test 6

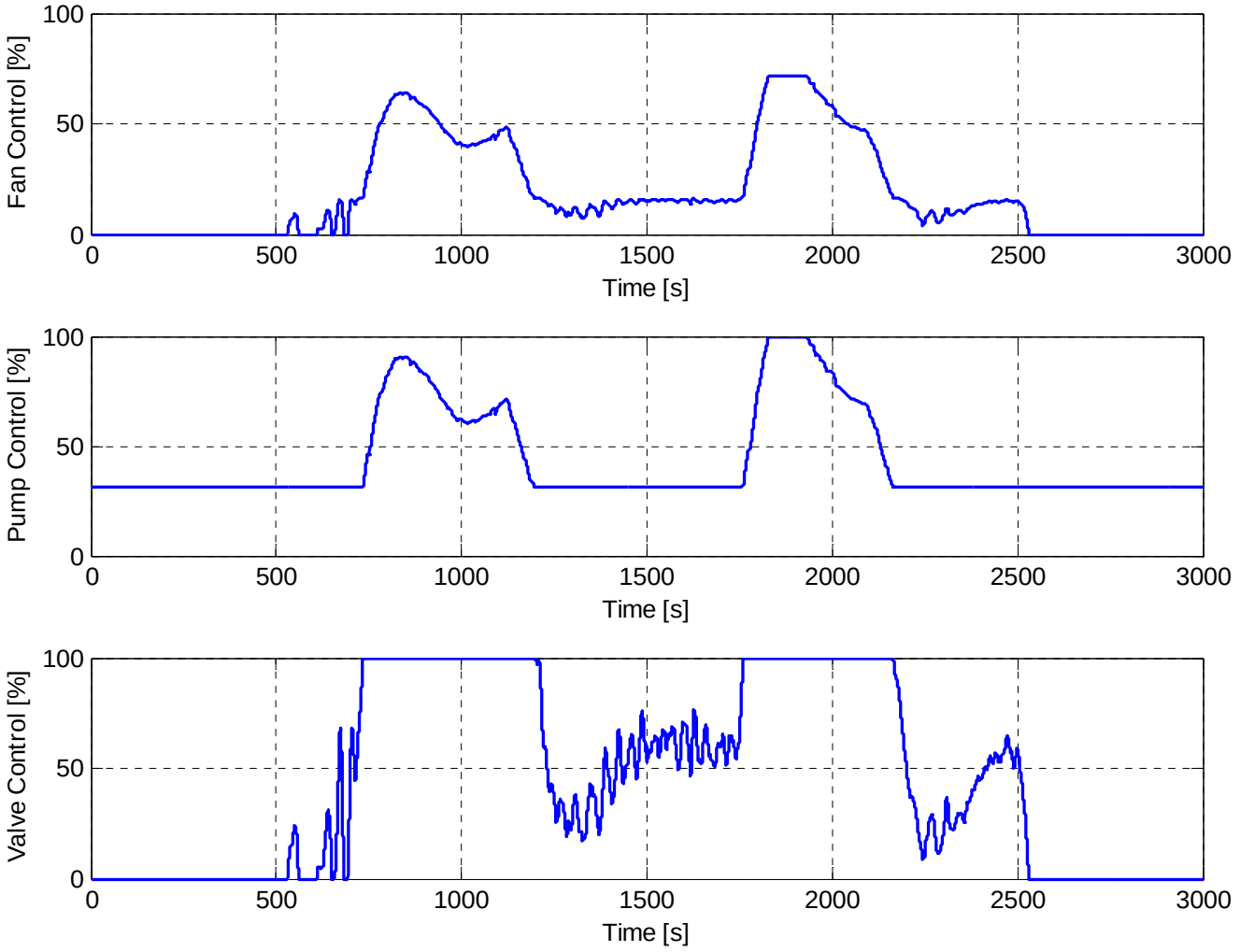

Figure F.23 Normalized control percentages: Test 6

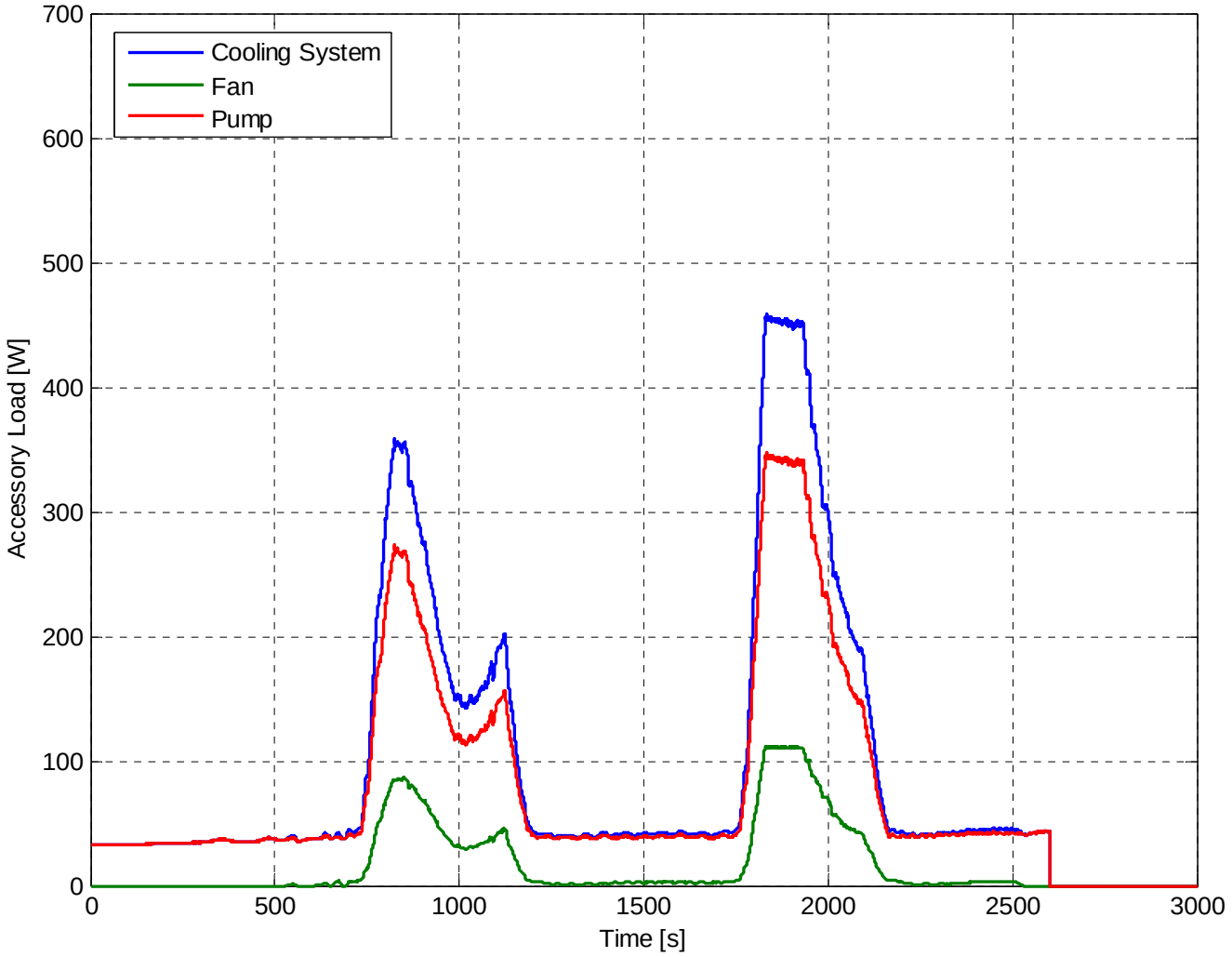

Figure F.24 Power consumption: Test 6

REFERENCES

Allen, D., and Lasecki, M., "Thermal Management Evolution and Controlled Coolant Flow", SAE paper no. 2001-01-1732, 2001.

Ap, N., and Tarquis, M., "Innovative Engine Cooling Systems Comparison", SAE paper no. 2005-01-1378, 2005.

Bejan, A., Entropy Generation through Heat and Mass Flow, John Wiley and Sons, Inc.: New York, 1982.

Bejan, A., Entropy Generation Minimization: The Method of Thermodynamic Optimization of Finite-Size Systems and Finite-Time Processes, CRC Press: Boca Raton, FL, 1996.

Bhat, N., Joshi, S., Shiozaki, K., Ogasawara, M., Yamada, M., and Somu, S., "Adaptive Control of an Externally Controlled Engine Cooling Fan -Drive" SAE paper no. 2006-01-1036, 2006.

Chastain, J., and Wagner, J., "Advanced Thermal Management for Internal Combustion Engines – Valve Design, Component Testing, and Block Redesign", SAE paper no. 2006-01-1232, 2006.

Chalgren, R., and Allen, D., "Light Duty Diesel Advanced Thermal Management", SAE paper no. 2005-01-2020, 2005.

Chalgren, R., and Barron, L., "Development and Verification of a Heavy Duty 42/14V Electric Powertrain Cooling System", SAE paper no. 2003-01-3416, 2003.

Chanfreau, M., Gessier, B., Farkh, A., and Geels, P., "The Need for an Electrical Water Valve in a Thermal Management Intelligent System", SAE paper no. 2003-01-0274, 2003.

Chmela, F., and Orthaber, G., "Rate of Heat Release Prediction for Direct Injection Diesel Engines Based on Purely Mixing Controlled Combustion", SAE paper no. 1999-01-0186, 1999.

Driskell, L., Control-Valve Selection and Sizing, Instrument Society of America: Research Triangle Park, NC, 1983.

Eberth, J. F., Wagner, J. R., Afshar, B. A., and Foster, R. C., "Modeling and Validation of Automotive Smart Thermal Management System Architectures", SAE paper no. 2004-01-0048, 2004.

Figliola, R., and Tipton R., "An Exergy-Based Methodology for Decision-Based Design of Integrated Aircraft Thermal Systems", SAE paper no. 2000-01-5527, 2000.

Frick, P., Bassily, H., Watson, H., and Wagner, J., "A Hydraulic Fan Driven Heat Exchanger for Automotive Cooling Systems", Proceedings of the IMECE 2006, IMECE2006-13464, 2006.

Friedrich, I., Pucher, H., and Offer, T., "Automatic Model Calibration for Engine-Process Simulation with Heat-Release Prediction", SAE paper no. 2006-01-0655, 2006.

Goldstick, Robert and Thumann, Albert, Principles of Waste Heat Recovery, The Fairmont Press, Inc.: Atlanta, 1986.

Hutchison, J. W., ISA Handbook of Control Valves, 2nd edition, Instrument Society of America: Pittsburgh, 1976.

Incropera, F. P., and DeWitt, D. P., Introduction to Heat Transfer, 4th edition, John Wiley and Sons, Inc.: New York, 2002.

Kays, W. M., "Heat Transmission from the Engine to the Atmosphere", Heat and Mass Transfer in Gasoline and Diesel Engines, pp. 333-362, Hemisphere Publishing Corporation: New York, 1989.

Li, H., and Figliola, R., "Optimization of an Automotive Cooling System Based on Exergy Analysis", SAE paper no. 2004-01-3541, 2004.

Luptowski, B., Arici, O., Johnson, J., and Parker, G., "Development of the Enhanced Vehicle and Engine Cooling System Simulation and Application to Active Cooling Control", SAE paper no. 2005-01-0697, 2005.

Luptowski, J., Adekeye, D., and Straten, T., "Coupled Engine/Cooling System Simulation and its Application to Engine Warm-up", SAE paper no. 2005-01-2037, 2005.

Miles, V. C., Thermostatic Control: Principles and Practice, C. Tinling & Co., Ltd.: London, 1965.

Moran, M. J. and Shapiro, H. N., Fundamentals of Engineering Thermodynamics, 4th edition, John Wiley and Sons, Inc.: New York, 2000.

O'Dwyer, A., Handbook of PI and PID Controller Tuning Rules, Imperial College Press: London, 2003.

Page, R., Hnatczuk, W., and Kozierowski, J., "Thermal Management for the 21st Century – Improved Thermal Control & Fuel Economy in an Army Medium Tactical Vehicle", SAE paper no. 2005-01-2068, 2005.

Redfield, J., Surampudi, B., Ray, G., Montemayor, A., McKee, H., Edwards, T., and Lasecki, M., "Accessory Electrification in Class 8 Trucks", SAE paper no. 2006-01-0215, 2006.

Setlur, P., Wagner, J., Dawson, D., and Marotta, E., "An Advanced Engine Thermal Management System: Nonlinear Control and Test", *IEEE/ASME Transactions on Mechatronics*, vol. 10, no. 2, pp. 11, 2005.

Shinskey, F. G., Energy Conservation through Control, Academic Press: New York, 1978.

Stoecker, Wilbert F., Design of Thermal Systems, McGraw-Hill Book Company: New York, 1971.

Vagenas, A., Hawley, J., Brace, C., and Ward, M., "On-Vehicle Controllable Cooling Jets", SAE paper no. 2004-01-0049, 2004.

Visnic, B., "Thermostat, Thy Days are Numbered", *Ward's AutoWorld*, vol. 37, no. 6, pp. 53-54, June 2001, 2001.

Wagner, J., Paradis, I., Marotta, E., and Dawson, D., "Enhanced Automotive Engine Cooling Systems – A Mechatronics Approach", *International Journal of Vehicle Design*, vol. 28, nos. 1/2/3, pp. 214-240, 2002.

Wagner, J., Srinivasan, V., Marotta, E., and Dawson, D., "Smart Thermostat and Coolant Pump Control for Engine Management Systems", SAE paper no. 2003-01-0272, 2003.

White, F. M., Fluid Mechanics, 4th edition, McGraw Hill: Boston, 1999.

Zeng, P., Prucka, R., Filipi, Z., and Assanis, D., "Reconstructing Cylinder Pressure of a Spark-Ignition Engine for Heat Transfer and Heat Release Analyses", Proceedings of ASME Internal Combustion Engine Division 2004 Fall Technical Conference, ICEF2004-886, 2004.